

City Research Online

City St George's, University of London

Citation: Alsalim, H. S. (1972). Surface treatment of titanium alloys for adhesive bonding. (Unpublished Doctoral thesis, The City University)

This is the accepted version of the paper.

This version of the publication may differ from the final published version. To cite this item please consult the publisher's version.

Permanent repository link: https://openaccess.city.ac.uk/id/eprint/38443/

Copyright and Reuse: Copyright and Moral Rights remain with the author(s) and/or copyright holders. Copies of full items can be used for personal research or study, educational, or not-for-profit purposes without prior permission or charge, unless otherwise indicated, provided that the authors, title and full bibliographic details are credited, a hyperlink and/or URL is given for the original metadata page and the content is not changed in any way. For full details of reuse please refer to City Research Online policy.

City Research Online: http://openaccess.city.ac.uk/ publications@citystgeorges.ac.uk

SURFACE TREATMENT OF TITANIUM ALLOYS

FOR ADHESIVE BONDING

A thesis submitted for the degree of Doctor of Philosophy in

The City University, London

by

HIKMAT SAID ALSALIM, B.Sc.(LONDON)

THE CITY UNIVERSITY LIBRARY,
ST. JOHN STREET, LONDON, E.C.1.

October 1972

ABSTRACT

This work investigates the effect of surface treatments of two titanium alloys on adhesive joint strength over a wide range of temperatures using two commercial adhesives.

The literature surveyed is divided into two. The first deals with the metallography and surface chemistry of titanium and its alloys; while the second deals with theories of adhesion and locus of failure in metal-metal bonding. This indicates that interfacial failure is unlikely in properly formulated bonds.

In the first part of the experimental work tensile testing in shear was used to examine the effect upon joint strength of various oxidation methods of the alloys. The results show that to obtain strong bonds, a rough and thin rutile surface is required. Then torsional shear testing was used to explore the effect on the joint strength of these oxidation methods over a wide range of temperatures. The results agree with those obtained by tensile testing.

Several techniques were employed to examine the fractured joints in order to study the locus of failure. The results indicate that some separation near the interface was taking place with the two adhesives. A mechanism for substrate failure was advanced and it suggests that a considerable element of mechanical adhesion is involved.

CONTENTS

		Page
	ABSTRACT	1
	PREFACE	5
	UNITS	6
1	INTRODUCTION	7
2	CRITICAL REVIEW OF EXISTING KNOWLEDGE	10
2.1	Structure and metallography of IMI-318 and IMI-205 alloys	11
2.1.1	IMI-318 alloy	11
2.1.2	IMI-205 alloy	15
2.2	Surface reactivity of titanium alloys	16
2.2.1	Air oxidation	16
2.3	Surface reactivity towards hydrogen	22
2.4	Surface reactivity towards nitrogen	23
2.5	Surface reactivity towards acids	24
2.5.1	Hydrofluoric acid	24
2.5.2	Hydrochloric acid	24
2.5.3	Sulphuric acid	25
2.5.4	Nitric acid	27
2.6	Oxidation in alkaline hydrogen peroxide solutions	28
2.7	Electrolytic oxidation	29
2.8	Metal-Metal adhesion	30
2.8.1	Surface preparation	30
2.8.2	Methods of adhesion testing	34
2.8.2.1	Tensileshear test	35
2.8.2.2	Torsional shear test	37
2.9	Adhesives for structural uses	41
2.9.1	Thermoplastic adhesives	41
2.9.2	Elastomeric adhesives	41
2.9.3	Thermosetting adhesives	42
2.9.4	Phenolic-vinyl adhesives	42
2.9.5	Phenolic-rubber adhesives	42
2.9.6	Epoxide adhesives	43
2.10	Theories of adhesion to high energy substrates and locus of failure	44
2.11	Poor adhesion	48
2.11.1	Interfacial forces	48

		Page
2.11.2	Critical surface tension	50
2.11.3	Importance of adequate wetting	54
2.12	Weak layers	56
2.13	Effect of temperature on bond strength	58
3	DESCRIPTION OF EXPERIMENTAL WORK	61
3.1	Optical microscopy	62
3.2	Transmission electron microscopy	62
3.3	Scanning electron microscopy	64
3.4	X-ray powder diffraction	64
3.5	Transmission electron diffraction	64
3.6	Reflection electron diffraction	65
4	SURFACE STUDIES OF TWO TITANIUM ALLOYS	66
4.1	Metallographic examination	67
4.1.1	IMI-318 alloy	67
4.1.2	IMI-205 alloy	68
4.2	Air oxidation of IMI-318 and IMI-205 alloys	71
4.3	Oxidation of IMI-318 alloy in alkaline hydrogen peroxide solutions	75
4.3.1	X-ray powder diffraction	78
4.3.2	Reflection electron diffraction	82
4.3.3	Colorimetric analysis of oxides formed in alkaline hydrogen peroxide and air oxidation	84
4.4	Etching IMI-318 with hydrochloric acid	87
4.5	Etching IMI-318 with sulphuric acid	92
4.6	Etching IMI-318 and IMI-205 alloys with hydrofluoric acid	95
4.7	Electrolytic oxidation of IMI-318 and IMI-205 alloys	102
4.8	Discussion	105
4.9	Etchants for titanium and its alloys	109
5	PRELIMINARY EXPERIMENTS	111
5.1	Bonding IMI-318 alloy and mild steel with Araldite	112
5.2	BSL-308 Adhesive	115
5.3	Hidux 1197C Adhesive	115

		Page
5.4	Bonding IMI-318 alloy with BSL-308 adhesive	116
5.4.1	Method of preparing the joints and testing	116
5.4.2	Effect of pressure and temperature during curing on bond strength	119
5.5	Effect of etching IMI-318 alloy on bond strength	125
5.6	Oxidation in alkaline hydrogen peroxide and bond strength	131
6	TORSIONAL SHEAR TESTING JOINTS	142
6.1	Description of apparatus used	143
6.2	Calculation of bond strength	145
6.3	Procedure for making the joints	147
6.4	Heating and cooling the joints	147
6.5	Effect of temperature on bond strength using IMI-205 alloy and BSL-308 adhesive	148
6.5.1	Discussion of results	157
6.6	Effect of temperature on bond strength using IMI-318 alloy and BSL-308 adhesive	165
6.6.1	Discussion of results	169
6.7	Bonding IMI-318 alloy with Hidux 1198C adhesive	171
6.8	Effect of etching IMI-318 alloy with aqueous hydrofluoric acid on bond strength	171
6.9	Effect of temperature on bond strength using IMI-318 and Hidux adhesive	182
6.9.1	Discussion of results	193
7	GENERAL CONCLUSION AND DISCUSSION	201
	POSSIBLE FUTURE WORK	209
	APPENDIX -1	210
	REFERENCES	213

PREFACE

The work presented in this thesis was carried out in the Department of Chemistry between November 1969 and September 1972, under the joint supervision of Professor W.C.Wake and Mr.K.W.Allen, to whom I am greatly indebted for their guidance and encouragement.

I am grateful to Mr. [redacted] for discussions on metallography; to [redacted] for his guidance in electron microscopy and Nomarski's interference contrast device and to [redacted] of Imperial Metal Industries (Kynoch) Limited, for his help on metallography.

In addition I would like to record my thanks to many of the other research students and to the staff in this Department, particularly [redacted] and [redacted] and also to the Secretariat, particularly [redacted] for typing this work.

Finally, I am indebted to the Ministry of Defence for supporting this research financially under Agreement No. AT/2090/017/Mat.,and to [redacted] and [redacted], for their help and advice.

[redacted]

26th OCTOBER 1972.

H. S. ALSALIM

UNITS EMPLOYED IN THIS THESIS

In the literature cited, the units reported here are those used by the authors while in the experimental section, S. I. Units were employed.

The following relationship will show their magnitude compared to MKS system.

1 kg/mm^2 = 9.81 MN/m^2

1 kg.cm torque = 0.0981 N.m torque.

Where more than one reading is presented, the standard error of the mean (S.E.M.) is indicated.

CHAPTER 1

INTRODUCTION

The use of structural adhesives has become more widespread in recent years particularly in the aircraft industry. With the advent of high speed aircraft, structural adhesives capable of withstanding high temperatures have become necessary, due to the high skin temperatures associated with speeds in excess of Mach-1. Further,aluminium has been considerably superseded by steel and titanium alloys.

This thesis is devoted to a study of titanium bonding and considers the effect of temperature and surface pretreatments on joint strength.

The napkin ring torsional testing method was used in which a simple stress is applied to the bond, avoiding the complex stress distribution in lap joints. Also special attention was given to failure patterns. The locus of failure was studied by several techniques including electron and optical microscopy particularly the Nomarski's interference contrast method.

A considerable number of techniques for surface inspection and identification has been used in this work. These include various diffraction techniques both of electrons and X-rays and metallography.

In an endeavour to keep the project at a technological level so that the results should be directly applicable to industry, model systems were avoided. The work was carried out with commercial materials; two titanium alloys and two adhesives known to give high strength with titanium alloys and to be in use at the present time.

The immediate technological aims of this work were:

1. To determine the nature of substrate when the surface has been pretreated.
2. To see if one treatment can be regarded as preferable to the others and if so, why?
3. To determine the temperature-strength profile of the adhesives and to see if the failure pattern altered radically over the temperature range.
4. To see if any general conclusions could be drawn about the surfaces and their morphology as a result of various pretreatments.

Most of these aims have been achieved and it is felt that this thesis does throw light on the mode of failure. Contrary to much that is published on the theory of adhesion it will be seen that there is considerable element of mechanical adhesion involved.

The alloys contained principally beta phase in the one and a mixture of alpha and beta phases in the other. It was found to be important to understand the metallography of the surfaces since the final surface roughness was controlled by the ratio of the phases present. This surface roughness was of considerable importance in determining the characteristics of the eventual adhesion bond.

Contrary to some previous reports, no evidence was found for the presence of hydrides or fluorides in the surface. Irrespective of the treatment applied, the surface layer was always of oxide.

CHAPTER 2

CRITICAL REVIEW OF EXISTING KNOWLEDGE

		Page
2.1	Structure and metallography of IMI-318 and IMI-205 alloys.	11
2.1.1	IMI-318 alloy.	11
2.1.2	IMI-205 alloy.	15
2.2	Surface reactivity of titanium alloys.	16
2.2.1	Air oxidation.	16
2.3	Surface reactivity towards hydrogen.	22
2.4	Surface reactivity towards nitrogen.	23
2.5	Surface reactivity towards acids.	24
2.5.1	Hydrofluoric acid.	24
2.5.2	Hydrochloric acid.	24
2.5.3	Sulphuric acid.	25
2.5.4	Nitric acid.	27
2.6	Oxidation in alkaline hydrogen peroxide solutions.	28
2.7	Electrolytic oxidation.	29
2.8	Metal-Metal adhesion.	30
2.8.1	Surface preparation.	30
2.8.2	Methods of adhesion testing.	34
2.8.2.1	Tensil shear test.	35
2.8.2.2	Torsional shear test.	37
2.9	Adhesives for structural uses.	41
2.9.1	Thermoplastic adhesives.	41
2.9.2	Elastomeric adhesives.	41
2.9.3	Thermosetting adhesives.	42
2.9.4	Phenolic-vinyl adhesives.	42
2.9.5	Phenolic-rubber adhesives.	42
2.9.6	Epoxide adhesives.	43
2.10	Theories of adhesion to high energy substrates and locus of failure.	44
2.11	Poor adhesion.	48
2.11.1	Interfacial forces	48
2.11.2	Critical surface tension.	50
2.11.3	Importance of adequate wetting.	54
2.12	Weak layers.	56
2.13	Effect of temperature on bond strength.	58

2.1 Structure and metallography of IMI-318 and IMI-205 alloys

(A glossary of metallographic terms is given as Appendix 1 on page 210 of this thesis).

2.1.1 IMI-Titanium 318 (commercially known as Ti-6Al-4V).

The chemical composition of IMI-318 as given by manufacturer[1] is:

Aluminium	5.5 - 6.75
Vanadium	3.5 - 4.5
Iron	0.30 max.
Hydrogen	0.0125 (0.015 in forgings)
Hence Titanium	91 88.4

IMI-318 is an (alpha + beta) alloy. The aluminium stabilises and strengthens the alpha phase, so raising the beta-transus temperature, as well as reducing the density of the alloy. The vanadium is a beta stabiliser which leads to a greater amount of the more ductile beta phase during hot working[1]. The (alpha + beta)/beta transus temperature is $995 \pm 15^{o}C$[2].

The phases present in this alloy depend on the temperature from which the alloy is quenched and the heat treatment given. Figures (2.1) show the system Ti-Al-V at various temperatures and as can be seen the volume of phases present varies enormously between them[3]. These diagrams are reproduced in detail because they were used in assessing the thermal history of the alloy supplied. The work reported later in this thesis shows a connection between the volume fraction of the phases present and surface roughness and these are determined by thermal history.

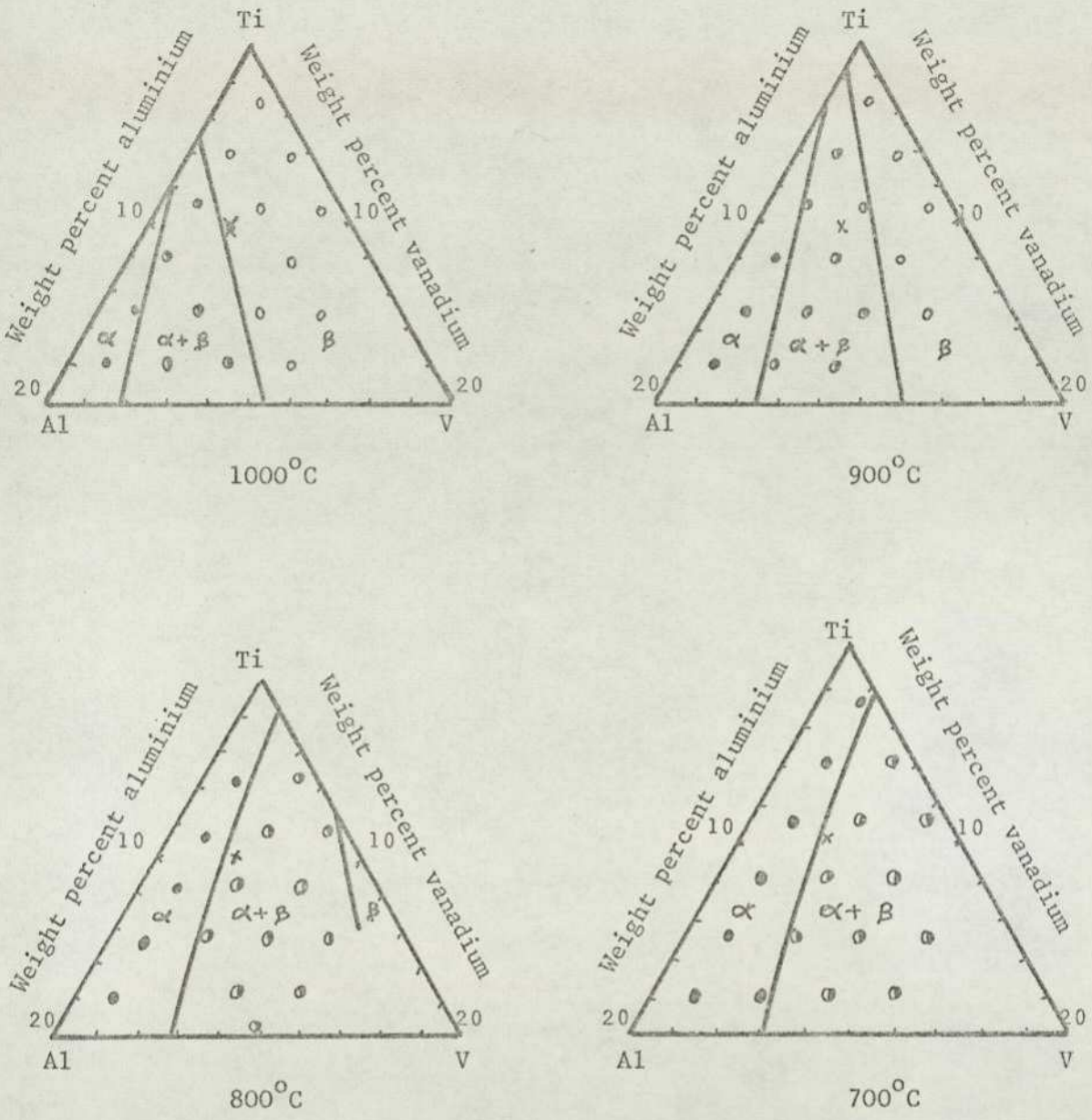


Figure 2.1 - Partial isothermal section of Ti-Al-V system at various temperatures. Closed and open circles each represent one phase (● = α, ○ = β); divided circle, two phase. (x) marks the composition (Ti -6Al-4V).

Williams and Blackbury[4] studied the phase transformations in Ti-6Al-4 alloy. Their findings are summarised in table 2-1. They identified the various phases using electron microscopy and selected area diffraction techniques.

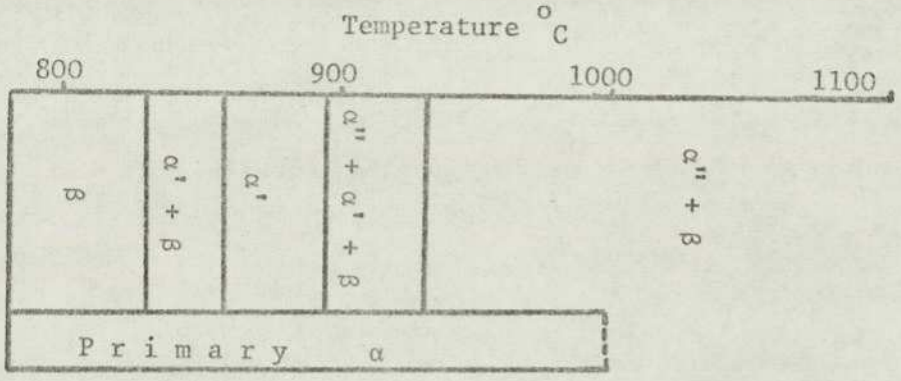


Table 2 - 1. Phases present after quenching from temperatures ranging from 800°C to 1100°C.

They have identified two martensites; α' which is an face centred cubic or face centred tetrahedron and α" which is hexagonal, and showed that α' can be strain-induced in the metastable β phase. On tempering, both α' and α" form a dispersion of β-phase in an α-phase matrix. However, they did not find any precipitation of the ordered phase α_2 (Ti_3Al). They obtained rather diffuse superlattice reflections, however, such reflections were only found in some alpha grains.

The existence of Ti_3Al phase after annealing in Ti-6Al-4V alloy has been confirmed by several workers[5][6]. This phase appears if the concentration of aluminium in the alpha phase exceeds 5.5%. The presence of this phase plays a significant part in hydride formation and consequent embrittlement of the alloy.

The distribution of Al and V through the alloy depends upon which of these phases are present[7]. Aluminium, an α-stabilizer, is very soluble in α-phase, up to 26% by weight but only slightly soluble

in β phase; whilst vanadium, a β-stabilizer, is completely soluble in β phase but only slightly soluble in α phase[8]. The changes in the composition of the phases with the temperature are important and have been studied by Fopiano et al[9]. They used electron microscopy and X-ray diffraction methods to identify the various phases present in the quenched specimens. The volume fraction of the phases was determined by lineal analysis. Table 2-2 is adapted from their results with β and α' phases both considered as β phase.

Solution temperature °C	Phases present after quenching	Volume % β and or α' phases	Weight % in α phase		Weight % in β, and α' phase	
			Al	V	Al	V
750	α,β	8	6	3	1	14
800	α,α'	14	7	3	1.5	11
850	α,α'	25	8	2.5	2	8
900	α,α'	32	9	2.5	2	6.5
950	α,α'	64	10	2	4	5
1000	α'	100	-	-	6	4

Table 2-2. The composition of phases present at various solution temperatures.

Their results show that the solubility of Al and V changes with temperature. This affects the reactivity of the phases and may contribute to preferential attack of one phase more than the other when subjected to a chemical treatment.

2.1.2 IMI-Titanium 205 alloy

The chemical composition of IMI-205 as given by the manufacturers is 15% (wt) molybdenum and 85% (wt) titanium. Although it is classified as a beta alloy[10], it could contain alpha phase if quenched or air cooled from 725°C[10] and if aged at about 450°C a third 'omega' phase may appear[11].

The system Ti-Mo[12] is a simple one. Additions of molybdenum to titanium stabilises the beta phase, which, at high temperature, exists over the whole range of composition from 0-100 atomic percent molybdenum, as seen in figure 2.2.

No discussion is available about the distribution of molybdenum in beta, alpha, and omega phases. Preliminary studies[13][14][15] of Ti-Mo alloys indicated that molybdenum was extensively soluble in beta-titanium. Hansen et al[16] give 0.44 at % as the maximum solubility of molybdenum in the alpha phase, but have not included in their paper the experimental evidence from which this value was obtained.

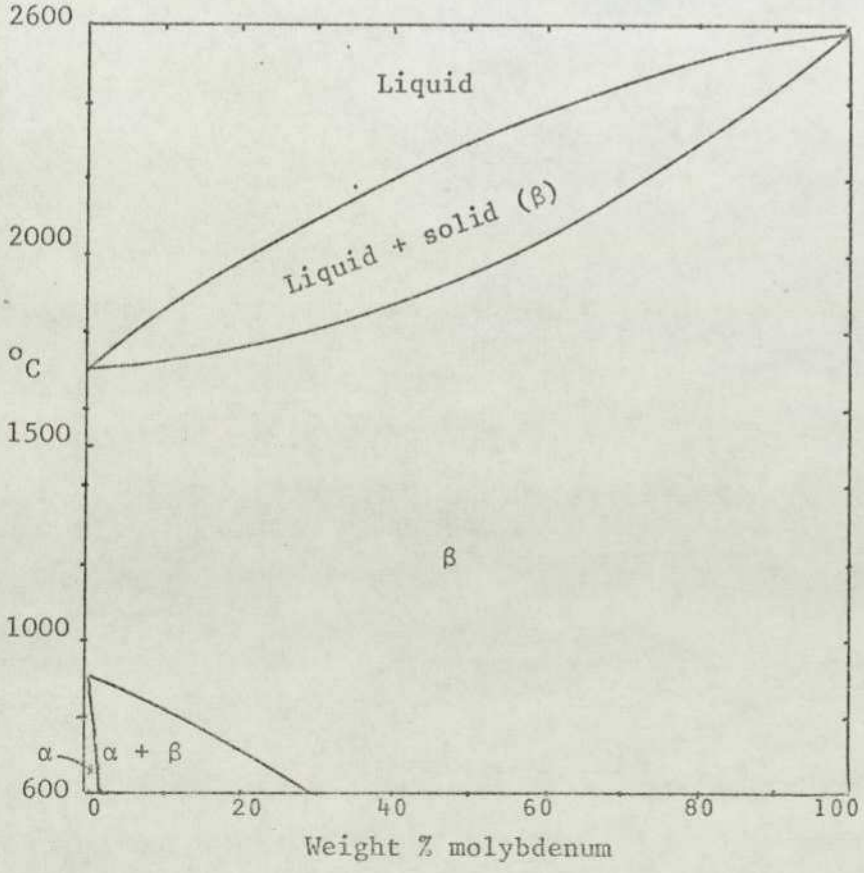


Figure 2.2
Titanium/Molybdenum phase diagram.

2.2 SURFACE REACTIVITY OF TITANIUM ALLOYS

While a great deal has been published on the surface reactivity of pure titanium, very little has appeared on the two alloys, IMI-318 and IMI-205 with which we are concerned.

Care must be exercised in extrapolating results both because of the effect of previous treatment and because of the unpredictable effect on a two component system of a third component.

2.2.1 Air oxidation

Titanium alone can form a series of oxides of the type Ti_nO_{2n-1} where $(4 \leq n \leq 19)$[17] and so far 16 oxides have been identified in addition to TiO_2.

Figure 2.3 shows the phase diagram of Ti-O[17a] It is rather complex and as can be seen various phases could exist at any one temperature. Titanium oxide scale therefore is rather complex and the complexity varies from one alloy to another and stresses which arise from density changes associated with varying composition.

It is expected that when an alloy is exposed to an oxiding atmosphere, the element with the greatest affinity for oxygen will be preferentially oxidised. The temperature dependence of the free energy of formation of oxides of aluminium and titanium are shown in figure 2.4[18]. If the oxides of the alloying element have a large difference in free energy of formation, a surface layer composed of only the more stable and least noble oxide will form.

From figure 2.4 one would expect Al_2O_3 to form at the surface at any temperature. However, selective oxidation of the more active component will take place only above a critical concentration of the component[19] and this critical concentration may be different for each

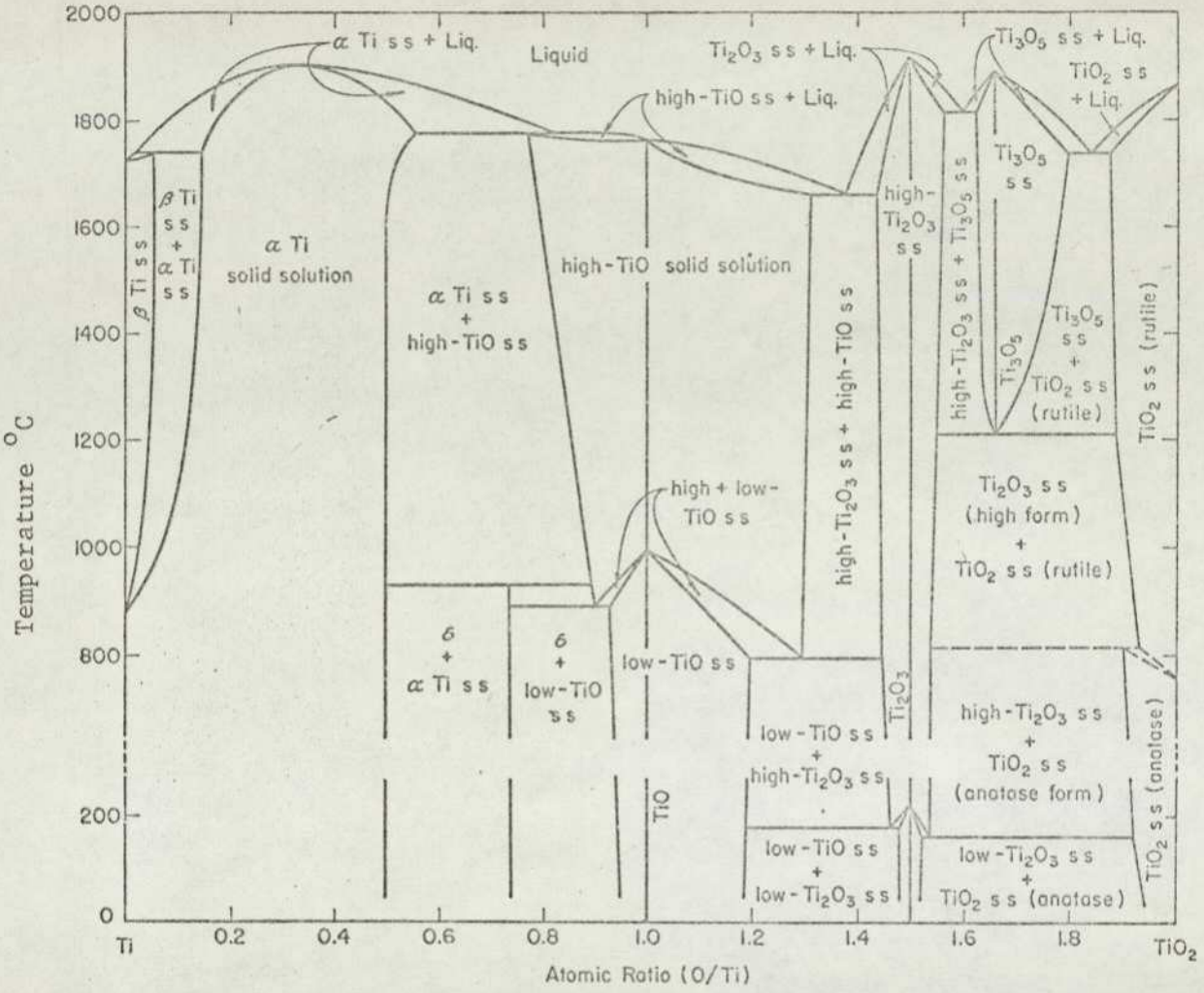


Figure 2.3 - Titanium - oxygen system.

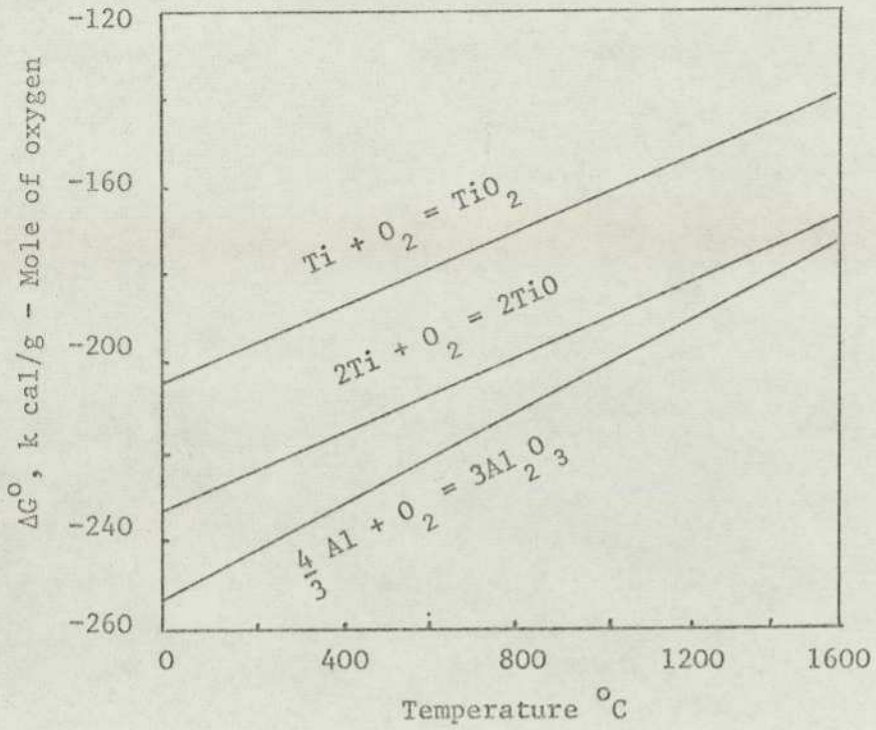


Figure 2.4 - Temperature dependence of ΔG^{o} of oxides of aluminium and titanium.

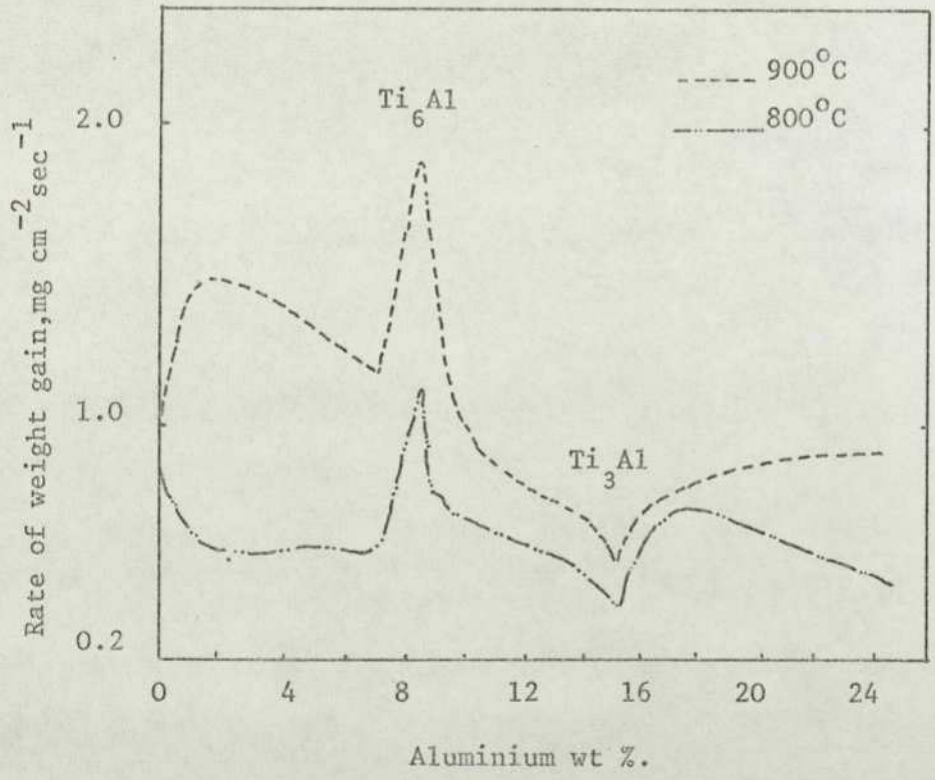


Figure 2.5 - Weight gain of titanium - aluminium alloys due to oxidation.

alloy, as it depends on the alloying elements. As the least noble constituent is oxidised, a depletion of this constituent in the underlying alloy occurs. The gradient of this depletion will be a function of both the oxidation rate and the rate of inter diffusion in the alloy. If the critical concentration of the next least noble of the remaining constituents is reached at the metal-oxide interface, then the oxide of this constituent will form and will be incorporated into the scale. The more noble constituent can also be incorporated into the scale despite a large difference in free energy of oxide formation. This occurs by diffusion of the metal into the oxide where it is subsequently oxidised.

Lainer et al[20] have investigated the oxidation of Ti-Al alloys, aluminium oxide was found on alloys with 2.85 and 5.05% only after oxidation at 1000°C or above, while for an alloy containing 11% Al it was found after oxidation under all conditions, in addition to TiO_2-rutile.

When oxidation was carried out in an atmosphere of steam-air, the scale consisted of rutile, and in the layers situated between the metal and the rutile, the following oxides were detected

TiO, Ti_3O_5, TiO_3 and Al_2O_3 at 200-800°C and γ-Al_2O_3 and α-Al_2O_3 at 900-1000°C. The most informative work on Ti-Al alloys was done by Glazova[21] the results of which are condensed into figure 2.5 Alloy compositions coinciding with the structure Ti_6Al and Ti_3Al show extreme oxidation behaviour at 800°C and 900°C. These compounds have been identified in the Ti-Al systems by Kornilov and Glazova in previous work; they also showed that the suboxides Ti_6O and Ti_3O can exist in the Ti-O system[22]. The oxidation behaviour of these suboxides follows the same trend as the Ti-Al compounds; i.e. an increase in oxidation rate was found at Ti_6O and a decrease at Ti_3O.

Anitov and Gorbunov considered the oxidation of titanium alloys containing 1.5, 5, and 10 wt% vanadium at 700-1000°C[23]. The 10% V alloy exhibited a catastrophic oxidation at all temperatures. This was attributed to the formation of a porous scale with subsequent cracking. Some of this cracking may be due to the large difference between the molecular volumes of V_2O_5 and TiO_2 (approximately 2.6 : 1).

Anitov and Gorbunov considered that the intensive oxidation of alloys with vanadium may be attributed to the formation of molten and volatile V_2O_5 in the oxide film. The oxidation does not become catastrophic unless the alloy contains 10% or more vanadium. Preferential oxidation of titanium effectively increases the concentration of vanadium in the alloy at the metal-oxide interface beyond the critical valve for oxidation leading to formation of V_2O_5 (m.p.690°C)[24] which then melts at the metal-oxide interface. If a crack opens both surface volatilization of the molten V_2O_5 can occur leading to a porous scale and subsequent further cracking and oxidation.

Anitov and Gorbunov investigated the oxidation in air at temperatures of 700-1000°C of Ti-Mo alloys containing 5 wt % Mo[23]. The molybdenum protects the titanium against oxidation at 700-900°C to some extent. However, at 1000°C "catastrophic" oxidation is observed. They attributed this behaviour to the action of fusible (m.p.795°C)[24] and volatile MoO_3 which forms in the TiO_2 oxide. If a liquid phase appears in the oxide film, the rate of diffusion of oxygen will rise considerably, and thus increasing the oxidation rate[25].

Stringer et al considered Ti-15% (wt) Mo alloy oxidised in temperature range 650-1000°C[26]. Behaviour was similar to that observed by Anitov and Gorbunov, with catastrophic oxidation beginning at about 800°C. MoO_3 was identified within the rutile scale. Considerable intergranular

oxidation was observed in the alloy and oxygen-rich alpha-titanium plates were found within the beta-titanium grains.

The stresses in the oxide scale arise from volume differences between rutile and the oxides of the alloying elements which, as has been discussed, may become incorporated in the scale. The molecular volumes of the relevant oxides are listed in the following table[27].

Compound	Molecular volume	Compound	Molecular volume
Mo	9.41	Al	9.99
$Mo(OH)_3$ or $Mo_2O_3.3H_2O$	-	Al_2O_3 α	25.68
$MoO(OH)_3$ or $Mo_2O_5.3H_2O$	-	Al_2O_3 γ	27.63
$MoO_3.2H_2O$	57.63	$Al_2O_3.H_2O$	39.81
MoO_2	19.77	$Al_2O_3.3H_2O$	64.47
Mo_2O_3	-	$Al_2O_3.3H_2O$	61.66
Mo_2O_5	-		
MoO_3	30.68		
Ti	10.60	V	8.55
TiO_2 brookite	19.16	VO (or V_2O_2)	11.63
TiO_2 anatase	20.81	VO_2 (or V_2O_4)	19.12
TiO_2 rutile	18.76	V_2O_5	54.18
TiO	12.96	V_2O_3	30.78
Ti_2O_3	31.26		

TABLE 2.3 Molecular volumes of molybdenum, titanium, aluminium and vanadium oxides.

The stresses arising from the oxides and the various possible titanium oxides have not been calculated but Vasilev et al[28] have calculated the stresses in oxidised Ti-4% Al annealed and hardened specimens, and have shown that the stresses at the surface of the diffusion layer are of the order of 10 kg/mm^2. Removal of the oxide film relieves the stresses in the diffusion layer. It will be appreciated that such stressed oxide layers are important when surfaces are bonded and could contribute towards substrate failure.

2.3 Surface reactivity towards hydrogen.

The effect of hydrogen on the mechanical properties of titanium and its alloys has received considerable attention because it causes embrittlement of the metal. Kotfila and Erbin[29] studied ($\alpha + \beta$) alloys and found that a marked ductile/brittle transition occurs at low temperatures when hydrogen is absorbed. The embrittlement is now known to be due to precipitation of titanium hydride within the alpha phase while hydrogen remains in solution in the beta phase[30]. The hydride phase is not seen in ($\alpha + \beta$) alloys unless the hydrogen content is high[31].

Recently it was discovered that the ordered phase α_2 (Ti_3Al) takes a part in this[32]. Hydrogen first enters octahedral sites of Ti_3Al causing expansion, and which disappears later as the hydrogen shifts to tetrahedral sites in Ti Al and later to the body of the alloy.

Gegel and Fujishiro[33] have studied the mechanism of embrittlement of Ti-6Al-4V alloy hydrogen and found it to be connected with the precipitation of hydride phases associated with the present of Ti_3Al. Hydrogen is evolved when titanium or its alloys is etched by reducing acids, a fact which should be remembered, Bomberger et al[34] found that addition of nitric acid to these acids reduces considerably the amount of hydrogen picked up. It is for this reason most pickling solutions contain either nitric acid or another oxidising agent.

2.4 Surface reactivity towards nitrogen.

The effect of nitrogen on titanium and its alloys has not received much attention, possibly because of the slow reaction between titanium and nitrogen. However, it is well known that nitrogen stabilises the alpha phase[35]. Titanium nitride TiN is a stable compound over a wide range of temperatures and can be obtained on the surface of titanium (or its alloys) by heating at 500°C in an atmosphere of nitrogen. The TiN layer thus obtained is very coherent.

2.5 Surface reactivity towards acids

2.5.1 Hydrofluoric acid

The oxide(s) on titanium metal is not resistant to hydrofluoric acid, and a strong chemical attack takes place on immersion in even 1% aqueous solution of the acid. It is for this reason that hydrofluoric acid is one of the princial ingredients of many etching and pickling solutions for titanium and its alloys. The initial reaction is believed to be [36][37]:

$$2Ti + 6HF = 2TiF_3 + 3H_2$$

TiF_3 is not stable in aqueous media containing dissolved oxygen and Ti^{III} is oxidised to Ti^{IV} and held in solutions as a complex ion(s). In hydrofluoric acid solutions the predominant ion is $[TiF_6]^{2-}$ [38].

The presence of oxidising agents such as nitric acid in hydrofluoric acid solutions appears to inhibit the attack. Kieffer has attributed this to formation of oxide(s) on the metal surface which diminishes reactivity of hydrofluoric acid but nevertheless solutions containing hydrofluoric acid are extremely corrosive[39].

2.5.2 Hydrochloric acid

Titanium or its alloys are strongly attacked by hydrochloric acid solutions.

Sorokin and Babich[40] found that for an increase in temperature from 20 to 80°C the corrosion rate increased at least a hundredfold for all concentrations of the acid; while for an increase in concentration from 1.5 to 37.8% hydrochloric acid the corrosion rate increased by about two-hundredfold at any temperature. The results obtained by

Neroslavskaya and Artemev[41] are in agreement with Sorokin's and Babich's.

The presence of nitric acid in hydrochloric acid reduces the corrosion rate considerably, Sorokin and Babich[40] found that the addition of 0.003M nitric acid to 37.8%(wt) hydrochloric acid reduces the rate from 11.5 to 5.0 gm/m^2/hour at 20°C; and when 12M nitric acid was added to the same solution of hydrochloric acid at 80°C the rate decreased from 245.2 to 0.115 gm/M^2/hour. They attributed this to passivation of the metal in the presence of nitric acid but they did not provide any evidence of the nature of coating formed on the metal.

The initial mechanism of dissolution of the metal is believed to be [38][40][41]:

$$2Ti + 6HCl = 3H_2 + 2TiCl_3$$

Ti^{3+} is easily oxidised by dissolved oxygen to Ti^{4+}.

Titanium remains in solution as hydrated ions of chlorocomplexes of the type:

$$\left[TiCl_5(H_2O)\right]^{2-} \text{ and } \left[TiCl(H_2O)_5\right]^{3+}$$ [38]

Koizuni and Nakayama[42] have studied the grey coating formed on titanium after etching in boiling 0.2% (wt) hydrochloric acid, using electron diffraction techniques. They found a layer structure consisting of TiO_2-rutile deposited over a film consisting mainly of brookite. However, Chiganova and Batashev[43] obtained a hydride on specimens of titanium etched in 20% (wt) hydrochloric acid. The hydride thickness increased to a maximum of 0.151 microns at 70°C and then decreased to a limiting value of 0.125 microns.

2.5.3 Sulphuric acid

Golden et al[44] investigated the rate of corrosion of titanium in sulphuric acid. Their results are presented graphically in figure 2.6

The corrosion reached a first maximum at a concentration of 40%, fell to a plateau around 60%, and rose to a larger maximum about 80%. No satisfactory explanation was advanced except that more soluble complex ions are formed in the region of the two maxima.

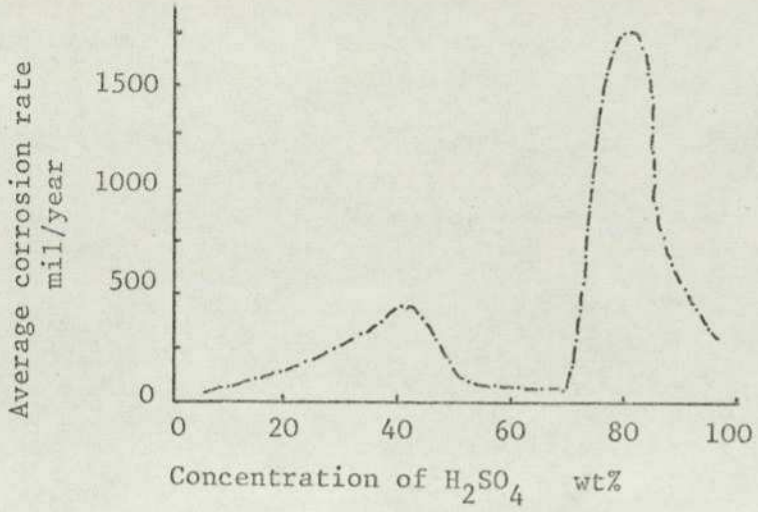


Figure 2.6 - Corrosion rate of CP-Ti at 35°C in various concentrations of sulphuric acid.

The process of dissolution of the metal by the acid can be represented according to Chiganova and Batashev [43] by:

$$2Ti + 3H_2SO_4 = Ti_2(SO_4)_3 + 3H_2$$

They also claim that when the metal is etched in boiling 60%(wt) sulphuric acid only a hydride is formed. The thickness of the hydride layer at 70°C increases to a maximum of 0.124 microns and then decreases to a limiting value of 0.075 microns.

Investigation by Koizumi and Nakayama [42] have shown that in boiling 0.1% (wt) sulphuric acid thornshaped crystals are deposited on a continuous film consisting of mainly anatase.

Titanium is held in sulphuric acid solutions largely as $\left[Ti(OH)_3HSO_4\right]$ and $\left[Ti(OH)_2HSO_4\right]^+$ [38][45] and on increasing the pH polymerisation and further hydrolysis eventually gives colloidal or precipitated hydrated TiO_2.

2.5.4 Nitric acid

Red fuming nitric acid attacks titanium violently leading to an explosion. The explosion is usually preceded by formation of a pyrophoric material[46]. More dilute solutions of the acid passivate the metal. Weiman[47] suggested that when titanium dissolves in nitric acid solutions it is always present as Ti^{4+} and that if the concentration of the Ti^{4+} ion exceeds a certain value $\left[\text{"}Ti^{4+}\text{ critical"}\right]$ then a mixture of hydrates, some of which are insoluble, is formed. If this value is not reached then more metal is dissolved until this equilibrium value is reached. He attributed passivation of titanium to precipitation on the surface of the insoluble hydrate.

Cotton and Wilkinson[38] mention the formation of the insoluble hydrates. However, Koizumi and Nakayama[48] have examined the surfaces of titanium immersed in boiling concentrated nitric acid for 4 to 24 hours by reflection diffraction, prior to stripping the film. The reflection patterns they obtained were due to anatase only while transmission diffraction indicated the presence of rutile as well. They suggested that a double layer structure is formed and that anatase formed the outer layer while rutile formed the inner layer, and that the rutile layer would grow with immersing time. This is based on results obtained from specimens immersed for short periods; they were covered with anatase only. Ogawa and Watanabe[49] obtained similar results.

2.6 Hydrogen peroxide - alkaline solutions

Alkaline solutions of hydrogen peroxide have the ability to act simultaneously as oxidising and corroding agents - in the case of titanium, soluble pertitanates are formed in concentrated solutions. Sodium hydroxide is generally used with hydrogen peroxide and depending on the concentrations titanium either becomes passive and is coated by a protective, glossy and translucent film; or is coated by an oxide whose colour varies from yellow to black; or is quickly corroded. Bianchi et al[50] have studied this and their results are summarised in figure 2.7 .

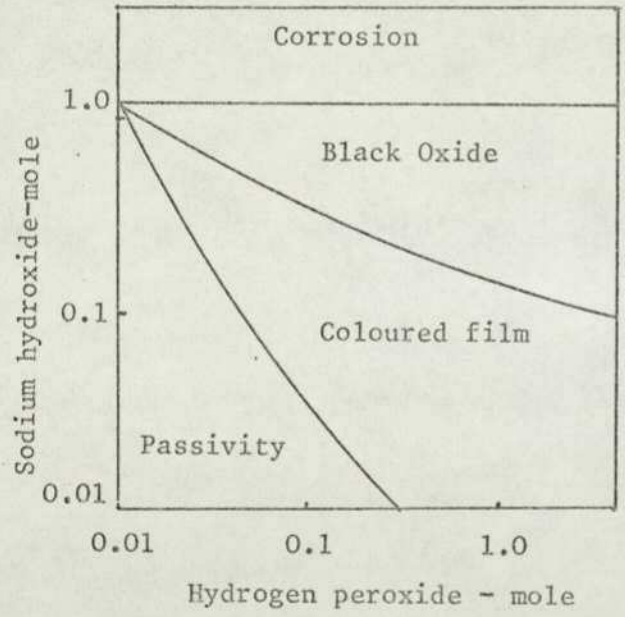


Figure 2.7 - Conditions of corrosion, passivity and black oxide formation for titanium in NaOH + H_2O_2 solutions.

The colour of the oxide is a sign of a nonstoichiometric structure. This can be formed under a variety of conditions of which alkaline hydrogen peroxide is only one specific example[50][51]. According to Bianchi et al the rate of decomposition of the oxidising agent determines the colour of the oxide layer. Oxide layers of thickness up to 0.1 mm

have been been obtained on titanium in alkaline hydrogen peroxide, some of which were incoherent and offered little protection against further oxidation. They did not identify the oxides formed.

2.7 Electrolytic oxidation

In the majority of aqueous solutions except those containing complexing agents such as fluoride ions, titanium can be oxidised anodically. Titanium forms "a barrier film" which is non-porous (generally) and has a low ionic and electronic conductivity, therefore, anodic polarisation leads to passivation. Because oxygen is not evolved in the process, the oxide thickness can be increased by increasing the voltage applied. Moreover, over a wide range the TiO_2 formed is stable and pitting will only take place at high voltages, the exact nature of which is a function of the electrolyte used[52].

Oxide layers formed anodically on titanium range in colour from white to straw colour, gold, green, various shades of blue to purple and finally black. These can be formed by varying the applied voltage. The colouration is believed to be due to interference and the various colours are due to various thicknesses of the oxide layer[53] while Bianchi et al[50] believe that the "coloration" is due to nonstoichiometric oxides and have postulated a mechanism for its formation:

$$Ti = Ti^{+} + e$$

$$4Ti^{+} = Ti^{4+} + 3Ti$$

They claim that "metallic atoms" remain dispersed within the oxide layer giving excess metal. The oxides formed by electrolytic oxidation, are believed to be TiO_2 - rutile[52], while Yamaguchi[53] found brookite in the stripped films, but rutile and anatase as well as hydrated oxides were detected under various conditions by Rivolta[54].

The changes in the topographical features of anodically oxidised specimens seems to have received no attention, but preliminary studies by Young[52] indicate that such oxides merely replicate the original surface.

2.8 METAL-METAL ADHESION

2.8.1 Surface preparation

Since adhesion is a surface phenomenon the methods used to prepare the surfaces of the adherends are vital to the success of a bond. Titanium and titanium alloys are frequently contaminated with layers, which may include rolling lubricant, mill scale,oxidation products or incidental contaminants. This layer is usually so thick that the surface has the properties of the layer material and consequently providing the layer is not dissolved by or displaced in the adhesive, the strength of bonded joints made between adherends having such surface layer will be limited by the forces between the adhesive and the layer, or the layer and the metal, or by the cohesive strength of the layer material, whichever is the weakest. It is therefore vital that such a contaminated layer should be removed prior to application of the adhesive either by mechanical, chemical or electrolytical means. Mechanical means leads to a "clean" surface but it is invariably covered with oxide film with varying amouts of water, either in the form of adsorbed molecules or as hydrated oxides.

The change in surface area by mechanical means is limited but the maximum roughness - hence surface area - is produced by blasting the machined surface with a fine grit. Blasting a surface before bonding could, in addition to cleaning, modify the surface topography whereby sharp-edged, deep pits or those with recessed angles are replaced by shallow, open structures, which are more likely to be interconnecting or, in any case, more easily filled with adhesive[55]. However, the danger

of trapping gases in a rough surface is a problem by itself and has been pointed out by de Bruyne[56]. Ultimately this leads to a weakness and could affect the mode of failure. The effect of surface roughness on bond strength was investigated by Jennings[57]. Using aluminium and stainless steel with a variety of adhesives, his results indicate sand blasted adherends lead to a significant increase in bond strength.

Chemical means have the ability of leaving a clean surface, increasing the total surface area as well as providing a better surface for bonding than the machined metal surface. Electrolytic means require polishing followed by anodisation. Usually electrolytic polishing is carried out in an electrolyte containing perchloric acid in glacial acetic acid. Other methods have been used but the choice of electrolyte as well as procedure depend on the alloy[58][59].

As far as titanium and its alloys are concerned, chemical means are believed to be the most convenient and easy to handle even on an industrial scale.

The choice of pretreatments for surface preparation is dictated by the ability of the reagent(s) to attack the oxide film which is present on the surface of titanium. The various pretreatments available invariably contain reagents able both to dissolve and form oxides, at the surface. Surface preparation often consists of hydrofluoric acid or its salts together with other mineral acids, sometimes with an oxidising agent to reduce the pick up of hydrogen evolving during the process. Basically, industrial usage has concentrated on three main recipes

Recipe I[60] (5-10 minutes at room temperature)

Sodium fluoride	10 parts/wt.
Chromium trioxide	5 " / "
Sulphuric acid	50 " / "
Water	250 " / "

Recipe II[60] (10-15 minutes at room temperature)

Hydrofluoric acid	5 Parts/Wt.
Conc.nitric acid	30 " / "
Water	100 " / "

Recipe III[61] consists of two parts, A. and B, commonly known as phosphate-fluoride etch.

III-A (30 seconds at room temperature)

Nitric acid (70%)	15% by volume
Hydrofluoric acid(50%)	3% " "
Water	82% " "

III-B (etching for 2-3 minutes at room temperature)

Trisodium phosphate	5.0% by weight
Sodium fluoride	0.9% " "
Hydrofluoric acid	1.6% " "

All three recipes leave a grey coating, the nature of which has received little attention. Capriolo and Turris[62] believe a fluoride coating exists on titanium and its alloys when pretreated as in recipe-III but they do not mention how they established this improbable result.

The surface roughness obtained with each pretreatment depends mainly on the concentration of hydrofluoric acid and the temperature. Very little is known about the degree of roughness obtained in each case. Bijlmer[63] measured surface roughness on titanium treated in hydrofluoric acid to which various amounts of nitric acid had been added and his findings are shown graphically in figure 2.8 .

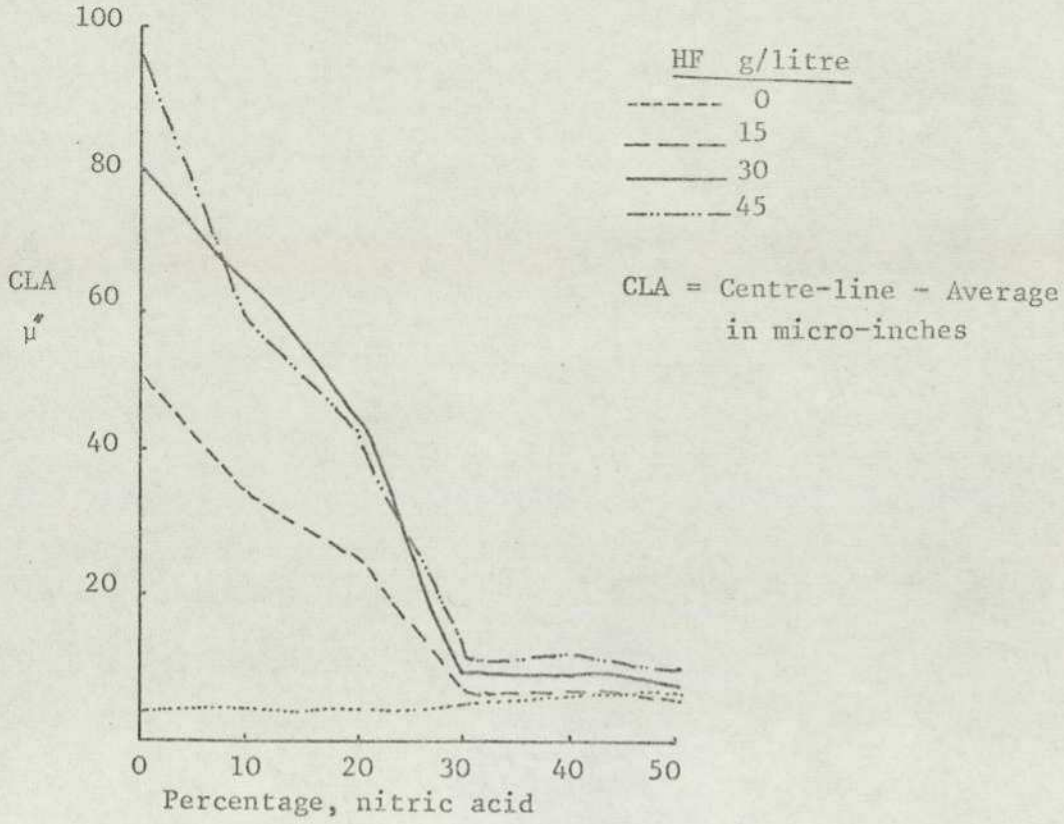


Figure 2.8 - Surface roughness after 10 minutes pickling in relation to nitric acid content.

His results indicate that roughness decreases rapidly as the concentration of nitric acid increases and above 30% (wt) nitric acid, only a slight increase in roughness was observed.

As previously mentioned, bond strength is a function of "surface preparation" and can be improved by a variety of methods such as degreasing, polishing, grinding, and pickling[64] ... etc. e.g.Breshears[65] has obtained with electrolytically oxidised titanium laps, bonds which were 50% stronger than those attainable by phosphate-fluoride pretreatment. It is generally recognised that chemical oxidation of titanium adherends can lead to strong bonds[65] but this author does not give the methods employed nor the type of oxide formed. Alkaline hydrogen peroxide solutions are powerful oxidising media for titanium and give a variety of coloured oxide coatings depending on the concentration of both reagents[50] but unfortunately it seems no work on bonding such oxidised adherends has previously been published.

2.8.2 Methods of adhesion test

The word "adhesion" is used in several senses, but only in the sense of that interaction which exists between two materials in contact does it have any real meaning. The most convenient and straight forward way to measure adhesion is to separate the two materials and measure the force or energy which is required,but it appears that separation does not occur exactly at the interface, so that the quantity measured in a so-called "adhesion test" is not necessarily the true adhesion. No mechanical test can be directly related to thermodynamic adhesion but such tests do serve as an empirical comparison of the effectiveness of different adhesives or other parameters such as surface pretreatments.

Most tests can be classified as tensile, shear, or peel tests[66]. In tensile testing the adherends are separated by a force normal to the interface, and if failure is initiated at a flaw in the interface, subsequent separation will occur either by cleavage or peel mechanism. Shear tests are of two main types; the napkin ring tests in which the joint is broken in pure shear, and lap-shear tests in which flat strips are bonded together with a small overlap and then tested in tension. In this test a peel or cleavage force component is superimposed on the shear force. In a peel test a strip of metal, or other flexible adherend is bonded with adhesive to either a rigid substrate, or another flexible strip, and bond strength is measured by peeling them apart. The force required will depend, among other things, on the rate of peeling, and the angle at which the force is applied[67].

In the present work two methods were employed; tensile shear and torsional shear tests.

2.8.2.1 Tensile shear test using single lap joints

Tensile shear strength is most widely adopted as a measure of the ultimate shear strength of an adhesive bond backed in tension. In this type of loading the forces act in the plane of the adhesive bond. Shear strength is expressed by the ratio of failure load to bond area:

$T = F/A$ where F = failure load

A = bonded area

T = shear strength.

The mechanical properties of bonded joints are the highest at loads in shear. For this reason simple lap joints are the most commonly used adhesive joints and have been most studied so far.

The mean tensile shear strength of a lap joint is affected above by all the factors, which do not depend on the adhesive: adherend material, adherend thickness, and adhesive bond thickness[68]. The distribution of forces in this type of joints is complex[68][69][70]. The distribution of stress over the bonded area is affected not only by stretching but also by bending of adherends and adhesive which is bound to occur during testing of such specimens, specially if the adherends are thin. In the absence of any bending, the shear stress in the adhesive layer is a maximum at each end of the overlap[68][69][70]. Bond failure starts at this point when the shear stress exceeds the cohesive strength of the adhesive. Detailed work on reduction of stress concentration at the ends of bonded areas was carried out by de Bruyne[71] and Greenwood[68]. They found that the stress concentration can be reduced by:

i. Reducing the length of overlap

ii. Reducing the shear modules of adhesive

iii. Increasing the Young's modules of the adherend

iv. Increasing the thickness of the adherend

v. Increasing the thickness of adhesive bond.

The effect of (ii) (iii) and (iv) are obvious but (i) and (or) (v) are debatable. A reduction in the length of the overlap leads to an increase in the mean shear stress and this leads to a reduction in the stress concentration. But one should not forget the fact that the length of the overlap is dictated by the practical application of such bonds on one hand, and a point is reached when the mean shear stress in the joint is equal to the failing shear stress on the other hand. De Bruyne[71] has shown, using adherends $\frac{1}{4}$ inch thick that bond strength was independent of the length of overlap down to a length of about 2 inches, beyond this the bond strength was proportional to the length of overlap.

The role played by adhesive bond thickness is not very clear, but generally an increase in bond thickness will lead to a decrease in shear stress of the adhesive layer and although this leads to a reduction in the stress concentration it could lead to a reduction in the strength of the joint. If the strain rate is kept constant then, as Bryant[72] demonstrated, an increase in bond thickness should have no effect on joint strength.

The main difficulty one encounters with lap joints is to find conditions under which reproducible bond strength values can be obtained. The results in the literature obtained with single lap joints generally show large scatter which could be attributed to a variety of reasons such as a non-uniform stress distribution, poor alignment and the amount of bending during testing.

With high strength adhesives another factor may contribute towards scatter is the presence of the adhesive on the boundaries of the bonded areas (fillet). This has received but little attention despite the fact that some surplus adhesive is usually present. Again this could modify the distribution of stresses within the joint and may contribute to initiation of bond failure.

It was considerations such as as these which lead to the adoption of torsional shear testing method rather than lap shear.

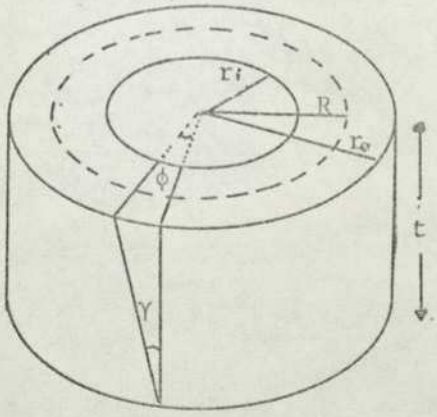
2.8.2.2 Torsional shear test using napkin rings

The torsional shear test was first suggested by de Bruyne[73] in 1951. It uses circular coaxial thin walled cylinders commonly known as 'napkin rings' of thickness $(r_o - r_i)$ and a mean radius R are joined end to end and subjected to a torque T. Adhesion results obtained by this method first appeared in 1956 by Gillespie and Rideal[74].

The theory of torsional shear test is simple, the applied torque T is given by :

$$T = 2\pi \int_{r_i}^{r_o} Sr^2 \, dr \qquad \ldots\ldots\ldots 1$$

where r_i and r_o are inner and outer radii of ring respectively. For elastic case we have , S is the shear stress. If the shear modulus of adhesive is G, then from the following diagram



$S = G\gamma$ where γ = shear strain $= \frac{\phi r}{t}$, ϕ = angle of strain and t is the thickness of adhesive layer .

Therefor , $S = \frac{G\phi r}{t}$ 2

Substituting in equation 1 , we get :

$$T = \frac{2G\pi\phi}{t} \int_{r_i}^{r_o} r^3\, dr = \frac{G\pi\phi}{2t}\left(r_o^4 - r_i^4\right) \qquad \text{..... 3}$$

It will be noted in passing that for a solid bar $T = \frac{G\pi\phi r_o^4}{2t}$. This result is required later in the discussion for preliminary experiments.

Returning to the napkin ring, let S_f and T_f be shear stress and torque at failure , then from equation 2 , the maximum shear stress S_o ,is at r_o . When $S_o = S_f$ we have catastrophic failure. This is because fracture at the outer boundary causes a higher average stress for the remaining intact bonded area. This in turn means that the new outer boundary is instantaneously supporting S_f , thus :

$$T = \frac{S_f\pi\left(r_o^4 - r_i^4\right)}{2r_o}$$

i.e $$S_f = \frac{2r_o T_f}{\pi(r_o^4 - r_i^4)} \qquad \text{..... 4.}$$

For plastic case S in equation 1 is assumed to be uniform over the bonded area , therefore

$$T = \frac{2S\pi(r_o^3 - r_i^3)}{3} \qquad \text{i.e} \quad S_f = \frac{3T_f}{2\pi(r_o^3 - r_i^3)} \qquad \text{..... 5}$$

(Again for asolid bar $S_f = \frac{3T_f}{2\pi r_o^3}$)

If $r_o^2 \simeq r_i r_o \simeq r_i^2$ then equation 5 can be simplified further to :

$$S_f = \frac{T_f}{2\pi R^2(r_o - r_i)} \qquad \text{..... 6}$$

Where $R = \frac{r_o + r_i}{2}$

The thickness of the adhesive bond does not enter into equations 5 and 6, and one should expect S_f, therefore, to be unaffected by variation in bond thickness, but results obtained by Kraus and Manson, as quoted by Wake[75], Foulkes et al[76] and others, indicate that the thinner the adhesive bond, the stronger the joint. The gradual decrease in bond strength observed in their results with increase in adhesive bond thickness could be due to residual stress set up at the interfaces when the glue contracts on setting.

De Bruyne assumed that the stress over the whole annular width is uniform but in actual fact the stress varies radially and is a maximum at the outer perimeter, therefore, failure is expected to occur when the stress at the outer perimeter reaches the failing stress of the adhesive. The effect becomes pronounced when the width of the annulus is large compared with the radius. Bryant and Dukes[77], using a rubbery adhesive, found that equation 4 held for five different annular sizes by obtaining a linear relationship on a plot of T_f against

$$\frac{\pi(r_o^4 - r_i^4)}{2r_o}$$

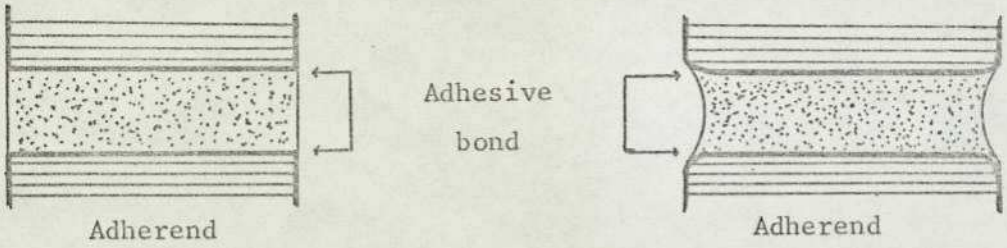
Foulkes et al[76] used equation 5 to relate T_f and annular dimensions of 14 different sized annuli bonded with Redux 775, a rigid adhesive. They have suggested that the bulk adhesive behaves as an elastic solid up to a given stress above which it behaves plastically.

The yield stress will first be reached in the adhesive at the perimeter of the annulus and an elastic-plastic boundary will then pass through the annulus to the inner radius. After this the stress will be constant over the whole annulus and related to torque by 5.

They plotted T_f against $\frac{2\pi}{3}(r_o^3 - r_i^3)$ and obtained a good linear relationship but a large scatter was observed in their plot especially with larger diameter napkin rings which they attributed to variation in the speed of test.

The main drawbacks of this test are :

1. A uniform stress distribution is assumed over the whole bonded area. This is true only if $(r_o - r_i)$ is very small. Therefore thin-walled napkin rings are preferred in this test.
2. It is not easy to maintain the napkin rings concentric during bond formation.
3. The relationship between this test and other tests is not yet clear.
4. A curved edge as illustrated below is always produced and special apparatus is required for polishing the test pieces. Equations



Assumed conditions Practical conditions

4,5 and 6 do not allow for this and assume parallel adherends always.

Despite these drawbacks , the torsional shear test method is valuable because only torsional stress is involved; i.e. all shear even if not as uniform as the equations suggest. There are no cleavage, tensile or peel components.

2.9 ADHESIVES FOR STRUCTURAL USES[78-81]

Adhesives in general are discussed in many places and structural adhesives have received widespread discussion. For the purposes of this introductory survey, references (78-81) were those principally used.

Adhesives of many types are used for assembling load-carrying components and structures in various industrial and technological aspects such as electrical, automobile, aircraft and aerospace industries.

The term 'structural adhesive' is used to refer to adhesives capable of forming bonds which can sustain indefinitely loads involved in engineering structures. They are all synthetic organic polymers. Other adhesives may be used when the load sustained is smaller in magnitude. These are mainly thermoplastic and elastomeric.

2.9.1 Thermoplastic adhesives

These are based on thermoplastic resins. They can be softened by heat and hardened by cooling without undergoing chemical change. This group includes for example, vinyl and vinyl-modified products, polyacrylics, polyamides, and polyethylenes. Thermosetting resins are sometimes added to this group of adhesive to improve properties.

2.9.2 Elastomeric adhesives

These are based on natural or synthetic rubbers such as styrene-butadiene, nitrile, polychloroprene, ethylene, polysulphide and polysiloxanes. As formulated they generally include not only elastomers but also solvents, fillers, and additives to impart some desirable characteristics such as high flexibility. When used for structural purposes a thermoplastic or thermosetting resins is added to them, e.g. nitrile-phenolic adhesives.

2.9.3 Thermosetting adhesives

These are based on thermosetting resins which change into infusible and insoluble products as the result of chemical reaction, i.e.curing. Curing is a polymerisation process brought about by "hardner" and which may require heat. These types of adhesives do not soften significantly on heating to temperatures below their decomposition temperature. Thermosetting resins used in adhesives include among others phenolic, urea, melamine, epoxide, unsaturated polyester, polyurethane and polyimide. Thermosetting adhesives find their widest use in serving as the basis of structural adhesives, modified with other types of resins, because they produce strong bonds with high strength and low creep.

At present, there are two main classes of adhesives that outstrip by far all others that are employed in metal-to-metal bonding: these are the modified phenolic and epoxide systems.

2.9.4 Phenolic-vinyl adhesives

The most important formulations contain a phenolic resin combined with polyvinyl formal or polyvinyl butyral.They provide good shear and peel strengths at room temperatures, but have limited resistance to higher temperatures. These adhesives give off vapours during curing either from solvents or from products of the polymerisation process, therefore, should be cured with pressure the magnitude of which depend on the type of adhesive used.

2.9.5 Phenolic-rubber adhesives

These have good flexibility and vibration absorption. Neoprene or nitrile rubber are used here as the elastomeric component, the latter is preferred because of their increased resistance to chemicals, oils, fuels as well as of their higher service temperature.

2.9.6 Epoxide adhesives

These are usually based on the reaction of bis phenol-A with epichlorhydrin and the resultant linear polymer is crosslinked by reaction of the terminal epoxy group with amine or anhydride. They provide excellent strength and remarkable versatility in meeting technical requirements. These adhesives do not contain solvents and generally contain a filler such as aluminium powder, aluminium oxide, talc or graphite to improve presumably their thermal conductivity. Elastomeric or thermoplastic resins are added sometimes to improve peel strength and impact resistance. These adhesives resist heat to a substantial degree and are normally unaffected by moisture or chemicals.

Epoxide resins cure without releasing by-products in vapour or liquid form, therefore, shringkage is negligible and requires little pressure. The curing agent is either an amine such as diethylene triamine, diethylamino-propylamine, polyamide,m-phenylenediamine or dicyandiamide, or an acid anhydride.

2.10 THEORIES OF ADHESION TO HIGH ENERGY SUBSTRATES AND LOCUS OF FAILURE

Adhesion is the attraction force between the molecules of two phases across the boundary separation between them. These are not special "adhesion" forces but the normal interactions between atoms and molecules, which may be of various types depending on the chemical constitution of the materials. They can be divided into two broad classifications, primary and secondary bonds. The primary bonds are those which bind atoms together and may have high energies (10-100 kcal/mole). They are ionic, covalent, and metallic bonds. The secondary, or Van der Waal's forces always include the London dispersion forces and for polar molecules, dipole interaction between two permanent dipoles (these include hydrogen bonds), ion-dipole interactions, or image forces, where a dipole generates an image charge at the surface of forces 2 $\sim$ 4 k cal/mole, but they lead to significant adhesion, and act over longer distances than the primary bonds. The effect of separation or mismatching of the atoms at the interface is thus not so important as with primary forces.

Although adhesion could not occur without these forces, there is a body of opinion which claims that their study is not relevant to the problems. In particular, it has been argued by Bikerman[82] that once a proper adhesive bond has been produced, the interface will nearly always be stronger than one of the two phases, and that in any case the statistical probability of failure propagating along the line of the interface is extremely small. His case rests on two main points. If Van der Waal's forces only are considered the interaction between the unlike molecules will be the geometric mean of the interactions between like molecules, i.e.

$$F_{12}^2 = F_1 F_2$$

where F_{12} is the force across the interface between molecules of types 1 and 2, and F_1 and F_2 are the intermolecular forces in phases 1 and 2. Because either F_1 or F_2 will be the larger of the two forces, one of them will be weaker than their geometric mean, and failure will occur in this phase rather than at the interface.

Sharpe and Schonhorn[83] have pointed out that if complete wetting of the surface occurs, then the work done in separating the two phases will be greater than that needed to cause cohesive failure in one of the phases. Dupre[84] defined the work of adhesion Wa as:

$$W_a = \gamma_1 + \gamma_2 - \gamma_{12} \qquad 1$$

Where γ_1 and γ_2 are surface free energies of the two phases 1 and 2, and γ_{12} is the surface free energy of the interface.

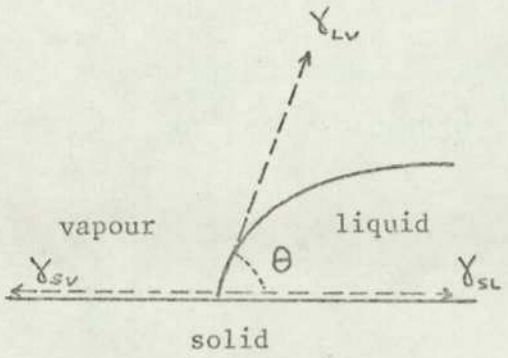
If one of the phases is a liquid and the other a solid, then molecules of the vapour from the liquid can be adsorbed on to the exposed solid surface. This will effectively lower γ_{solid} or change the work of adhesion to $W_a - \pi$ where π is the spreading coefficient[85]. Hence :

$$W_a = \gamma_{sv} + \gamma_{lv} - \gamma_{sl} + \pi \qquad 2$$

where γ_{sl} = surface free energy of the solid with the adsorbed film of vapour.

γ_{lv} = surface free energy of the liquid in equilibrium with its own vapour.

γ_{sl} = surface free energy of the solid-liquid interface.



From Young's Equation[86] (or more correctly from that of Sumner[87] who derived the result in terms of surface free energies rather than surface tension)

$$\gamma_{sv} = \gamma_{sl} + \gamma_{lv} \cos \theta$$

For complete wetting i.e. $\theta = 0$; $\cos \theta = 1$ and

$$\gamma_{sv} = \gamma_{sl} + \gamma_{lv} \qquad 3$$

Combining this result with equation 2

$$W_a = (\gamma_{sv} + \gamma_{lv}) + (\gamma_{lv} - \gamma_{sv}) + \pi$$

$$= 2\gamma_{lv} + \pi \qquad 4$$

The liquid adhesive will have solidified before any load is applied to the bond, but this will not greatly affect the surface energies (although it will introduce residual stresses), and the above expression will be a reasonable estimate of the work needed to break the adhesive bond at the interface and leaving a film of adsorbed vapour on the solid surface. Similarly, if the adhesive itself is broken then the work needed to produce the new fractured surfaces will be approximately $2\gamma_{lv}$ - the work of cohesion. Therefore, for perfect bond, the work needed to break a joint by cohesive failure of the adhesive will be less than that needed to break it at the interface.

Frequently when a joint is broken adhesive is visible on both adherends, so that failure is obviously cohesive in the adhesive, but in other cases failure appears to be at the interface. In such cases suitable techniques often detect a thin layer of adhesive on the adherends. Bikerman[88] dissolved residual polythene from the surface of aluminium from

which a coating had been peeled, and determined the total amount of polymer gravimetrically. He found that the residual layer had a mean thickness of nearly 20 μm. Schonhorn[89] applied coatings of polythene to aluminium covered with a monolayer of radioactive stearic acid. After the polymer had been stripped off he estimated the thickness of the polythene left behind by measuring the extent to which it shielded the radiation from the stearic acid. He estimated a thickness of about 100 μm was left on the adherend. Gromov et al[90] applied polypropylene labelled with C^{14} to various adherends and after peeling off the adhesive, measured the intensity of the radiation, which corresponded to a residual thickness of several monolayers.

Clearly in some cases in which the failure appears to be adhesive it is in fact cohesive, but this does not prove that there is never separation at the interface. There are several flaws in such a theoretical argument. First the fracture energy of the polymer is not equal to $2\gamma_{lv}$, because the long-chain polymer molecules will all be entangled with one another, and fracture cannot occur simply by separating sets of molecules on either side of a plane. Many molecules will pass through any plane and when the polymer is broken these chains must either be drawn out against the resistance of thevan der Waal forces acting along the whole of their length; or must themselves be broken by fracturing covalent rather than van der Waals bonds. For polythene $2\gamma_{lv}$ is about 7I ergs/cm^2 [91] but experiments on crack propagation[92] give the fracture energy as about 2×10^6 ergs/cm^2. The fact that the energy needed to break the interface is greater than $2\gamma_{lv}$ does not therefore prove that fracture must occur in the polymer. Secondly the strength of the forces across the interface will frequently be less than those theoretically predicted. The polymer may fail to wet the substrate properly, because there is air trapped in pits in the substrate surface. These

unfilled cavities will act as stress centres which can initiate cracks. In addition, shrinkage during solidification will set up stresses in the polymer, and these will be a maximum at or near the interface, thus favouring interfacial rather than cohesive failure. Lastly, experiments with molecular models of the polymer and various metallic surfaces[93] have shown that because the intermolecular distances in both metal and oxide surfaces are substantially different from those in polymers, when the polymer is adsorbed onto the metal there will be considerable mismatch between atoms and only about 10% will be in positions where they can exert maximum interaction. Indeed it has been demonstrated that interfacial failure does occur. Huntsberger[94] measured the residual films of polyisobutylene left on an alkyd base after stripping, by interferometric method, and found it was -1.3 ± 3.3Å, which corresponds to the interface within the experimental limits. Ilkka and Scott[95] have used the electron microscope to study fractured surface joints and have observed areas which appear to be bare metal.

2.11 POOR ADHESION

Three principle reasons can be recognised for poor adhesion:

1. Inadequate interfacial forces
2. Poor wetting
3. Weak boundary layers

2.11.1 Interfacial forces

In the expression for work of adhesion, W^*_a, given as in equation 2 only γ_{lv} can be measured directly. By using Young's equation and equation 2 we can obtain:

$$W^*_a = \gamma_{lv} (1 + \cos \theta) \qquad 5$$

Therefore, as $\theta \to o$, W^*_a increases, also an increase in γ_l leads to an increase in W^*_a. W^*_a can be determined by measuring

γ_{lv} and θ.

The contact angle of water on surface is frequently used as a measure of its wettability, or to determine the effectiveness of a surface pretreatment[96]. Bond strength generally increases with decreasing contact angle, but one cannot assume that the contact angle with the adhesive will necessarily behave in the same way as that with water. Raraty[97] has used ice as the adhesive in a napkin ring test. The cylinders were made of PTFE, polystyrene,(P.S.), or polymethyl-methacrylate (PMMA), which gave contact angles of 108°, 75° and a very low angle which in some other work by de Bruyne[98] was estimated as between 30° and 40°. Raraty's bond strengths do increase with decreasing contact angle, but if one computes the values of $(1 + \cos \theta)$ they are roughly proportional to the bond strengths, as shown below:

Surface	θ	$(1 + \cos \theta)$	shear strength (Kg/cm^2) at $-10^{\circ}C$	$-20^{\circ}C$	$-30^{\circ}C$
PTFE	108°	0.691	1.5	1.5	1.5
PS	75°	1.259	10	10	10
PMMA	$30\sim40^{\circ}$	(1.766~1.866)	12	17	17

But in general there does not seem to be any significant correlation between the shear strength of the joints and the theoretical work of adhesion.

Levine et al[99] measured the lap-shear strengths of steel strips with different surface pretreatments, bonded with an epoxy adhesive and compared them with the contact angles of the adhesive on the surface. The two quantities were clearly interrelated, but not sufficiently well to allow any detailed analysis.

There is also an indirect method of testing the relationship between these quantities, without having to measure contact angles and this depends on the concept known as the critical tension.

2.11.2 Critical Surface Tension

Zisman[100] has pointed out that the contact angle of a homologous series of liquids on any particular surface can be related empirically to their surface tensions by the equation:

$$\cos \theta = a - b \gamma_{lv} \qquad - \qquad 6$$

a and b are arbitrary constants. When $\theta = o$, γ_{lv} is defined as the critical surface tension = γ_c. Therefore, when $\theta = o$, equation 6 becomes

$$1 = a - b \gamma_c \text{ and } a = 1 + b \gamma_c$$

substituting for (a) in equation 6, we obtain:

$$\cos \theta = 1 + b (\gamma_c - \gamma_{lv}) \qquad - \qquad 7$$

A new expression for W^*_a from equations 5 and 7 can be obtained, namely

$$W^*_a = (2 + b\gamma_c)\gamma_{lv} - b\gamma^2_{lv} \qquad - \qquad 8$$

This is an equation of a parabola with the concave side towards the surface tension and it has a maximum value of W^*_a occurring at:

$$\gamma_{lv} = \frac{1}{b} + \frac{1}{2} \gamma_c \qquad - \qquad 9$$

and the W^*_a max. $= \frac{1}{b} + \gamma_c + \frac{1}{4} b \gamma^2_c \qquad - \qquad 10$

Levine et al[101] bonded sheets of different polymers between metal cylinders with an epoxy adhesive, and found that the tensile strengths of the joints were indeed proportional to γ_c of the polymers. In this example the bonding is chiefly by Van der Waal's forces, and the results agree well with the theoretical predictions.

Fowkes[102] has derived a way of estimating interaction energies when it is difficult to measure them experimentally, which is of particular use in cases where only London dispersion forces act. The

analysis depends on splitting the interfacial surface energy into two components, one for dispersion forces, and the other from any other forces, in a system where the intereactions arise solely from dispersion forces. The forces exerted on the molecules at the surface of phase 1 by those in the surface of phase 2 will be $\sqrt{\gamma_1^d \gamma_2^d}$ where γ_1^d and γ_2^d are the dispersion force components of the respective surface tensions. This will lower the surface tension of phase 1 to $\gamma_1 - \sqrt{\gamma_1^d \gamma_2^d}$ Likewise that of phase 2 will be $\gamma_2 - \sqrt{\gamma_1^d \gamma_2^d}$. The tension of the interface will be the sum of these two tensions i.e.

$$\gamma_{12} = \gamma_1 + \gamma_2 - 2\sqrt{\gamma_1^d \gamma_2^d}$$

From this expression the work of adhesion will be

$$W_a = \gamma_1 + \gamma_2 - \gamma_{12} = 2\sqrt{\gamma_1^d \gamma_2^d}$$

In order to determine W_a^* it is necessary to measure π_e, the equilibrium spreading pressure of the adsorbed vapour i.e.

$$\pi_e = W_a - W_a^* = \gamma_s - \gamma_{sv}$$

It if is assumed that the surface tension of hydrocarbon originates only from dispersion forces, then $\gamma_{lv} = \gamma_1^d$, and by measuring the interfacial tensions and contact angles with other materials it is possible to calculate γ^d for these materials. Fowkes found that with these results he was able to predict successfully the values of many parameters involved in interfacial phenomena where only dispersion forces act. In particular having determined γ_s^d for polymers which are used as adhesives, and for various metals he was able to calculate the works of adhesion of bonds between the metals and the polymers, and from these to estimate the tensile strength of the bond. For iron adherends joined with polythene, the tensile strength of the interface predicted by this theory is 157,000 psi, and that of polymer 105,000 psi, so that the joint should fracture in the polythene. The actual strengths

of such joints as measured by Kraus and Manson[102] were more than an order of magnitude less (6.500 psi).

This treatment also gives a useful insight into the role of other types of forces. The value of γ_{12} can be calculated assuming that only dispersion forces are acting, so that the contribution of other forces can be estimated from the actual value of γ_{12}. In particular the contribution of polar group- towards the interaction between the adhesive and substrate were examined. The polar component was as high as 20% with alkylhalides, and about 10% for acids. It does not appear that polar groups will cause any particularly large increase in the actual interaction between the adhesive and substrates.

The contribution from dipole forces can be determined from the dipole moment of a typical polar group, if it is assumed that the metal is completely polarisable. For the interaction with mirror charges in the metal the energy is[103]:

$$V = - \frac{\mu^2}{(2r)^3} (1 + \cos^2 \theta)$$

μ = dipole moment of the molecule (say 2×10^{-18} esu)

(for C = O it is 2.3×10^{-18} esu)

r = the distance from the surface , say 3 Å

θ = angle between dipole axis and the normal to the surface, which in the most favourable case = 0^o

V = dipole-metal interaction.

This leads to an energy of only 530 cal/mole, which is small compared with the dispersion forces. It appears that the dispersion forces make the major contribution to the bond strength, and that they are in themselves more than sufficient to account for the observed bond strengths.

Taylor and Rutzler[93] have also claculated the strength of bonds in terms of intermolecular forces, but instead of assuming perfect correspondence between molecules at the interface they have taken into account the atomic configurations of the adhesives and adherends. By using large scale models of the polymer molecules and the metal surface they were able to find the best configurations of the polymer chains. They found in some cases only 1-2% of the surface sites on the substrate will be able to participate in the formation of an adhesive bond, and the fraction is never likely to be more than 50%. The forces which they considered were the ion-dipole interactions. They have calculated the strength of bond, and the work required to break the bonds, and their calculations show clearly that ion-dipole forces are able to make an even larger contribution to the total adhesion force than dispersion forces. Again their calculation indicates that the failure of such bonds should be within the adhesive layer.

One other source of interaction, electrostatic forces, should perhaps be mentioned at this point. Deryagin[104] has noticed electrical discharges during peel tests, and the dependence of peel strength on peeling rate which he observed could be a rise from the separation of electrical charges. Furthermore, he found that changing the ambient gas pressure during the peel test changed the peel load, presumably by changing the dielectric constant. Skinner et al[105] have detected and measured the charges which are produced on the surface of the polymer when tensile tests are carried out on metal cylinders bonded with "Araldite" an epoxy adhesive. Kabanov et al[106], however, found that irradiating aluminium - polythene bonds with electrons while they were being tested did not affect the bond strengths, although this would allow dissipation of the charge.

It appears then, that electrostatic phenomena are sometimes associated with the fracture of adhesive joints, though this does not mean that a new theory of adhesion is needed. Many of the bonds mentioned already involve a redistribution of electrons, and charge separation may occur when the bond is fractured.

Chemisorption of active species can also play an important part in improving adhesion. Covalent or ionic bonds will have energies of up to 420 kJ /mole, and with selective adsorption they could make a large contribution to the total adhesion. The magnitude of this "contribution" requires rigorous mathematics and it is not surprising to find not many have attempted to relate their true effect on the total adhesion.

2.11.3 The importance of adequate wetting

When considering wetting we are not concerned with the case in which a liquid gives a high contact angle with a smooth flat surface; this is just a case of poor intermolecular forces and has already been considered. What we have to take into account is the effect of the roughness of the surface, which will lead to reduced bond strengths unless the adhesive is able to fill all the minute crevices. Roughness should lead to an increased area of contact, and therefore increased adhesion, but if the polymer only penetrates a short way into the cavities then the actual area of contact may be smaller than the true surface area. If fracture occurs near the interface,polymer will only be left behind at the points of attachment to the surface and it may appear to be interfacial failure. The air trapped in crevices will lead to stress concentrations, because the polymer above a hole will not be able to carry any load; the whole of the load on this area will be carried at the edges of the hole. This may lead to the initiation of cracks at the interface, but these will then propagate into the polymer.

Clearly the degree of penetration into the surface roughness will be of primary importance. This problem has been pointed out by Zisman[107], Huntsberger[108], and many others; and more detailed analyses have been carried out by de Bruyne[98] and Bikerman[109]. These show that the rate of penetration will be increased by a low contact angle, a high polymer surface tension, and a low polymer viscosity. The steeper the sides of the pit the slower will be the rate of entry, but a shallow pit will form a bigger stress raiser than a steep pit of similar volume when filled to the same depth. If the sum of the contract angle and the angle between the pit side and apparent surface is greater than 180^{o}, then the polymer will not be able to enter that pit at all. The capillary pressure during the adhesive into crevices will be greater the smaller the radius of the pit.

If pressure is applied to the adhesive it will speed penetration, which according to de Bruyne significantly increases adhesion[98]. When aluminium panels are bonded in a press with "Redux" adhesive the peel strength at the centre of the panel is often nearly twice that at the edge, when the pressure on the adhesive will be less.

If a pit is so shaped that the air cannot escape, then further entry will be prevented once the pressure of the trapped air equals the capillary driving pressure in the crevice, so the same factors will promote good adhesion as when the air can escape.

Any surface will contain crevices of different shapes and dimensions and for any particular adhesive some of these will be filled completely, and others to lesser degrees. There will not be an abrupt change from wetting to non-wetting at any particular contact angle but a gradual transition. The way in which adhesion varies with contact angle will depend on the topography of the surface. Any contamination of the surface can produce a very high contact angle, and completely prevent

penetration by the adhesive.

It appears that unless the existing topography is less favourable to wetting than a roughened surface, then roughening will not lead to any increase in bond strength.

If there is any special type of interaction between the adhesive and a given surface this will decrease γ_{12}, the energy of the interface, which from Young's equation will also decrease the contact angle. Polar interactions increase bond strength by decreasing γ_{12} tension.

2.12 Weak layer(s)

So far it has been considered that an adhesive bond as a two phase system, in fact there may be several distinct phases present as thin layers at the interface and (or) around fillers in the adhesive. The surface of metals will often carry a film of oxide, the adhesive and adherent may react together to form another layer, and as will be demonstrated later in this thesis, a layer can separate from the adhesive as it sets. Any of these might have poor mechanical properties and may break when only a small load is applied to the joint. If an alloy is oxidised, the oxides of alloying element may contribute to formation of a weak layer, and the ability of multiple oxide formation by some metals and their coexistence can lead to high stresses at the surface leading to a weak oxide layer.

However, the example which is probably of more general significance is that in which the weak layer originates solely from the adhesive. During setting of a polymer, low molecular weight (LMW) components may migrate towards the interface. This phenomenon has been observed with polythene by Sharpe and Schonhorn[83]. Before the completion of solidification the LMW constituents will be rejected to the surface of the polymer, and because of their short chain length the layer which is produced will have poor mechanical strength. Bikerman has found that if

metals are bonded together with molten polythene very weak joints are produced, but if the polymer is first purified by dissolving it in boiling toluene and reprecipitating with acetone, then strong joints are obtained[110]. Even small traces of impurities such as oleic acid, ethyl palmitate , or stearone added to the purified polymer, will lead to rapid loss of adhesion[111]. The point at which adhesion falls again corresponds to the first appearance of traces of the impurities on the surface as detected by surface resistance measurements[112]. These experiments led Bikerman to conclude that whenever poor adhesion occurs it is not because of weak adhesion forces, but because there is a weak layer somewhere in the joint. He regards adhesion primarily as a rheological problem.

2.13 EFFECT OF TEMPERATURE ON BOND STRENGTH

Generally, an increase in temperature weakens the joint strength. Figure 2.9 shows a typical behaviour of loaded lap shear and torsional joints with temperature

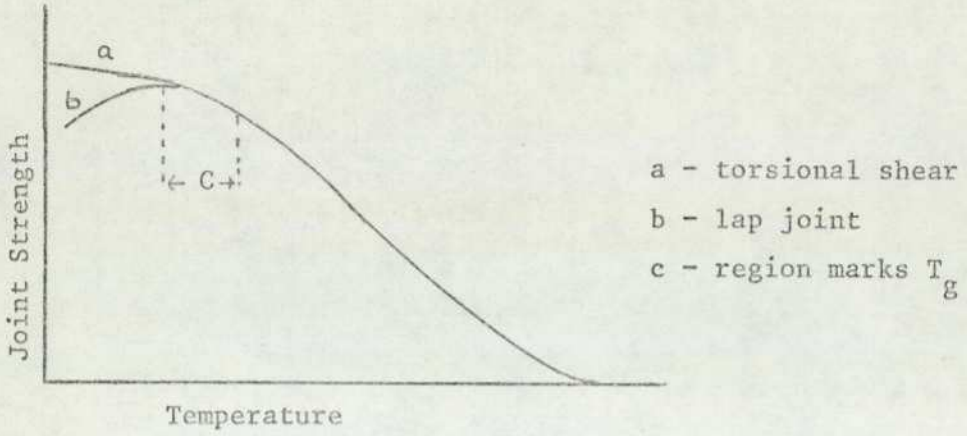


Figure 2.9 - Variation of joint strength with temperature

This change in bond strength could be due to one or more of the following reasons:

1. Increase in weak layer(s) with increasing temperature.
2. Increase in stress due to differences between thermal coefficients of adhesive and adherend.
3. Changes in primary, secondary forces and crosslinkage either within the adhesive or across the interface.
4. Changes in mechanical properties of adhesive.

The region (C) marks the transition from ductile (at high temperature) to brittle failure[113] (at low temperatures). This transition occurs in the region of the glass transition temperature (T_g) which is extremely sensitive to structural changes leading to changes in molecular mobility. Suffice it to state that cyclization, aromatic rings, bulky side groups and cross linkage all tend to raise T_g from about $-100^{\circ}C$ for flexible aliphatic hydrocarbon chains to above $200^{\circ}C$ and even much higher temperatures for condensed rings systems.

Generally for an epoxy resin T_g increases with increasing molecular rigidity of the diamine curative.

At the low end of temperature, levelling (curve a) is caused by brittle failure which is not significantly sensitive to temperature, i.e. the energy required to form two new surfaces is not temperature sensitive. Results obtained by Foulkes et al[114], Wake[115] and Krieger and Politi[116], using various adhesives and adherends indicate the validity of curve (a).

Salomon[114] has given an excellent account for the observed behaviour. He attributed the changes in shear modulus or Young's modulus of the adhesive to five reasons, namely:-

1. In the hard glassy region the shear modulus is high approaching that for other rigid solids, and is less temperature dependent.
2. Near T_g, molecular units become flexible, and sudden change is observed.
3. Further increase in temperature reduces "internal friction" sufficiently to allow for a ready uncoiling of polymer chain on mechanical loading of the material leading to a drop in modulus.
4. On further heating, material begins to flow. This region is sensitive to molecular weight distribution and that the low molecular weight fraction flows more readily.
5. The final phase is reached when intermolecular forces become weak enough to allow rapid flow, stresses are then relaxed so fast that the polymer does not show any elastic recovery.

Experiments with lap joints shows a decrease in joint strength at the lower end of temperature (curve - b). This is a property of the lap

joint whereby the stress distribution is changed and cleavage becomes more important than shear. This occurs when the rigidity of adhesive approaches more closely that of the adherends.

The presence of fillers or carriers in the adhesive can cause some variation on either side of the region C and generally they increase the shear strength and when added to a non-brittle adhesive they may increase brittleness and thereby reduce peel strength[118].

There is very little scientific knowledge on the role of fillers but generally they are added to improve thermal and electrical properties of the adhesive, or to thicken the uncured adhesive which can be handled more easily.

CHAPTER 3

DESCRIPTION OF EXPERIMENTAL WORK

		Page
3.1	Optical microscopy	62
3.2	Transmission electron microscopy	62
3.3	Scanning electron microscopy	64
3.4	X-ray powder diffraction	64
3.5	Transmission electron diffraction	64
3.6	Reflection electron diffraction	65

3.1 Optical microscopy

A conventional microscope was used for examination of surfaces and particularly for determining the locus of failure of joints. Magnifications up to 500 were most useful since most of the samples were too rough to give a sharp image at higher magnifications.

Nomarski's[119] method of interference contrast microscopy involving polarised light which produces a 3-dimensional impression was used extensively in examination of fractured surfaces. The device is used to produce image contrast in a variety of colours. The interference contrast equipment was used with Reichert type "MeF" camera microscope[120].

This technique enhances contrast and shows surface irregularities which were not visible by the conventional methods of incident light microscopy.

For metallographic examination, the individual areas of the different phases of the alloys were frequently very small, optical methods were not entirely satisfactory and alternative methods were used.

3.2 Transmission electron microscopy

Transmission electron microscopy of replicas was found to be an appropriate and convenient method for studying many of the surfaces. An Elmskop - 1A (Siemens) model electron microscope operating at 60kV was used.

Prior to replication platinum-carbon shadowing at angles ca.20-45^{o} was deposited on the surface to enhance contrast. The replicas were then prepared using an evaporated carbon deposited at ca. 90^{o} to the surface. The replicas were freed from the substrate with dilute solutions of hydrofluoric and nitric

acids. The latter was added to minimise hydrogen evolution which usually causes disintegration of the replicas.

In order to follow modes of attack by various reagents, stereo electron micrographs were made by tilting the replicas 6^{o} in one direction, taking a picture, then tilting in the opposite direction by similar angle (i.e. total movement 12^{o}) and taking a second picture. This method was extremely useful because it not only enabled the shape of phases to be constructed in a three dimensional manner but also their heights relative to each other.

Direct replication of the napkin rings fractured surfaces was not used as the specimens in question were rather large and because they were required for further use. Indirect replication was used on these specimens. Cellulose acetate sheet (0.005 inch thick) was softened by swabbing with acetone and pressed firmly on the fractured surface. The sheet was allowed to dry completely before it was removed, and the areas required for examination were cut and marked. The latter was then shadowed in the usual manner. The final carbon replicas were freed by dissolving the cellulose acetate sheet with acetone. This latter operation is rather tedious; it involved placing the cut areas on an electron microscope grid placed on fine wire mesh resting at an angle in a petri dish containing some acetone. Acetone was allowed to drip from a burette ca. 1 drop/sec. on the wire mesh from a height of about 1 cm. The thin stream of acetone moving downward, dissolved the cellulose acetate sheet gradually. This usually took about half an hour. Faster dissolution of the sheet causes disintegration of the replica.

The main advantage of this technique is that the original surface can be replicated as many times as desired without causing any appreciable damage to it. Also it is simple to produce a replica

of a desired area, therefore, the chance of examining the "wrong" area is eliminated. A danger which always accompanies direct replication.

3.3. Scanning electron microscopy (S.E.M.)

This is the latest method to be used in the fields of adhesion. It has the advantage that fractured surfaces can be examined directly. The 3-dimensional effect it produces makes it easier to study such surfaces in great detail. The process involves coating the fractured surfaces with a very thin metallic film in order to make the adhesive films conductors.

Examination by S.E.M. was used in the present work to confirm the results obtained by other techniques. Samples were examined on a stereoscan scanning electron microscope model 600[121], operating at 25 kV. The samples were coated with gold/carbon film (ca. 10 nm.)

Identification of chemical nature of the coatings formed by the various pretreatments was done by:

3.4. X-ray powder diffraction

Using either copper or molybdenum radiation, the material to be examined was placed in a fine glass capillary tube, mounted on a rotating disc and enclosed in a camera of 11.46 cm. in diameter, then exposed to the radiation for periods of 4-8 hours. The work was carried out using a Raymax 60[122] diffraction camera operating at 40 kV.

3.5 Transmission electron diffraction

This was carried out with the same electron microscope mentioned above, operating at 100 kV. The d-values were calculated using the equation:

$$d = K/R$$

where d = spacing in $\mathring{A}$

K = camera constant

R = radius of diffracted rings

Because of the dependence of K on the applied voltage, the system was calibrated using either gold or rutile.

The specimens examined by this technique are coatings removed from substrates with a methanol solution of bromine.

3.6 Reflection electron diffraction

The procedure here is similar to that described in 3.5 above, except that it was carried out on whole specimens. The instrument available can only be used at a glancing angle position. Therefore, only half diffraction rings are obtained. The intensity of diffracted lines obtained by this method varies, among other things, according to their position since partial blockage of the diffracted rays is inevitable but their positions are unaffected. The specimen surfaces were sufficiently conducting to enable these examinations to be carried out in the standard Siemens microscope without the use of discharging device.

CHAPTER 4

SURFACE STUDIES OF TWO TITANIUM ALLOYS

4.1	Metallographic examination.	67
4.1.1	IMI-318 alloy.	67
4.1.2	IMI-205 alloy.	68
4.2	Air oxidation of IMI-318 and IMI-205 alloys.	71
4.3	Oxidation of IMI-318 alloy in alkaline hydrogen peroxide solutions.	75
4.3.1	X-ray powder diffraction	78
4.3.2	Reflection electron diffraction.	82
4.3.3	Colorimetric analysis of oxides formed in alkaline hydrogen peroxide and air oxidation.	84
4.4	Etching IMI-318 with hydrochloric acid.	87
4.5	Etching IMI-318 with sulphuric acid.	92
4.6	Etching IMI-318 and IMI-205 alloys with hydrofluoric acid.	95
4.7	Electrolytic oxidation of IMI-318 and IMI-205 alloys.	102
4.8	Discussion.	105
4.9	Etchants for titanium and its alloys.	109

4.0 Surface Studies of Two Titanium Alloys

Preliminary work was carried out on IMI-318 alloy which was readily available to the author at an early stage in the development of this work and napkin ring test pieces were made from this alloy. Napkin ring test pieces made from IMI-205 alloy were obtained from the Rubber and Plastics Research Association but this alloy was not available in any other form in spite of the effort to obtain samples. Therefore most of the metallography and surface chemistry has been carried out using IMI-318 with only a necessary minimum of work on the surface of IMI-205 napkin rings.

4.1 Metallographic examination

Identification of the various phases in the present work was based on published works[123][124][125] and were later confirmed by D.F.Neal of IMI-Kynoch during a visit in April 1972.

4.1.1 Titanium alloy IMI-318 (Ti-6Al-4V)

Several specimens of this alloy were ground in the conventional manner on successive grades of emery paper using water as a lubricant. Further polishing was carried on a rotating disc using diamond powder down to 1μ size. An etchant containing 4% (w/v) hydrofluoric acid, 3.5% (w/v) nitric acid in water, was used by swabbing for 5-10 seconds. This etchant is said to reveal alpha, beta, transformed beta, and hydrides. However, due to the small sizes of the various phases present, high magnifications were required and no sharp boundaries were obtained by optical microscopy, and complete identification of all phases was not possible. However, alpha and beta phases were noted as (yellow to orange) and mauve colours respectively. Further examination of the metallographic structure was carried with the aid of electron microscope.

Specimens for electron microscopy were electrolytically polished at a current density of about 0.5 amp/cm^2 in a solution containing 4% (w/v) perchloric acid in glacial acetic acid at temperatures not exceeding 15°C.

The etched specimens were shadowed with platinum and carbon at an angle of about 20°-45°. Further carbon was sprayed (at an angle ca.90°) to strengthen the thin film produced by the first operation. A solution containing 0.1% (w/v) hydrofluoric acid and 1.4% (w/v) nitric acid was found to be most suitable for removing the replicas from the substrate.

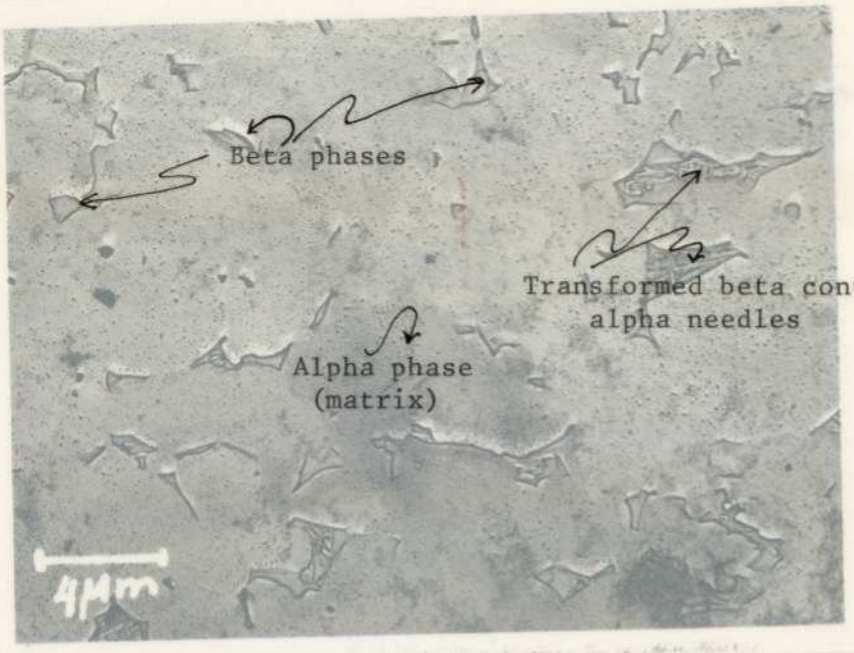
Examination of the replicas was carried out at 60 kv.Alpha,beta, transformed beta, and needles of alpha phase were identified and are indicated on electronmicrographs in figures 4.1 and 4.2.

The volume of beta phases was estimated from the total area occupied and found to be about 30% which suggests that the alloy was quenched from a temperature of about 850°C. (see figure 2.1).

Several types of structures were seen; equiaxed alpha with beta round the alpha, lightly deformed Widmanstatten structure, and in some cases spheroidal beta in an alpha matrix . No hydride phase was detected in all the specimens examined.

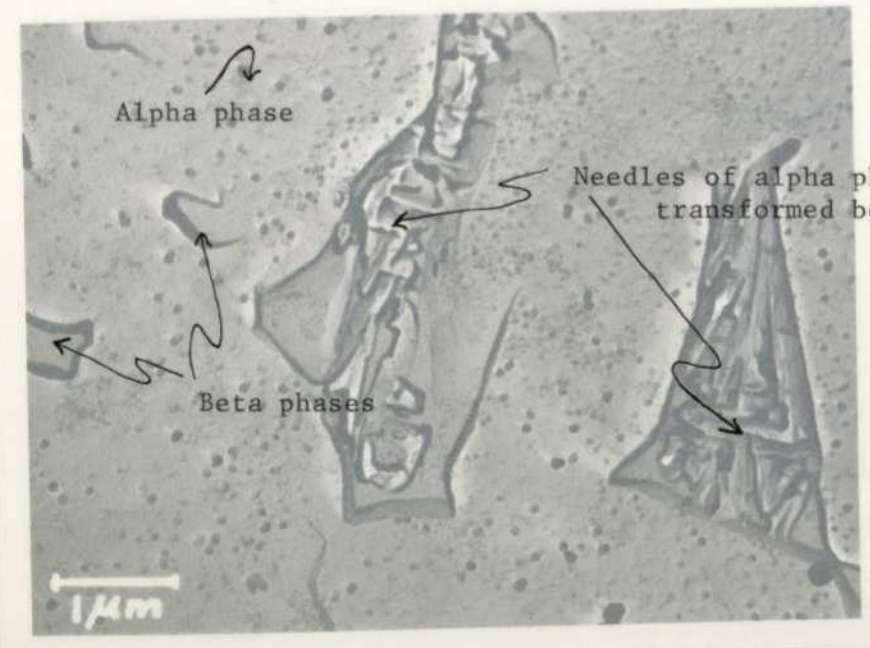
4.1.2 Titanium alloy IMI-205 (Ti-15%Mo)

Specimens for metallographic examination were prepared as with IMI-318 alloy and examined under similar conditions except that the etching solution used was 4% (w/v) hydrofluoric acid; 10.5% (w/v) nitric acid in water, and the solution used to detach the replicas from the specimens was 0.1% (w/v) hydrofluoric acid; 42% (w/v) nitric acid. This increase in the nitric acid content was necessary to dissolve the black molybdenum oxide which usually forms as a loose film on the surface.



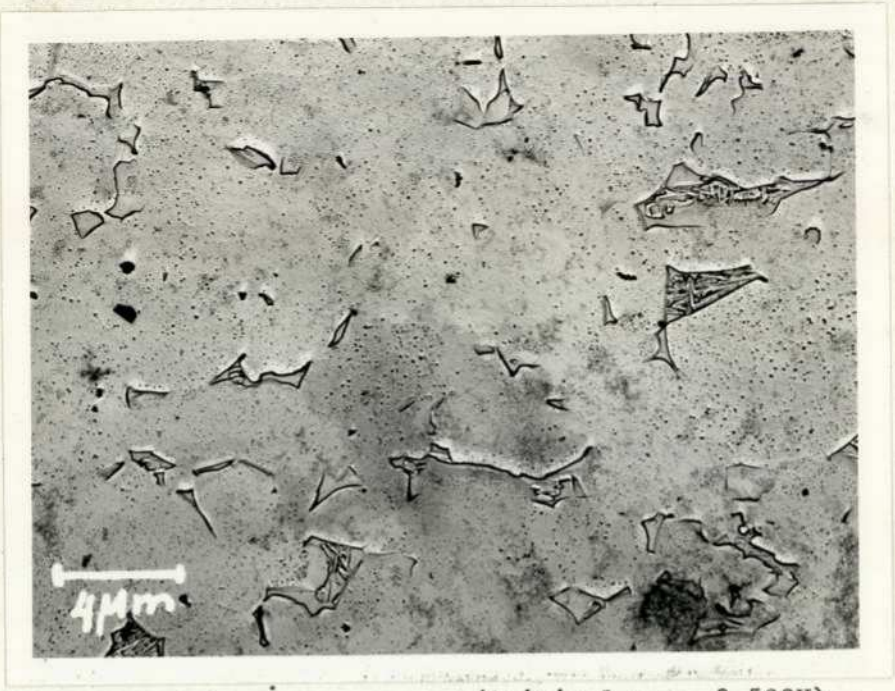
(Original mag. 2,500X)

Figure 4.1 : Electron micrograph of an etched IMI-318 alloy showing the following phases; alpha phase forming the matrix, alpha needles within transformed beta phase, and beta phase.



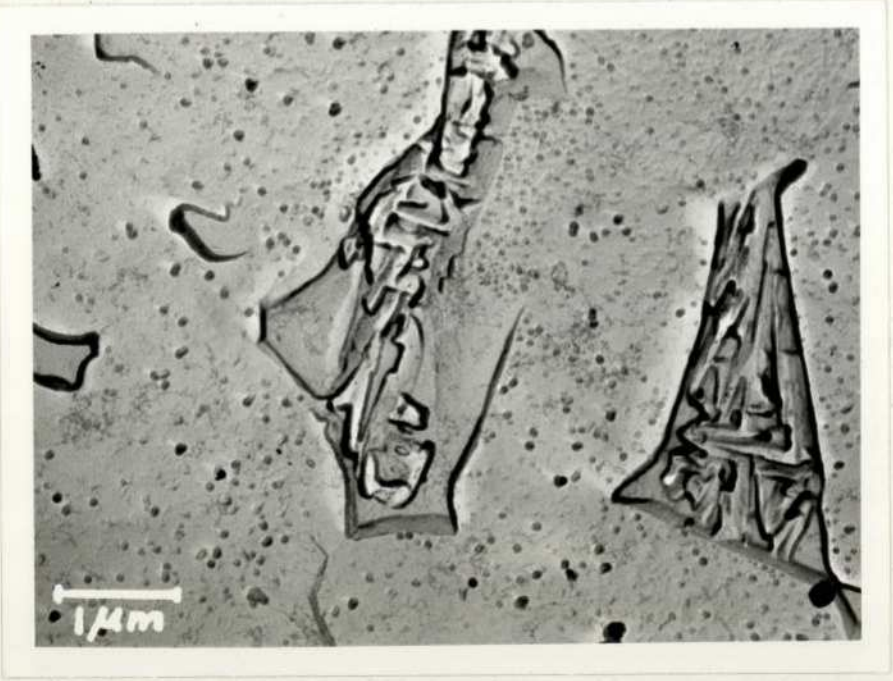
(Original mag. 10,000X)

Figure 4.2 : As in figure 4.1 but showing beta phases containing alpha needles surrouded with transformed beta.



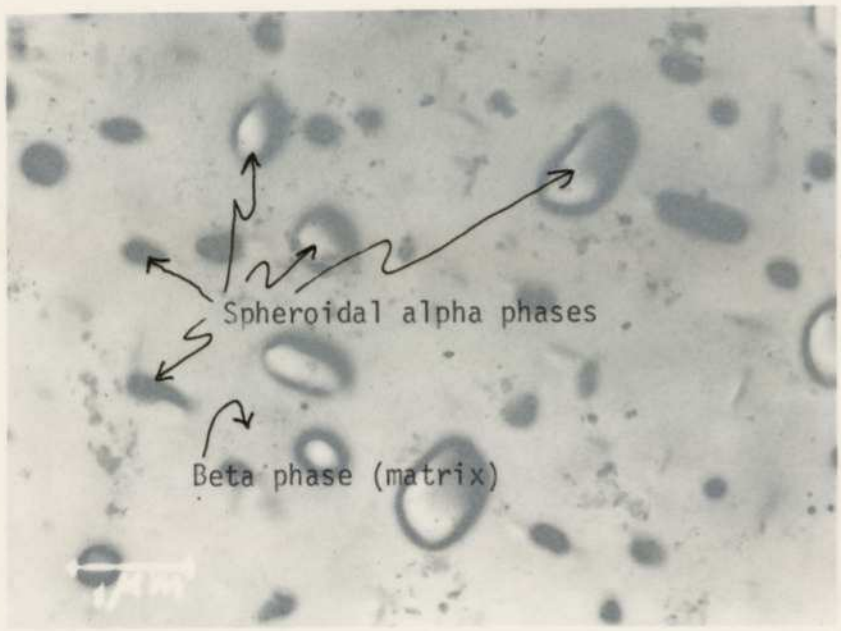
(Original mag. 2,500X)

Figure 4.1 : Electron micrograph of an etched IMI-318 alloy showing the following phases; alpha phase forming the matrix, alpha needles within transformed beta phase, and beta phase.



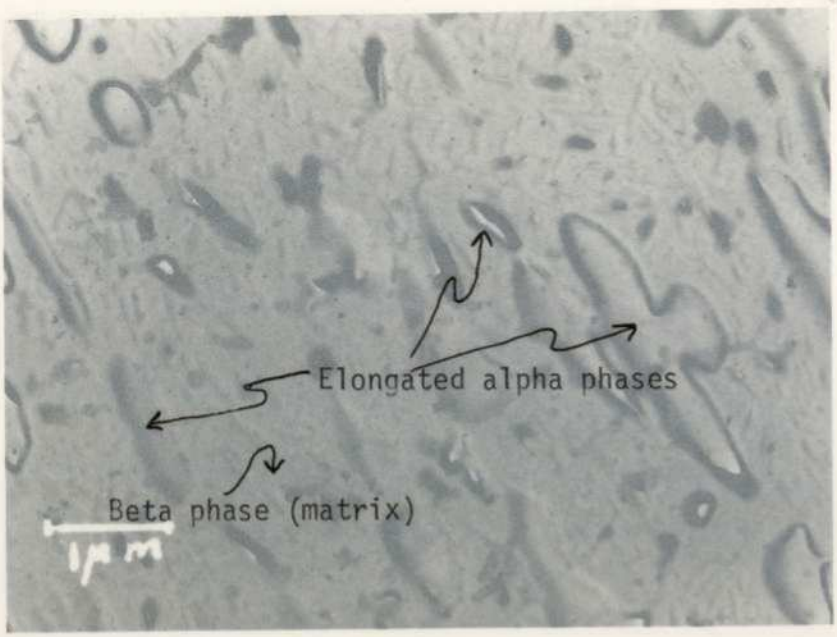
(Original mag. 10,000X)

Figure 4.2 : As in figure 4.1 but showing beta phases containing alpha needles surrouded with transformed beta.



(Original mag. 10,000X)

Figure 4.3 : Electron micrograph of an etched IMI-205 alloy showing the following phases; beta forming the matrix and spheroidal alpha phases.



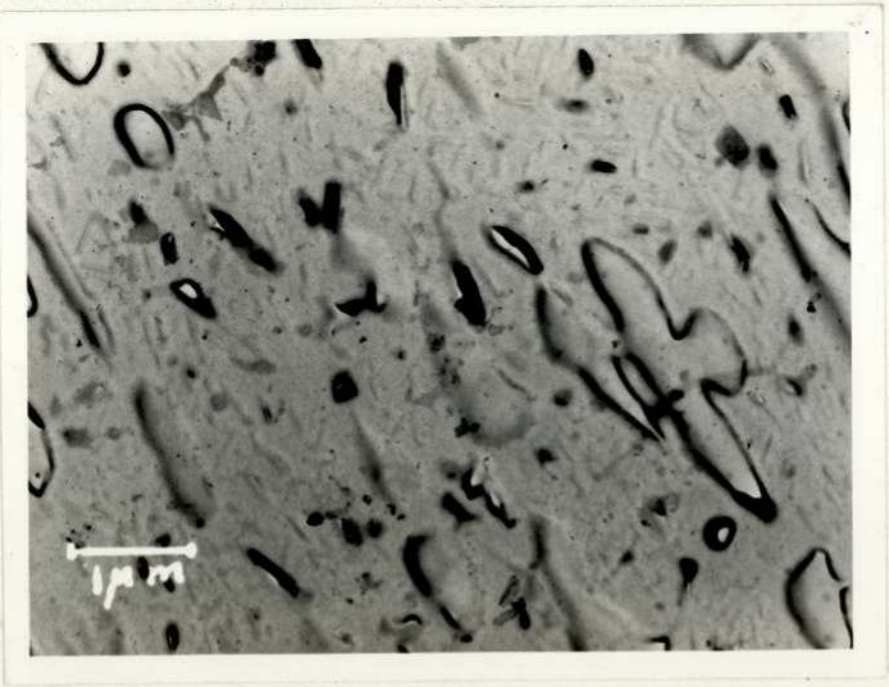
(Original mag. 10,000X)

Figure 4.4 : As in figure 4.3 but showing different alpha phases; spheroidal as well as elongated .



(Original mag. 10,000X)

Figure 4.3 : Electron micrograph of an etched IMI-205 alloy showing the following phases; beta forming the matrix and spheroidal alpha phases.



(Original mag. 10,000X)

Figure 4.4 : As in figure 4.3 but showing different alpha phases; spheroidal as well as elongated .

Alpha and beta phases were identified; the beta forming a matrix containing spheroidal alpha phase. The volume of the alpha phase varied among the specimens examined. The majority contained about 10% spheroidal alpha phases while others contained up to 25% of rather elongated alpha phase. The two types are illustrated in figures4.3&4.4.The black spots appearing on both micrographs are alpha phase which has been etched differently from the other alpha phases. This could be due to either size,composition or orientation effects[126]. Because of the different structures noted it can be deduced that the samples examined must have had a different thermal history. The samples containing the elongated alpha phase, most probably received a heat treatment at a temperature ca.650°C. This temperature is lower than that used for the samples containing spheroidal alpha phase, but high enough to prevent nucleation of the omega phase.

4.2 Air oxidation of IMI-318 alloy

Oxidation of IMI-318 alloy was carried out in an electric furnace coupled to a thermogravimetric balance capable of detecting changes in weight up to 10^{-3} gms. Oxidation below 600°C is rather slow but at 620 ± 5°C it becomes rapid. As the thickness of the oxide increases, the specimen passes through a series of colours; golden yellow, orange,mauve, blue, grey and finally black. Examination of oxidised specimens by optical microscope showed that alpha and beta phases were coloured differently. Obviously the difference in colour is due to different thicknesses of oxide layer on these phases which could have resulted from the presence of alloying elements in these phases in different concentrations. In addition, some orientations of phases enhance growth of an oxide more than others. Table 4.1 shows the colours of each phase in specimens oxidised between 400-800°C.

Temperature ^{o}C	Colour of α phase	Colour of β phase	Overall colour
400	Yellow	Yellow	Yellow
500	Yellow/orange	Metallic yellow	Golden
600	Orange/red	Blue	Mauve
700	Blue & orange	Blue/mauve	Blue
800	Pink & grey	Grey & blue	Sandy grey

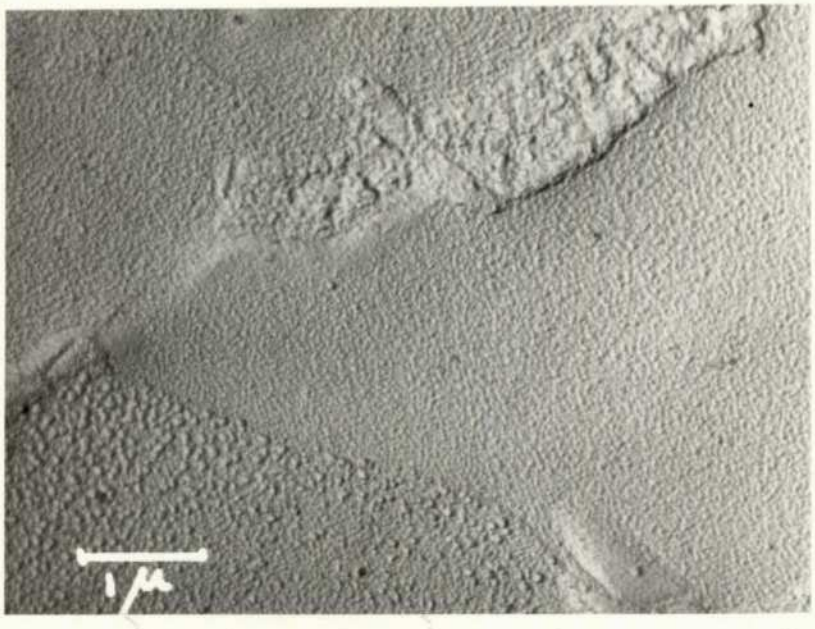
TABLE 4.1 - The colour of alpha and beta phases in IMI-318 alloy oxidised for five minutes at various temperatures.

The change in the surface topography was monitored by replications of oxidised specimens for examination by electron microscopy. Up to 400°C no change in the topography was observed, implying that the oxide layer replicates the surface of substrate. At temperatures above 500°C, the beta phase begins to swell. This continues until a temperature about 700°C is reached when suddenly most of the swelling disappears leaving behind a porous structure. Probably this is due to incorporation of vanadium oxide within the scale and because the molecular volume of V_2O_5 ca. 2.6 times larger than that of TiO_2. The disappearance of swelling could be due to melting and subsequent decomposition of V_2O_5(m.p.690°C)[24]. Figures 4.5 and 4.6 illustrate these effects. The basket-weave structure within the beta-phase could possibly be due to decomposition and subsequent agglomeration of the beta phase at the surface. The overall roughness produced by air oxidation is very poor. Examination of etched oxidised specimens by optical microscopy revealed the presence



(Original mag. 2,500X)

Figure 4.5 : Electron micrograph of IMI-318 alloy air oxidised for five minutes at 600°C showing swollen beta phases.



(Original mag. 10,000X)

Figure 4.6 : Electron micrograph of IMI-318 alloy air oxidised for five minutes at 700°C showing fine structure within the beta phases formed as a result of evaporation of V_2O_5 oxide.

of a layer consisting mainly of alpha phase below the oxide scale. This is not surprising since oxygen is an alpha-stabiliser. The total volume of beta phase at the surface decreased with rise in oxidation temperature; near 800°C about 50% reduction was observed.

The nature of the oxide scale formed by oxidation in air was examined by X-ray powder diffraction method on material removed mechanically from the surface and by transmission electron diffraction on scale removed from oxidised specimens by dissolving the substrate in 10% Br_2 in anhydrous methanol. The results obtained are listed in table 4.2 . No diffraction lines due to any aluminium or vanadium oxide(s) were detected by both techniques.

Experimental Results				ASTM data for TiO_2 - Rutile	
X-ray powder diffraction		Transmission electron diffraction			
dÅ	Intensity*	dÅ	Intensity*	dÅ	Intensity
3.233	vst	3.236	vst	3.245	100
2.492	m	2.453	st	2.489	41
2.281	vw	-	-	2.297	7
2.191	m	2.107	w/m	2.188	22
2.041	w	-	-	2.054	9
1.692	st	1.677	m	1.687	50
1.625	m	1.611	w	1.627	16
1.481	w	1.457	w	1.480	8
1.462	w	1.427	w	1.453	6
1.365	m/w	1.347	w	1.360	16
1.351	w	-	-	1.347	7

v = very ; st = strong; m = medium; w = weak.

TABLE 4.2 - X-ray powder and transmission electron diffractions of the oxide formed on IMI-318 alloy, when heated in air.

4.3 Oxidation of IMI-318 alloy in alkaline hydrogen peroxide solutions at room temperature

Oxidation was carried out at room temperature using specimens measuring 1 x 2 x 0.2 cm suspended by a nylon line in 200 ml of solution in a corked 250 ml conical flask. The duration of tests was limited to 72 hours maximum since hydrogen peroxide alkaline solution underwent a quick, spontaneous decomposition according to the reaction[127].

$$2H_2O_2 \rightarrow 2H_2O + O_2 \qquad \Delta H = -23.6 \text{ K.cal/mole}$$

The oxidised specimens were then washed with water and with acetone, and were dried at 80°C for half an hour before they were examined. 64 specimens were examined by optical microscopically and 26 by electron microscopy.

Because of the continuous decomposition of the stock solution of hydrogen peroxide, its concentration was determined volumetrically[128] using a standard solution of potassium permanganate before each set of solutions were prepared. 64 solutions were prepared containing different concentrations of both hydrogen peroxide and sodium hydroxide.

Depending on the concentration of hydrogen peroxide and sodium hydroxide, the alloy passivates and is coated by a protective glossy and translucent film, or is coated by a coloured oxide which ranged between yellow, mauve, blue, grey and black, or is quickly corroded. Figure 4.7 indicates the conditions under which each colour is formed, the boundaries are not precise and all the areas overlap.

The mode of attack differs considerably from one region to another. In the passivity region etching of the alloy increases with increasing hydrogen peroxide concentration. While in the yellow to blue regions a matt and patchy coloured oxide surface was obtained. In the grey-region generally both phases are dissolved but just before the black oxide region, the beta phase is preferentially removed and crevices around the alpha phase begin to form. The depth of these crevices increased

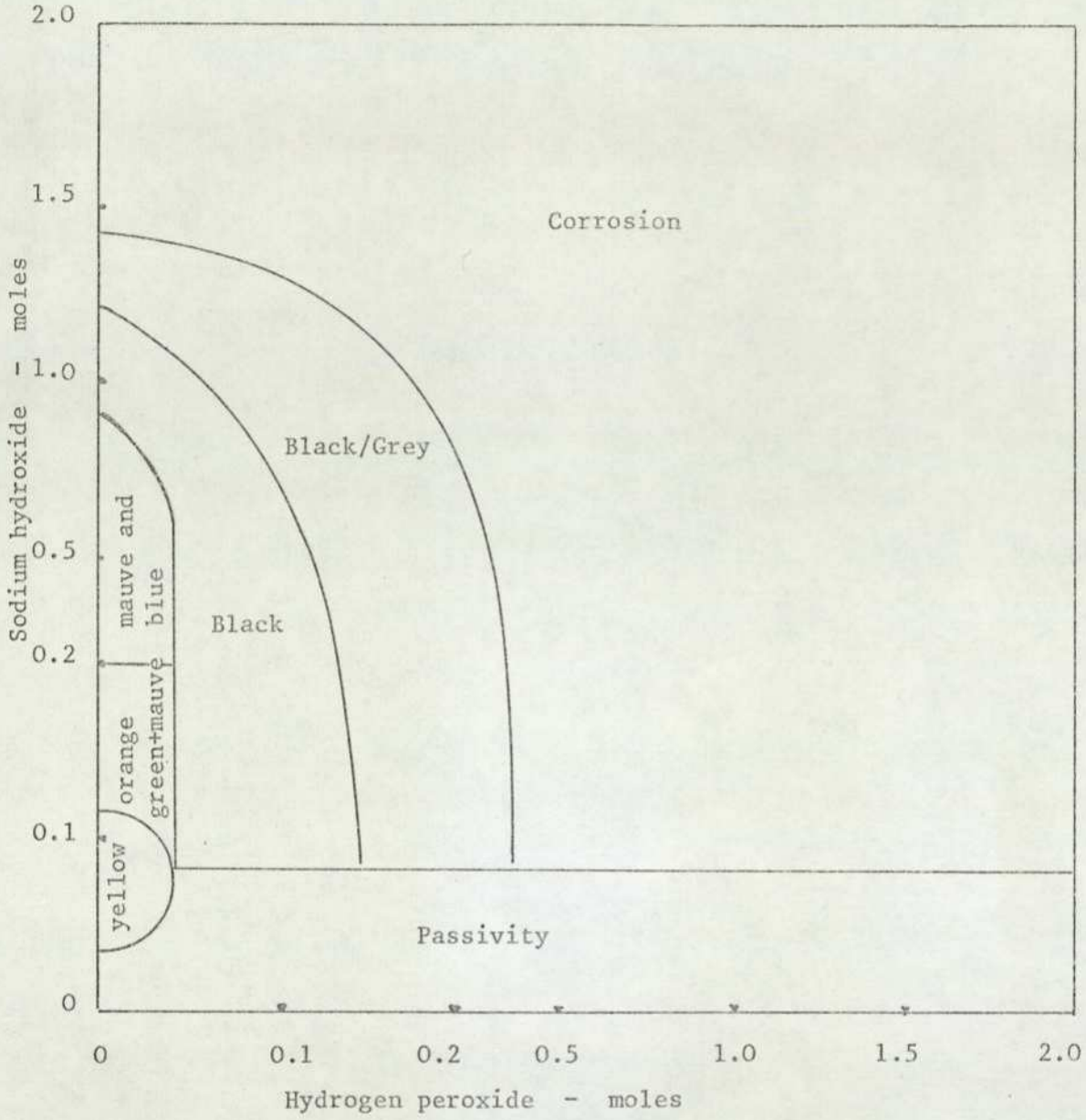


Figure 4.7 - IMI-318 alloy behaviour in sodium hydroxide - hydrogen peroxide solutions at 20 - 23°C. The actual data from which this figure was constructed are listed in table 4.3 .

Region	Concentration of NaOH · moles	Concentration of hydrogen peroxide in moles			
Passivity	0.02	0.08	0.16	0.60	
	0.04	0.12	0.40	0.80	
	0.06	0.08	0.16	0.40	1.00
Yellow	0.04	0.02	0.04		
	0.06	0.04			
	0.10	0.02			
Orange plus green and mauve	0.12	0.02			
	0.16	0.02			
	0.18	0.02			
Mauve and blue	0.20	0.02			
	0.40	0.02			
	0.60	0.02			
	0.80	0.02			
Various shades of black	0.08	0.08	0.12		
	0.10	0.08	0.12		
	0.20	0.06	0.08	0.12	
	0.60	0.06	0.08	0.12	
	0.90	0.02	0.04	0.08	
	1.00	0.02	0.06		
	1.20	0.02			
Black and grey	0.10	0.16	0.20		
	0.12	0.16	0.20	0.40	
	0.20	0.16	0.20	0.40	
	0.60	0.16	0.20		
	1.00	0.12			
	1.20	0.02			
	1.40	0.02	0.80	0.16	
Corrosion	0.10	0.60	0.80		
	0.20	0.60	1.40		
	0.50	0.40			
	1.00	0.40	1.00		
	1.20	0.16	0.60		
	1.40	0.12			
	1.50	0.02	0.80		
	1.80	0.02	1.00		
	2.00	0.02			

Table 4.3 : Oxidation of IMI-318 alloy in alkaline hydrogen peroxide solutions at room temperature.

with increase in both hydrogen peroxide and sodium hydroxide concentrations resulting in a porous surface. Dissolution of the two phases starts again towards the corrosion region.

Long oxide needles were seen to form on all coloured and corroded specimens. Their size as well as number increased towards corrosion region.

The black oxide region was studied closely by replicating specimens oxidised for various lengths of time. During the first 15 minutes etching of the surface takes place, this is followed (15-60 minutes) by rapid dissolution of the alloy and subsequent deposition of oxide on the two phases, leading to a rather rough surface and coherent coating. After one hour dissolution of this oxide and preferential attack on the beta phases begins leading to highly porous surface. Figures 4.8,9,10 & 11 show these observations.

The nature of the oxide formed in H_2O_2/NaOH solutions was studied by X-ray powder diffraction, reflection electron diffraction and colorimetric analysis based on the yellow-orange colour formed on addition of hydrogen peroxide to acidified solutions of titanium.

4.3.1 X-ray powder diffraction method

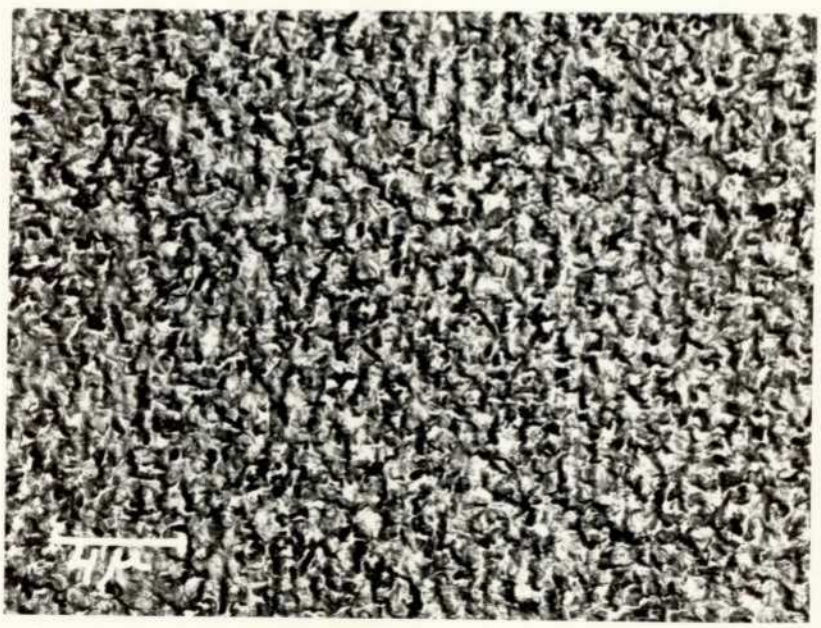
Samples removed mechanically from oxidised specimens did not reveal any oxide of titanium. The only diffraction lines obtained were those due to the alpha phase of Ti. Table 4.4 shows a typical set of d-values.

The absence of lines due to titanium oxide(s) does not imply that these oxides are definitely absent, it could well be that they are amorphous or nearly so. In fact the diffuse rings obtained with electron reflection diffraction method support the latter conclusion. Mechanical removal of the surface will always remove some subtrate but the absence of lines due to beta phase is explained in the following diagram.



(Original mag. 2,500X)

Figure 4.8 : Electron micrograph of IMI-318 alloy oxidised in hydrogen peroxide (0.05M)/sodium hydroxide (0.40M) for ten minutes at room temperature.



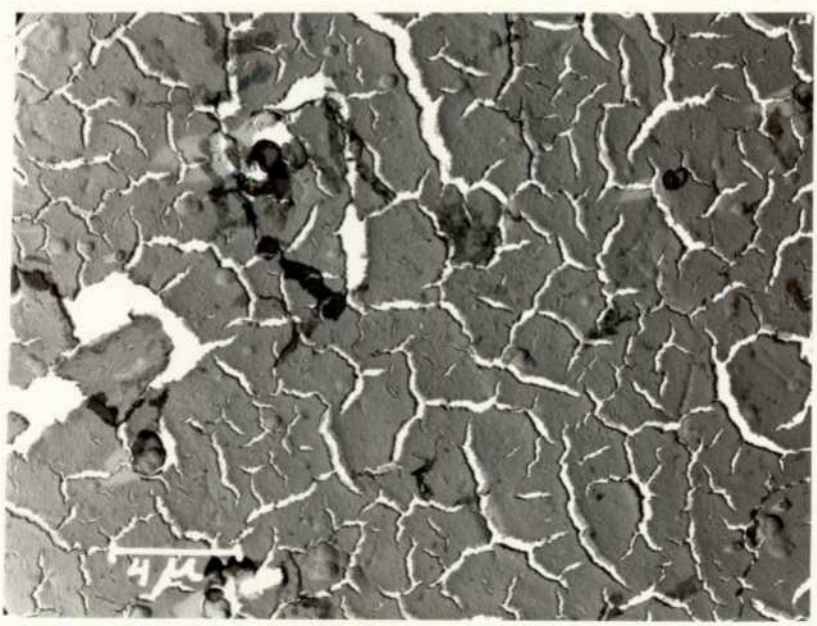
(Original mag. 2,500X)

Figure 4.9 : Electron micrograph of IMI-318 alloy oxidised in hydrogen peroxide (0.05M)/sodium hydroxide (0.40M) for one hour showing the coherent and rough oxide coating.



(Original mag. 2,500X)

Figure 4.10 : Electron micrograph of IMI-318 alloy oxidised in hydrogen peroxide (0.05M)/sodium hydroxide (0.40M) for two hours at room temperature..

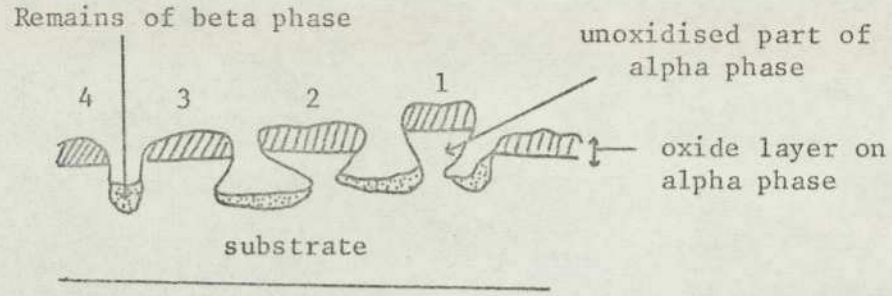


(Original mag. 2,500X)

Figure 4.11 : Electron micrograph of IMI-318 alloy oxidised in hydrogen peroxide (0.05M)/sodium hydroxide (0.40M) for 24 hours at room temperature showing a surface with alpha phases only . The surface is very porous due to preferential dissolution of beta phases.

Experimental Results		ASTM data for α - Titanium	
X-ray powder diffraction			
dÅ	Intensity	dÅ	Intensity
2.555	m	2.557	30
2.336	m	2.342	26
2.230	vst	2.244	100
1.710	m/w	1.726	19
1.470	m/w	1.475	17
1.325	m/w	1.332	16
-	-	1.276	2
1.236	m/w	1.247	16
-	-	1.233	13
1.172	vw	1.170	2
-	-	1.122	2
-	-	1.065	3
0.980	vw	0.989	6
0.935	vw	0.945	11
0.913	vw	0.917	10

TABLE 4.4 - X-ray powder diffraction data obtained from material mechanically removed from oxidised specimen (black oxide) in H_2O_2/NaOH.



Alpha phases 1,2,3 and 4 contain oxide as well as some unoxidised α-phase. Phases 1 and 2 can be removed easily as they are held on the substrate by small areas. It is believed that the unoxidised parts of α-phases similar to 1 and 2 are the source of diffraction lines observed.

4.3.2 Reflection electron diffraction

The method used was that of a glancing angle. This means that the intensities of lines recorded may not correspond with the ASTM data due to partial obstructions of the diffracted rays specially those near the centre of rings.

The experiment was repeated with several oxidised specimens. A typical set of d-values are listed in table 4.5 .

From table 4.5 it seems that the only "crystalline" oxide present at the surface is that of TiO_2-rutile.

The appearance of the diffraction lines suggests that the specimen contains some nearly amorphous material and the fact that only certain areas produced any diffraction lines at all indicated the considerable lack of uniformity.

Air oxidised		HF		HCl		H_2SO_4		H_2O_2/NaOH Black oxide		H_2O_2/NaOH Mauve oxide		Anodic oxide		ASTM data for TiO_2 - Rutile	
d Å	Int.*	d Å	Int.*	d Å	Int.*	d Å	Int.*	d Å	Int.*	d Å	Int.*	d Å	Int.*	d Å	Intensity
3.266	w	3.218	w	3.201	w	3.281	vw	3.266	vw	3.255	vw	3.295	vw	3.245	100
2.477	m/w	2.509	m/w	2.499	m/w	2.478	m/w	2.455	m/w	2.488	m	2.479	m	2.489	41
2.289	w	2.880	w	-	-	-	-	2.278	w	-	-	-	-	2.297	7
2.177	m	2.205	m	2.196	m	2.201	m	2.190	m	2.187	m	2.201	m/w	2.188	22
2.088	w	2.079	w	2.106	w	2.077	w	2.100	w	-	-	2.088	w	2.098	9
1.687	st	1.699	st	1.691	st	1.679	st	1.688	st	1.689	st	1.695	st	1.687	50
1.619	w	1.608	w	1.620	w	1.619	w	1.622	m	1.628	w	1.633	w	1.624	16
1.468	w	1.459	w	1.476	w	1.477	w	1.470	vw	-	-	1.478	vw	1.480	8
-	-	-	-	-	-	-	-	-	-	-	-	-	-	1.453	6
1.358	w	1.360	w	1.361	m	1.358	w	1.370	w	1.355	vw	1.359	vw	1.360	16
-	-	1.350	w	1.340	w	1.348	w	-	-	-	-	-	-	1.347	7
-	-	-	-	-	-	-	-	-	-	-	-	-	-	1.170	4
-	-	-	-	-	-	-	-	-	-	-	-	-	-	1.148	4

* Intensity v = very, st = strong, w = weak, m = medium.

TABLE 4.5 - Reflection electron diffraction examination of IMI-318 alloy surface given various treatments.

Specimens with yellow and mauve oxides were examined by this method. The results obtained were identical to those of the black oxide. It should be noted that samples oxidised for 20-30 minutes in the black oxide region produced sharper diffraction lines, implying that their surface is more crystalline than those oxidised for longer times.

4.3.3 Colorimetric analysis of the oxide coating formed on IMI-318 alloy in H_2O_2/NaOH solutions

The method used is based on the yellow-orange colour developed when hydrogen peroxide is added to acidified solution of Ti^{IV} ions. The colour is believed to be due to the peroxotitanyl group TiO_2^{2+} (aqueous)[129].

A calibration curve was prepared using TiO_2 (BDH assay> 98%) according to the method described by Scheffer[130]. Transmission was measured at 420 nm using 1 cm. Unicam glass-cell and doubly distilled water as reference, using SP500 Unicam Spectrophotometer. The TiO_2 used in preparation of the calibration curve was assumed to be 100% pure.

The reproducibility of application of this method was checked using TiO_2 (assay > 98%) obtained from British Titan Products (BTP). Assay found 98.48% and 98.54%. The Ti% in TiO_2 (BTP) was determined: 59.04% and 59.03%, (theoretical value is 59.995%).

The oxide coating was removed layerwise by dipping the oxidised specimens for 1½ minutes in a solution containing ammonium sulphate (A.R) in 98% sulphuric acid (1 gm salt per 10 ml acid) at $80^{\circ} \sim 85^{\circ}C$. This solution is known to dissolve all oxides of titanium and also oxidises any Ti^{+}, Ti^{2+} and Ti^{3+} to Ti^{4+}. This is important as the latter are the only ions capable of formation of TiO_2^{2+} ions. The last layer in each case was removed till the first signs of hydrogen evolution were seen. The solution was then diluted with water and hydrogen

Colour of oxide	Oxidation medium	Average distance from surface in μm	Percentage of titanium found
Mauve	H_2O_2(0.025M)/ NaOH(0.7M)	0.593	31.29
		1.016	34.59
		1.104	68.80
		1.186	83.90
Black	H_2O_2(0.08M)/ NaOH (0.3M)	0.440	37.04
		0.475	46.38
		1.105	87.60
Metallic Blue	air oxidation at 700°C for 10 minutes	0.482	60.75
		1.508	68.52
		2.149	80.73
		2.788	91.76
Grey Brown	air oxidation at 800°C for 5 minutes	0.497	60.38
		1.009	66.90
		1.391	74.60
		1.759	82.30

TABLE 4.6 - Colorimetric analysis of the oxide coating formed on IMI-318 alloy under various conditions of oxidation.

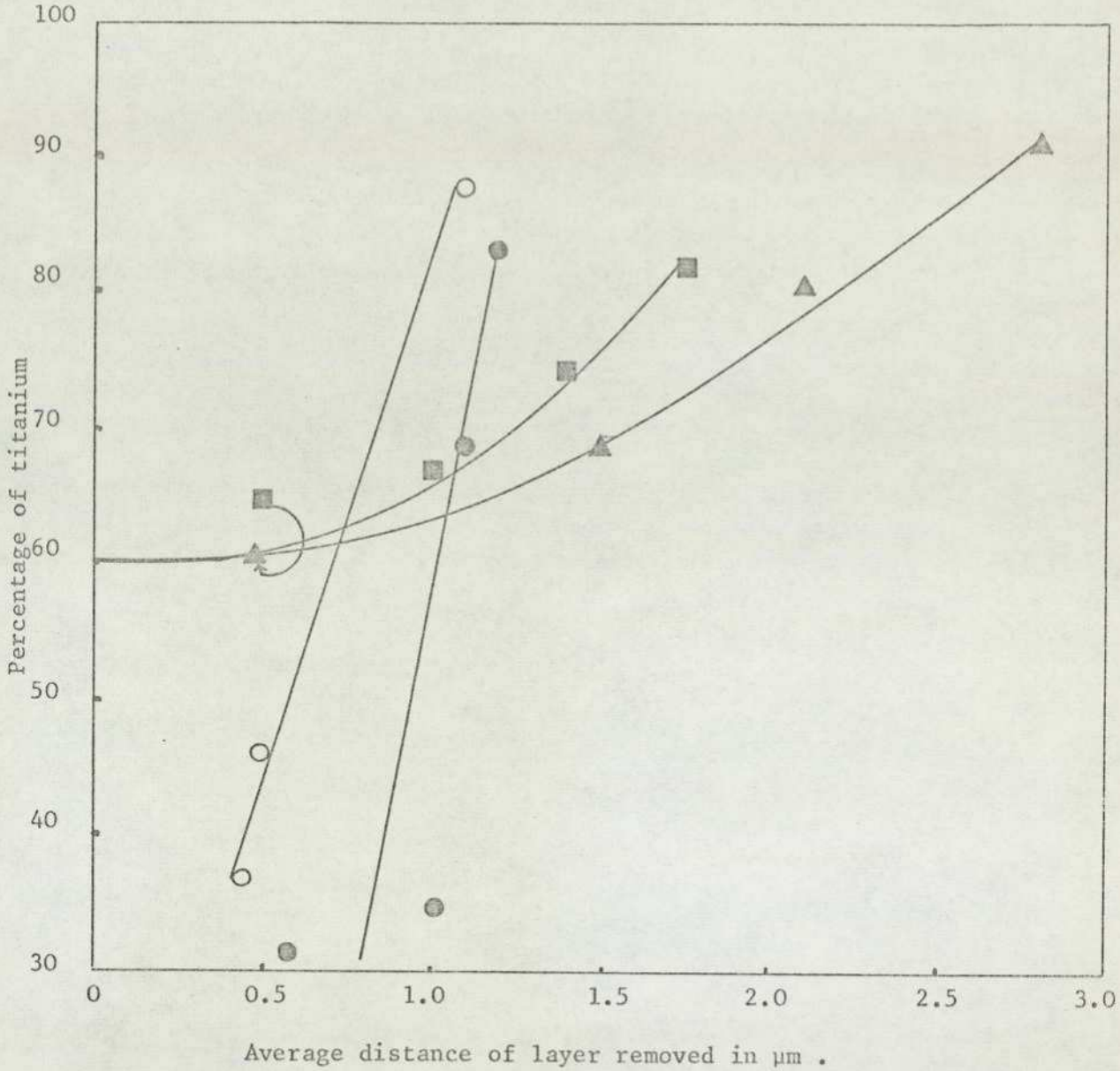


Figure 4.12 - Percentage of titanium in successive oxide layers.

● Mauve Oxide , formed in H_2O_2(0.025M)/NaOH(0.7M)

○ Black oxide, formed in H_2O_2 (0.08M)/NaOH(0.3M)

▲ Metallic blue, Air oxidation (10 minutes at 700°C)

■ Grey brown, Air oxidation (5 minutes at 800°C)

peroxide (AR 20 volume) to 100.0 ml in a previously calibrated volumetric flask. Absorbance was recorded after 3 hours. From the loss in weight of the oxidised specimens and their total surface areas, the average thickness of the oxide layer removed was calculated. Two specimens oxidised in alkaline hydrogen peroxide and two oxidised by heating in air were investigated by this method. Table 4.6 shows the results obtained and are represented graphically in figure 4.12 .

The results show that the oxide obtained by these methods is not any simple stoichiometric oxide of titanium, and that the colour of these oxides could not be due to excess of titanium, but could be due to excess oxygen. Hydration is another possibility which could lead to such results but oxidised specimens heated at 200°C for 24 hours suffered no loss in weight or change in colour.

4.4 Etching IMI-318 alloy with hydrochloric acid

The reaction between titanium and hydrochloric acid at room temperature is rather slow, but increases very rapidly with temperature. Hydrogen gas is evolved in the process according to the reaction:

$$2Ti + 6HCl = 3H_2 + 2TiCl_3$$

The colour of the solution obtained by this reaction is purple-mauve, which suggests Ti^{III} hydrated ions in solution. A UV/visible spectrum of the solution was recorded and absorption band was obtained at 490-500 nm. which corresponds to $[Ti(H_2O)_6]^{3+}$. These solutions were noted to change colour slowly on standing and colourless solutions were obtained within 2 weeks implying that Ti^{3+} was being oxidised to Ti^{4+}. This was attributed to oxygen dissolved in the solutions since solutions which had been freed from oxygen with pure nitrogen remained purple for 3-4 months.

The attack by HCl was studied by electron microscopy, by direct replication of etched specimens with 10% HCl at 100°C for various times. The acid attacks all phases to the same degree at the beginning, but after about an hour the interphase boundaries begin to dissolve at faster rates. After 1½ hours laminated structure begins to appear within each grain and after four hours a very rough surface is produced, as seen in figure 4.13 .

The final features on the surface are due to the lattice etching effect which shows the difference in orientation of the various grains. All the etched specimens had a grey coating which was examined by X-ray powder diffraction method, transmission and reflection electron diffraction. The only diffraction lines obtained from a powder mechanically removed, were those of alpha-phase titanium.

The grey coating was removed using bromine-methanol as previously described. Prior to stripping, the grey coating was strengthened by depositing alloprene (a chlorinated natural rubber prepared by ICI Limited) from chloroform solution on the specimens. Alloprene was removed later from the stripped coating by gentle washing with chloroform. Figure 4.14 shows some of the stripped coating, together with figure 4.15 the transmission electron diffraction pattern obtained at 100 kV.

No trace of any hydride was obtained and the diffraction rings seen in figure 4.15 correspond to spacings, 3.245Å and 1.687Å of TiO_2-rutile. These indicate that the grey coating is composed of almost amorphous oxide.

Reflection electron diffraction results indicate the presence of TiO_2-rutile at the surface. Table 4.5 shows a typical set of d-values obtained. The TiO_2 thus formed is believed to be due to hydrolysis of $TiCl_3$.



(Original mag.2,500X)

Figure 4.13 : Electron micrograph of IMI-318 alloy etched in (10%w/v) hydrochloric acid at 100°C for four hours.



(Original mag. 2,500X)

Figure 4.14 : Oxide coating (grey) formed on IMI-318 alloy when etched with hydrochloric acid.The oxide coating was removed with 10% w/v bromine in anhydrous methanol.



Figure 4.15 : Transmission diffraction pattern obtained from coating shown in figure 4.13 . The two rings seen above correspond to spacings 3.245 Å and 1.687 Å of TiO_2- rutile repectively. The diffuse rings indicate that the coating is composed of amorphous material.

Concentration of HCl (w/v %)	Temperature of test °C		
	20	40	60
0.5	0.0005*	0.0005*	0.009
1.0	0.0005*	0.008	0.012
2.5	0.007	0.008	0.012
3.0	0.008	0.015	0.088
5.0	0.018	0.020	0.795
10.0	0.018	0.308	1.583
20.0	0.044	1.008	3.215
30.0	1.635	5.225	25.775
30% HCl plus 0.1 mole nitric acid	0.008	0.091	0.205

* approximate measurement.

TABLE 4.7 Dissolution rate of IMI-318 alloy in hydrochloric acid at various temperatures as $gm/m^2/hour$.

Reaction of IMI-318 with hydrochloric acid solutions at elevated temperatures was studied using specimens 4 x 1 x 0.2 cm (total surface area = 10 cm^2). The specimens were suspended for 1 hour with platinum wire in 500 ml of solution. The temperature was controlled to $\pm$ 2°C. The difference between the initial and final weight of specimens was recorded to an accuracy of $\pm 10^{-4}$gm. The results obtained are shown in table 4.7 .

Presence of oxidising agents with hydrochloric acid reduces dissolution rate by a factor depending on the concentration of hydrochloric acid and the oxidising agent. For example, 0.1 mole of nitric acid in 30% hydrochloric acid solution causes a decrease in dissolution rate by a factor of 125. This is mainly due to oxidation of Ti^{3+} to Ti^{4+} and the latter increases the rate of TiO_2 (or hydrated oxides) formation which tends to passivate the alloy.

4.5 Etching IMI-318 alloy with sulphuric acid

Sulphuric acid attacks titanium at room temperature more than hydrochloric acid according to the reaction:

$$2Ti + 3H_2SO_4 = Ti_2(SO_4)_3 + 3H_2$$

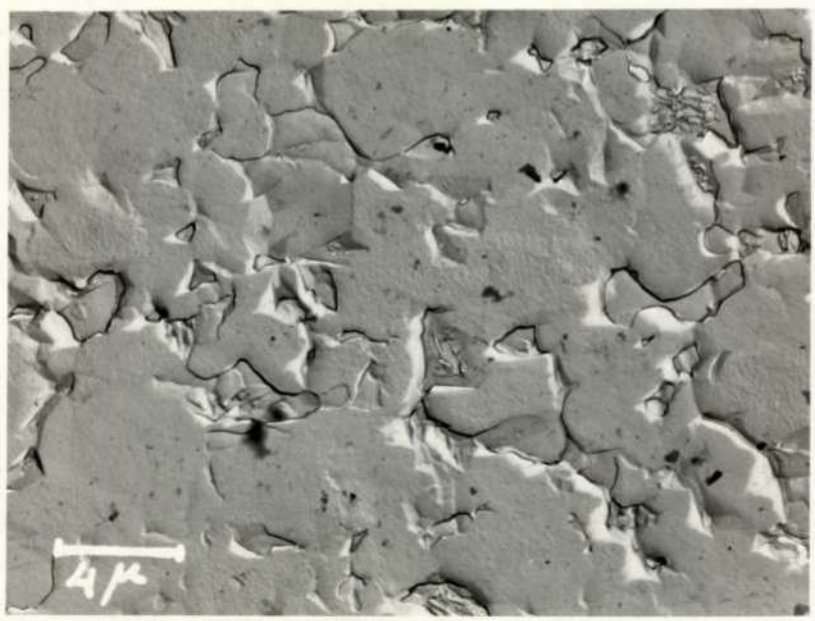
Titanium ions are held in solution as hydrated ions of the type $[Ti(H_2O)_6]^{3+}$ giving the solution a mauve colouration, and other complex ions of the type $[Ti(OH)_3HSO_4]$ and $[Ti(OH)_2\ HSO_4]^+$ (38)(45). The existence of $[Ti(H_2O)_6]^{3+}$ was confirmed as with hydrochloric acid with UV/visible spectroscopy.

The rate of dissolution increases with temperature. The mode of attack by boiling 10% (w/v) H_2SO_4 solution on IMI-318 alloy was followed in a manner similar to that used with hydrochloric acid, and although the final topographical features obtained are similar to those produced by hydrochloric acid, the mode of attack, however, differs considerably. Within the first 3 minutes only alpha phase is



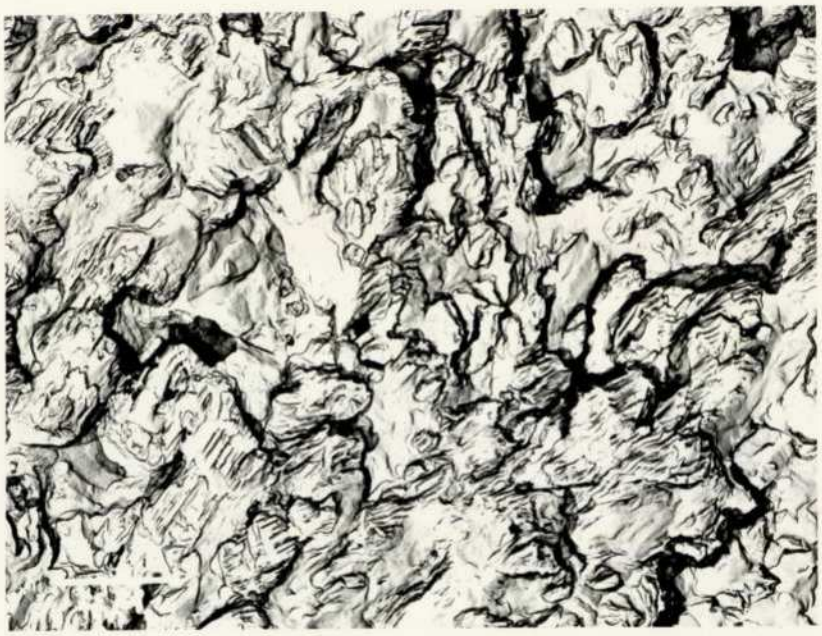
(Original mag. 2,500X)

Figure 4.16 : Electron micrograph of IMI-318 alloy etched in 10% w/v sulphuric acid at 100°C for two minutes. The fine structure seen is due to preferential dissolution of alpha phases leaving behind all beta phases.



(Original mag. 2,500X)

Figure 4.17 : Electron micrograph of IMI-318 alloy after etching in 10% w/v sulphuric acid at 100°C for 15 minutes, showing various beta phases . The fine structure within some of the beta phases is due to dissolution of alpha phase needles.



(Original mag. 2,500X)

Figure 4.18 : Electron micrograph of IMI-318 alloy after etching in 10%(w/v)sulphuric acid at 100°C for 3½ hours . cf.Fig.4.13 .

attacked leaving behind retained and transformed beta phases. It is worthwhile mentioning at this stage that as far as the author knows no one single etchant is available capable of showing those two types of beta phases. Figure 4.16 shows these phases clearly. The fine needle-like structure within the transformed beta is produced as a result of dissolution of alpha needles. Dissolution of alpha and some beta phases begins after that, leaving some beta phase relatively unattacked. The situation continues for about half an hour after which it does not follow a special pattern and a structure almost identical to that produced by hydrochloric acid is obtained, as seen in figures 4.17 and 4.18 . The colour of the etched specimens at this stage is grey. X-ray powder diffraction and reflection electron diffraction examination of the grey coating produced results identical to those obtained with hydrochloric acid (table 4.5) i.e. nearly amorphous oxide containing TiO_2-rutile with no hydride at all.

4.6 Etching IMI-318 and IMI-205 alloys with hydrofluoric acid

The reaction between hydrofluoric acid and titanium is rather vigorous and is accompanied by evolution of hydrogen. The initial reaction is:

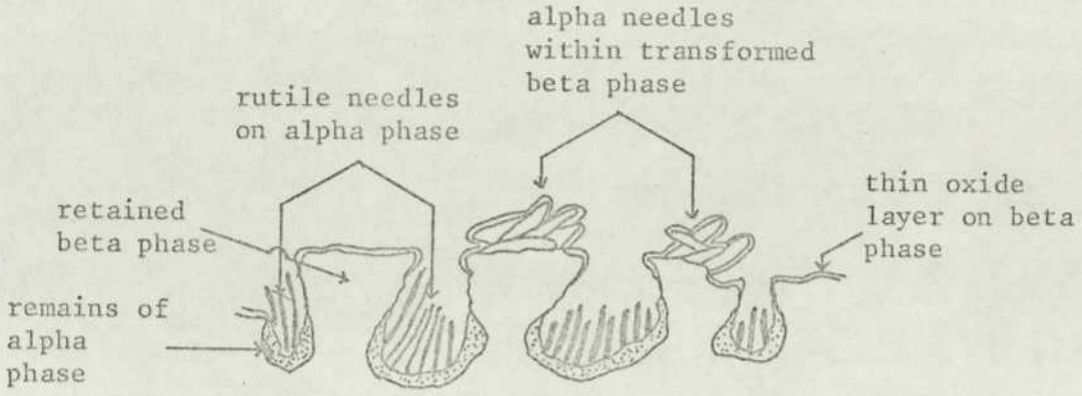
$$2Ti + 6HF = 2TiF_3 + 3H_2$$

This is followed by rapid hydrolysis of TiF_3 and/or formation of complex ions such as $[TiF_6]^{2-}$ which are stable in such aqueous media.

The mode of attack on IMI-318 alloy by hydrofluoric acid 4% (w/v) solution was followed by examination using electron microscopy. Initially,hydrofluoric acid attacks the alpha phase at a much faster rate than retained and transformed beta phases.

Eventually , a structure illustrated in figures 4.19 and 4.20 is

formed in which beta phase protruding well above alpha phases. The alpha needles within the transformed beta phase are attacked even less than the beta phase and the final state is represented by the following diagram, which is constructed from stereoelectron micrographs.



The fine structure seen on alpha phases is composed of oxide needles. Their height as judged from stereoelectron micrographs is of the same order as that of the retained beta phase. These needles have been shown to be TiO_2-rutile by X-ray powder diffraction method, and transmission electron diffraction. They have been successfully removed by several methods. The easiest, was to cover the etched surface with Araldite adhesive [131], curing the adhesive at 130°C for half an hour, and after cooling the specimen to room temperature, it was immersed in De Solv 8090[132]. This solvent is known to remove rapidly cured epoxy adhesives by penetrating along the interface. Rapid removal of the cured Araldite causes some of these needles together with some beta phases to break off. Further immersion leads to freeing of these detached needles and beta phase from the

Araldite and they sink to the bottom of the test tube while the Araldite remains floating. By repeating the whole procedure 3 to 4 times enough sample was isolated for examination by X-ray powder diffraction method.

The second method is similar to the previous method, except that cellulose acetate sheet was softened by swabbing with acetone and pressed firmly on the etched surface. Upon drying, some of the oxide needles usually break off and can be recovered by dissolving the cellulose acetate sheet in acetone. If the dried cellulose acetate sheet is replicated in the conventional manner for examination with the electron microscope, some of the oxide needles end up on the carbon replica when the cellulose acetate is dissolved. Figure 4.21 shows these needles. The second method was used to collect samples for X-ray powder diffraction and transmission electron diffraction, the results obtained are shown in Table 4.8 .

The final topographical features produced by hydrofluoric acid solutions are the same regardless of concentrations. Presence of oxidising agents such as nitric acid in hydrofluoric acid solutions slows down its reaction, leading to smoother surfaces because nitric acid oxidises the surface and in the presence of an oxide preferential attack is reduced. The oxide needles formed in such solutions are usually thicker and shorter than those produced by hydrofluoric acid alone. Their number decrease very rapidly with increasing nitric acid concentration. These features are illustrated in Figure 4.22 .

Reflection electron diffraction examination indicated the presence of TiO_2-rutile on the surface and that it is more crystalline than that produced by hydrochloric or sulphuric acids, as indicated by the sharper and better defined diffraction rings. The results obtained are contained in Table 4.5 .



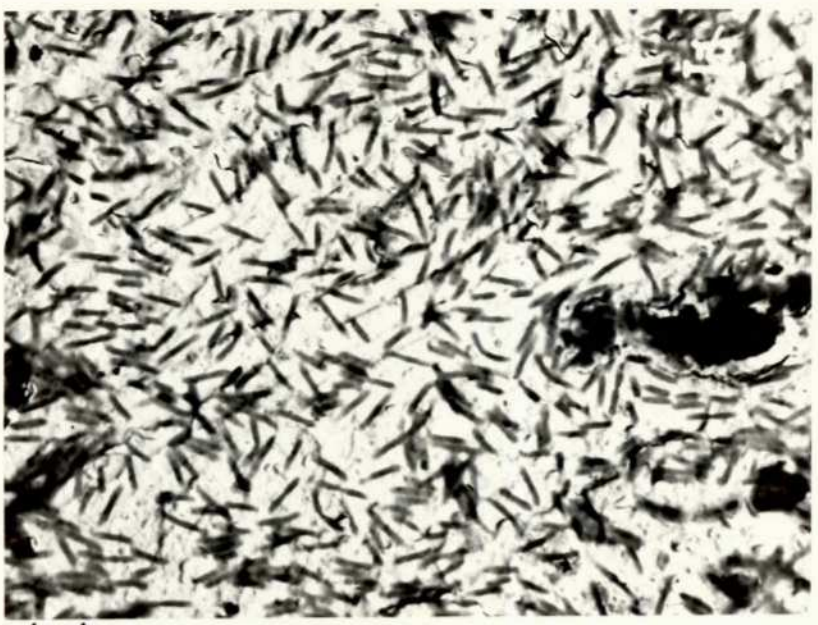
(Original mag. 2,500X)

Figure 4.19 : Electron micrograph of IMI-318 alloy etched for 1½ minutes at room temperature in 4% w/v aqueous hydrofluoric acid. The fine structure seen on alpha phases is due to oxide needles of TiO_2- rutile.



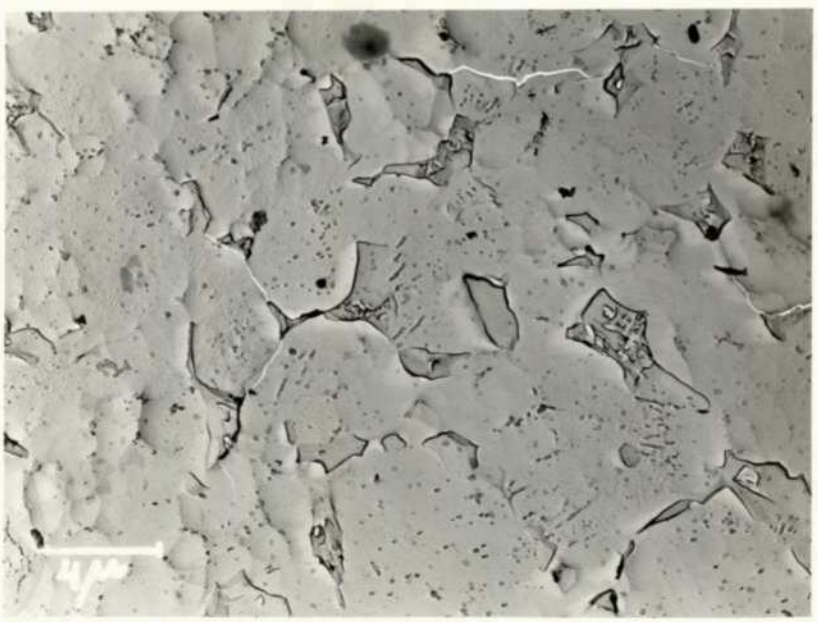
(Original mag. 10,000X)

Figure 4.20 : As in figure 4.19 , showing two types of beta phases with alpha phase needles within transformed beta phase.



(Original mag. 40,000X)

Figure 4.21 : Actual oxide needles of TiO_2 supported on a carbon replica. Transmission electron diffraction of these needles showed that they were TiO_2 -rutile.The actual data obtained are listed in table 4.8 .



(Original mag. 2,500X)

Figure 4.22 : Electron micrograph of IMI-318 alloy etched for 1½ minutes at room temperature in 4% w/v aqueous hydrofluoric acid containing 10% w/v nitric acid, showing fewer oxide needles on alpha phases cf. figure 4.19.

Experimental Results				ASTM data for TiO_2 - Rutile	
X-ray powder diffraction		Transmission electron diffraction			
dÅ	Intensity	dÅ	Intensity	dÅ	Intensity
3.238	vst	2.238	vst	3.245	100
2.487	m	2.485	st	2.489	41
2.291	vw	-	-	2.297	7
2.190	m	2.180	w/m	2.188	22
2.049	w	2.049	vw	2.054	9
1.691	st	1.690	st	1.687	50
1.624	m	1.619	w	1.627	16
1.481	w	1.477	w	1.480	8
1.463	w	1.449	vw	1.453	6
1.368	m/w	1.358	w	1.360	16
1.346	w	1.346	vw	1.347	7

v = very; st = strong; m = medium; w = weak.

TABLE 4.8 - X-ray powder and transmission electron diffractions of oxide needles formed on IMI-318 alloy when etched in hydrofluoric acid.

Experimental Results		ASTM data for MoO_3	
X-ray powder diffraction			
dÅ	Intensity	dÅ	Intensity
6.928	st	6.930	34
3.808	vst	3.810	82
3.462	vst	3.463	61
3.258	vst	3.260	100
3.010	vw	3.006	13
2.705	vw	2.702	19
2.653	m	2.655	35
2.607	vw	2.607	6
2.526	w	2.527	12
2.330	w	2.332	12
2.308	m	2.309	31
2.271	m	2.271	18
2.132	vw	2.131	9
1.992	vw	1.996	4
1.980	w	1.982	13

v = very; st = strong; m = medium; and w = weak.

TABLE 4.9 - Black powder formed on IMI-205 alloy when etched in hydrofluoric acid solutions, heated at 400°C for one week.

The reactions involved between hydrofluoric acid and IMI-205 alloy are similar to those of IMI-318 except that with hydrofluoric acid alone in solution, a black and rather loose material is formed on the alloy. This is known to be due to molybdenum[126]. The distribution of this powder is almost entirely on the beta phase areas as seen on freshly etched specimens . This is not surprising since molybdenum is mainly retained within the beta phase.

Addition of nitric acid to hydrofluoric acid solutions reduce the amount the black powder formed, and at about 30% (w/v) nitric acid its formation is inhibited completely. This could be due either to formation of colourless oxide, or the black oxide is dissolving as it is formed, or both.

The black oxide formed in hydrofluoric acid was examined by X-ray powder diffraction method. No diffraction lines at all were obtained even with exposures as long as 24 hours, implying that it is composed of amorphous material. However, when the "black oxide" was heated at 400°C for one week its colour changed to greenish white. When the latter was X-rayed, numerous lines were observed and as seen from Table 4.9 they correspond to MoO_3, confirming that the "black and rather loose material" is due to molybdenum.

4.7 Electrolytic oxidation of IMI-318 and IMI-205 alloys

Titanium and its alloys are easily oxidised by anodic currents in aqueous electrolytes. The oxidised specimens are usually covered with "a coloured" oxide. The colour depends mainly on the applied potential. In 0.1N sulphuric acid solution, oxidation of IMI-318 and IMI-205 alloys produce the following colours between 8-60 volts.

Applied Potential In Volts	Colour of oxide coating
8	Yellow
15	Orange/mauve
18	Mauve
24	Blue
30	Blue (metallic)
40	Yellow/blue
50	Yellow (metallic)
60	Mauve/orange

The sequence of these colours was repeated several times by increasing the potential applied. Pitting was not observed even at potentials as high as 200 volts.

The observed colours arise from interference due to various thicknesses. Thick oxide layers can be obtained (by increasing the applied potential) on titanium because the oxide layer has a low electronic conductivity which prevents oxygen evolution in the process.

Transmission and reflection electron diffraction examination of the oxide formed anodically indicated that it was TiO_2-rutile. The diffuse character of the lines obtained indicated that it was not well crystallised. The anodic oxide always replicated the substrate and no visible change in topography was observed at all. Generally these oxides are coherent and firmly attached to the substrate.

A summary of conclusions regarding the nature as well as crystallinity of oxide coatings formed by different oxidation methods is contained in table 4.10 .

Method of surface treatment	Colour obtained	Oregin of colour	Chemical nature of oxide formed	Crystallinity of oxide formed
Heating in air	Yellow Blue Mauve grey Black	interference	Rutile	Coherent and substantially crystalline
Alkaline hydrogen peroxide	Yellow Green Blue Mauve Grey Black	Different ratios of metal to oxygen	Unknown stoichiometry with some rutile	Short treatments give rather crystalline and coherent rutie layer . Prolonged treatments give incoherent oxide layer.
Anodic oxidation	yellow Blue Mauve	interference	Rutile	Very coherent and well crstalline at surface. Crystalinity decreased towards metal/oxide interface.
Etching in mineral acids	Grey	Uncertain	Rutile in amorphous matrix	Oxide needles formed in aq.HF on alpha phase are well crystalline,while oxide coating on beta phase is amorphous. HCl and sulphuric acid give rather amorphous oxide but more crystalline at the surface.

Table 4.10 - Summary of conclusions regarding oxides formed by different methods

4.8 DISCUSSION OF SURFACE CHEMISTRY

Metallographic examination of different sampels of IMI-318 alloy indicated that the alpha/beta ratio was not the same in each specimen implying they were either quenched from different temperatures within the (alpha + beta) field or they may have different thermal histories through annealing at different temperatures. Combination of the two reasons could not be ruled out. Exact thermal history of these alloys cannot be established from metallographic examinations alone. Tensile strengths,hardness measurements as well as phase identification by transmission electron microscopy and diffraction on the actual samples are required completely to establish their nature and hence history.

Distribution of the various phases as well as their size and shape indicate that the majority of the samples examined were quenched from different regions within the (alpha + beta) field, possibly 825^{o}C.

The napkin rings of IMI-318 alloy could have had a heat treatment at about 830^{o}C and possibly air cooled, as judged by the large and rather elongated alpha phase.

Similar conclusions, such as differences in quenching temperatures and thermal history apply to specimens of IMI-205 alloy. Samples which show rather elongated alpha phase are believed to have had a heat rreatment about 650^{o}C, as judged by the absence of any omega phase which appears in specimens given heat treatment between 450 - 600^{o}C.

The presence of different alpha/beta ratios in the two alloys had a great effect on the final topographical features obtained by chemical pretreatments. A factor which could have contributed to

the observed large scatter in bond strength values compared to those obtained with IMI-318 napkin rings which are known to have the same alpha/beta ratios.

The results obtained from oxidation in air are in agreement with those obtained by other workers. Failure to detect oxides of vanadium and aluminium by X-ray and electron diffraction does not necessarily mean that they are absent. Identification of oxides present in small amounts require specialised techniques such as microprobe analyses. The formation and disappearance of swelling of the beta phases in IMI-318 is possibly due to inclusion of vanadium pentoxide with rutile on beta phases.

Etching with hydrochloric and sulphuric acids left TiO_2-rutile on the surface of IMI-318. No hydride was detected even under conditions described by Chiganova and Batashev[43]. The decrease in thickness of the hydride layer which they obtained was not explained in their work and it could well be due conversion of the hydride to TiO_2, according to the equation:

$$2TiH_2 + 3O_2 = 3TiO_2 + 2H_2O$$

in which dissolved oxygen participates.

No trace of anatase or brookite was ever detected in this work. Koisumi and Nakayama[42] have obtained on commercially pure titanium under similar conditions a brookite layer in HCl and anatase in sulphuric acid beneath thorn shaped rutile crystals. No such crystals were observed in the present work.

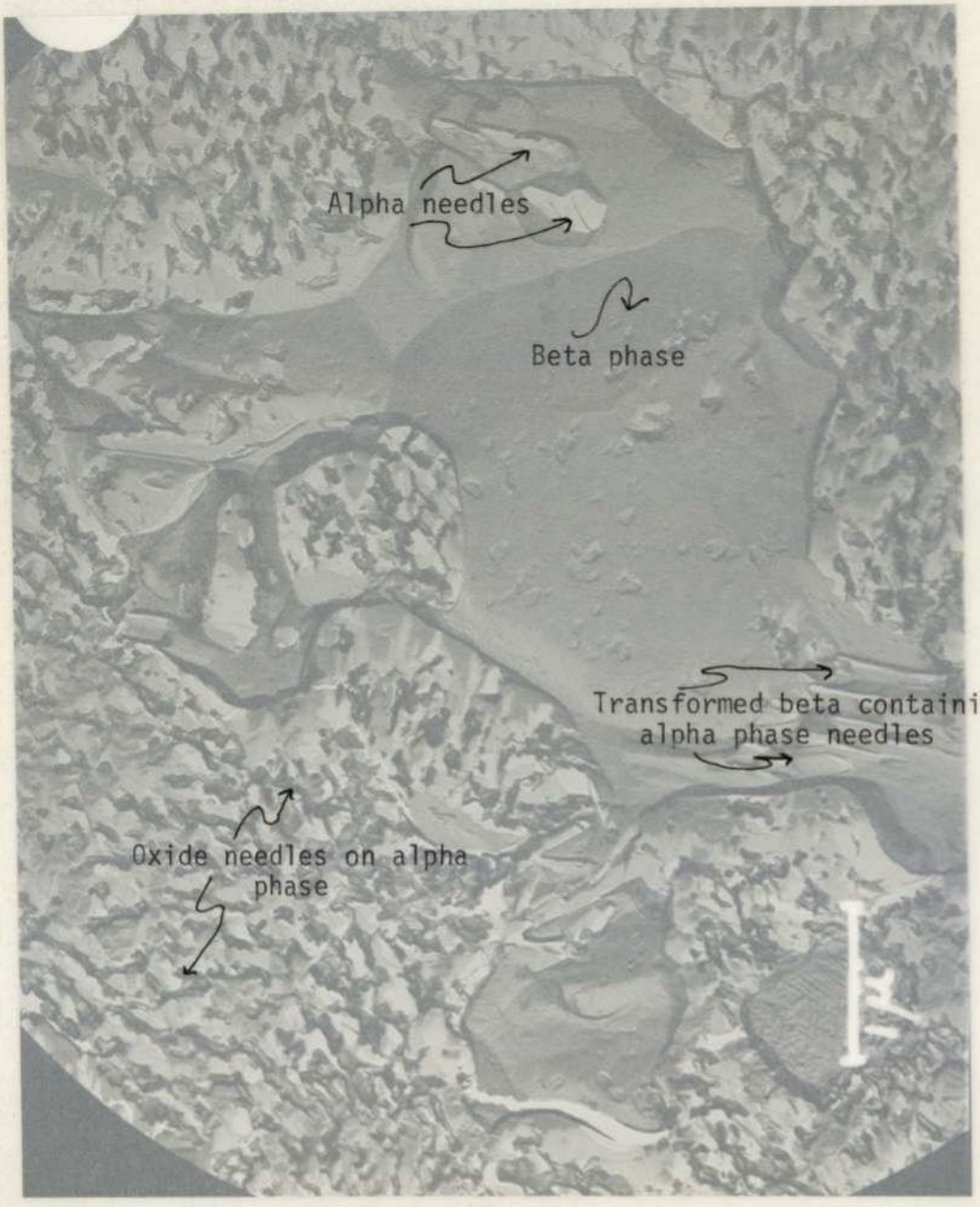
Etching by boiling for about 3 minutes in 10%(wt/vol)sulphuric acid has been shown to be the most satisfactory solution for

revealing in great detail both retained and transformed beta phases. This seems to be a new observation as no reports of any satisfactory single etching solution have been found. Most workers use two different methods to characterise the types of beta phase.

The chemical reactions involved in dissolution of titanium in hydrochloric and sulphuric acids are rather complex. It seems unlikely that Ti^{+} or Ti^{2+} will exist in acid solutions but are oxidised to Ti^{3+} (hydrated) which is stable in such media. Formation of TiO_2-rutile from such ions is still the subject of great controversy and no justified mechanisms are known apart from the participation of dissolved oxygen in the process.

Etching with solutions containing hydrofluoric acid has been shown to leave TiO_2-rutile with IMI-318 alloy on all phases. The TiO_2 formed on beta phases (retained and transformed) was smooth and continuous, while the TiO_2 formed on alpha phases was mainly needles. A possible explanation for their formation on alpha but not beta phases is that aluminium oxide, which is known to form in such media, forms nuclei on which TiO_2 grows. (Aluminium is almost entirely retained within the alpha phases). Further evidence comes from the fact that the alpha needles within the transformed beta phase which have very little aluminium, had no TiO_2 needles. These facts are shown clearly in Figure 4.23 .

Lack of specimens as well as the formation of molybdenum oxide of unknown composition on IMI-205 alloy in solutions containing hydrofluoric acid, hindered examination of such surfaces in great detail, but the existing evidence points out that this oxide is rather loose and nearly amorphous and that it is mainly formed on beta phase.



(Original mag. 10,000X)

Figure 4.23 : Electron micrograph of IMI-318 alloy etched for 1½ minutes at room temperature in 4% w/v hydrofluoric acid. It shows clearly that oxide needles are formed on the large alpha phases only. No such needles are formed on beta phases or alpha phase needles within the transformed beta phase.



(Original mag. 10,000X)

Figure 4.23 : Electron micrograph of IMI-318 alloy etched for 1½ minutes at room temperature in 4% w/v hydrofluoric acid. It shows clearly that oxide needles are formed on the large alpha phases only. No such needles are formed on beta phases or alpha phase needles within the transformed beta phase.

Alkaline hydrogen peroxide solutions leave amorphous oxide which has been shown to contain some TiO_2-rutile. The results obtained from estimation of titanium in successive layers indicate that the various colours observed on oxidised specimens are definitely not due to excess metal but excess oxygen. The observed colours in this case are due to movements of electrons within the oxygen layers in the lattice. Different ratios of metal to oxygen lead to different colours. On the other hand air oxidised specimens owe their colours to interference due to different thicknesses of rutile layer.

Electrolytic oxidation of IMI-318 and IMI-205 was carried out to produce coherent TiO_2 on the surface. The effects of pH and temperatures were not examined. The "colours" observed by Bianchi et al[50] on their anodically oxidised specimens and attributed by them to "excess metal" are more likely interference colours due to various thicknesses of oxide film.

The differences between this work and others could have originated from presence of the alloying elements. Most of the published work was carried out with the so called commercially pure titanium and it should be noted that this material produced by different methods and from different sources will contain different impurities.

4.9 Etchants for titanium and its alloys

An etchant acts by dissolving the oxide which is present on the surface. Solutions containing hydrofluoric acid serve such purpose but the reaction is vigorous and generally an oxidising agent is added to show the rate of attack. The three recipes for etching mentioned earlier are probably based on trial and error. No explanations were given to justify the presence of the various additives or their proportions, or the role which they play during etching.

The oxidation agent probably serves the following purposes:

a. It slows down the rate of attack and the process can be controlled more easily.

b. It minimises the loss in weight of material being etched.

c. It helps to remove surface contamination, by rendering it soluble.

d. It reduces "pick up" of hydrogen which is usually evolved in the etching process.

All the three etching recipes mentioned contain an oxidant, e.g. chromic acid, in which titanium and its alloys passivate; phosphoric acid which can act as an oxidising agent.

The choice of additives is also influenced by the alloying elements e.g. any recipe for etching an alloy containing molybdenum which does not include nitric acid in large amounts will leave a black and rather loose molybdenum oxide on the surface.

Hydrochloric or sulphuric acids have received very little attention in this field and as has been demonstrated earlier they can produce a very desirable surface for bonding.

CHAPTER 5

PRELIMINARY EXPERIMENTS

		Page
5.1	Bonding IMI-318 alloy and mild steel with Araldite.	112
5.2	BSL-308 Adhesive.	115
5.3	Hidux 1197C Adhesive.	115
5.4	Bonding IMI-318 alloy with BSL-308 adhesive.	116
5.4.1	Method of preparing the joints and testing.	116
5.4.2	Effect of pressure and temperature during curing on bond strength.	119
5.5	Effect of etching IMI-318 alloy on bond strength.	125
5.6	Oxidation in alkaline hydrogen peroxide and bond strength.	131

5.1 Bonding IMI-318 alloy and mild steel with Araldite

Pending the arrival of the napkin ring torsional shear testing apparatus, preliminary experiments were made with torque spanner and the well known lap shear joints. The torque spanner was taken from work reported by Holloway and Walker [133] in which steel specimens (napkin rings and solid bars) were bonded and removed by means of a recording torque spanner, the force applied being a shear force only.

The work started by testing reproducibility of bonds made with Araldite (AV100 and HV100) with mild steel and IMI-318 alloy as the adherends. The steel specimens were cut from one hexagonal bar 2.5 cm long and one end was machined to 1.0 cm in diameter, thus providing an area 0.788 cm^2 for bonding.

Both adherends were polished to 1μm smoothness and were solvent degreased in benzene, carbon tetrachloride and acetone before each experiment. Drying was carried out under vacuum at room temperature for at least 20 hours.

The adhesive was prepared by mixing manually equal weights of "adhesive" and "hardener" (to within $\pm 10^{-3}$gm), it was then applied to both adherends and cured at the desired temperature. No pressure was applied.

Testing was carried out at room temperature using a torque spanner[134] fitted with a universal joint and capable of applying torques up to 13.72 N.m. The experiments were designed primarily for testing bond reproducibility. A summary of these results is contained in Table 5.1

Interfacial failure on both sides of the adhesive dominated all experiments, leaving on the average about 50% of the adhesive on each adherend. The general appearance of fractured surfaces indicate that failure was ductile in nature. Because of the variability

Experiment number	1	2	3	4	5	6
Operators A,B or C	A,B	A,B	A,B	A,C	A,B	A,C
Number of adhesive batches used	2	1	1	1	1	1
Total number of bonds made	20	20	32	32	32	32
Number of bonds tested by operator A,B or C	10A 10B	10A 10B	16A 16B	16A 16C	16A 16B	16A 16C
Curing temperature in ^{o}C	20	20	20	120	120	130
Mean bond strength in N m torque	2.99A 2.55B	4.43A 2.73B	3.58A 3.48B	12.25A 11.03C	11.79A 7.84B	12.68A 12.16C
Standard error of the mean	0.25A 0.26B	0.55A 0.93B	0.18A 0.34B	0.69A 0.32C	0.35A 0.81B	0.41A 0.42C

TABLE 5.1- (mild steel and IMI-318 alloy as adherends/"Araldite" adhesive).

Reproducibility of bond formation and torque spanner adhesion test.

experience comparison was made of the results obtained by different operators.

Air bubbles were seen to be present in all joints. It is believed that these bubbles were formed during mixing the two components of the adhesive. Their size as well as number decreased when the curing temperature was raised from 20°C to 120°C. It was soon apparent that mixing of the two viscous components of the adhesive was a source of difficulty and probably the cause of the very wide scatter obtained. The short shelf life of the mixed adhesive prevented the use of single batch for testing the reproducibility of bonds.

In Table 5.1 the standard error of the means vary very much between the results obtained by each operator which indicates that reproducible bond strengths were not achieved by this method.

There are basically four main reasons which could cause the large scatter:

a) Presence of air bubbles which was not eliminated.

b) Manual mixing of the adhesive components did not produce homogenous compounds.

c) The rate of turning the torque spanner cannot be standardised, leading to different strain rates.

d) Variation in adhesive bond thicknesses.

None of these faults can be easily rectified, and these experiments, which were conceived as preliminary studies, were discontinued. But it is interesting to note that increasing curing temperatures increased bond strengths considerably. This is undoubtedly due to presence of fewer air bubbles within the adhesive bond. Further work therefore avoided the use of two component adhesives and concentrated on the two modified epoxy adhesives BSL-308 and Hidux 1197C.

5.2 BSL-308 adhesive (also known as Redux BSL-308) made by CIBA-Geigy, is said to be a modified epoxy adhesive employing a blend of resins based on bis-phenol A together with a hardner and is supplied as an unsupported film of about 0.010 inch thick. It contains dispersed aluminium powder and carbon black. The film is supplied sandwiched between protective sheets and has a shelf life of at least 12 months when stored at room temperatures.

The film was cut to size and shape before removing the protective sheets and placed on the area to be bonded. The film sometimes required gentle warming to be tacked in the desired position.

5.3 Hidux 1197C adhesive: made by CIBA-Geigy, is said to be a modified epoxy phenolic-adhesive, and is supplied as a film (0.016 inch thick), supported on a glass cloth carrier and contains aluminium powder. It is green in colour, with protective polythene sheets on either side.

It has a shelf life of three months at room temperature which can be increased to six months if stored at $0^{o}C$.

The film was used in a manner similar to BSL-308.

5.4 Bonding IMI-318 alloy with BSL-308 adhesive

5.41 Method of preparing the joints and testing

A jig shown in figure 5.1 was constructed to secure up to 10 lap joints. In order to minimize friction between the laps and the jig walls, steel rods of desired diameter were placed vertically between the two. Pressure was applied to the laps by a compression spring. When the joints had been assembled, the jig was placed in an air oven at the appropriate temperature for 90 minutes to cure the adhesive. The jig was removed and allowed to cool to room temperature with the joints still under pressure.

The small overlapping areas of only 0.78 to 0.80 cm^2 had to be employed to obtain breaking loads within the range of the Instron model 1026 tensile test machine seen in Figure 5.1a .

The machined laps were polished to 1μ smoothness using the conventional methods. Water was used as a lubricant. The laps were solvent degreased using trichloroethylene (or dichloromethane) and dried ca. 50°C. They were used in this condition or subjected to the desired pretreatment, followed by flushing with water and given an acetone rinse before drying.

Adhesive bond thickness was taken to be the difference between the thickness of the bonded joint and the total thickness of the laps and the mean of four readings quoted. The lap joints were tested by clamping them vertically and sheared at a constant rate of 5cm/minute jaw separation. The work started by finding the optimum conditions for bonding.

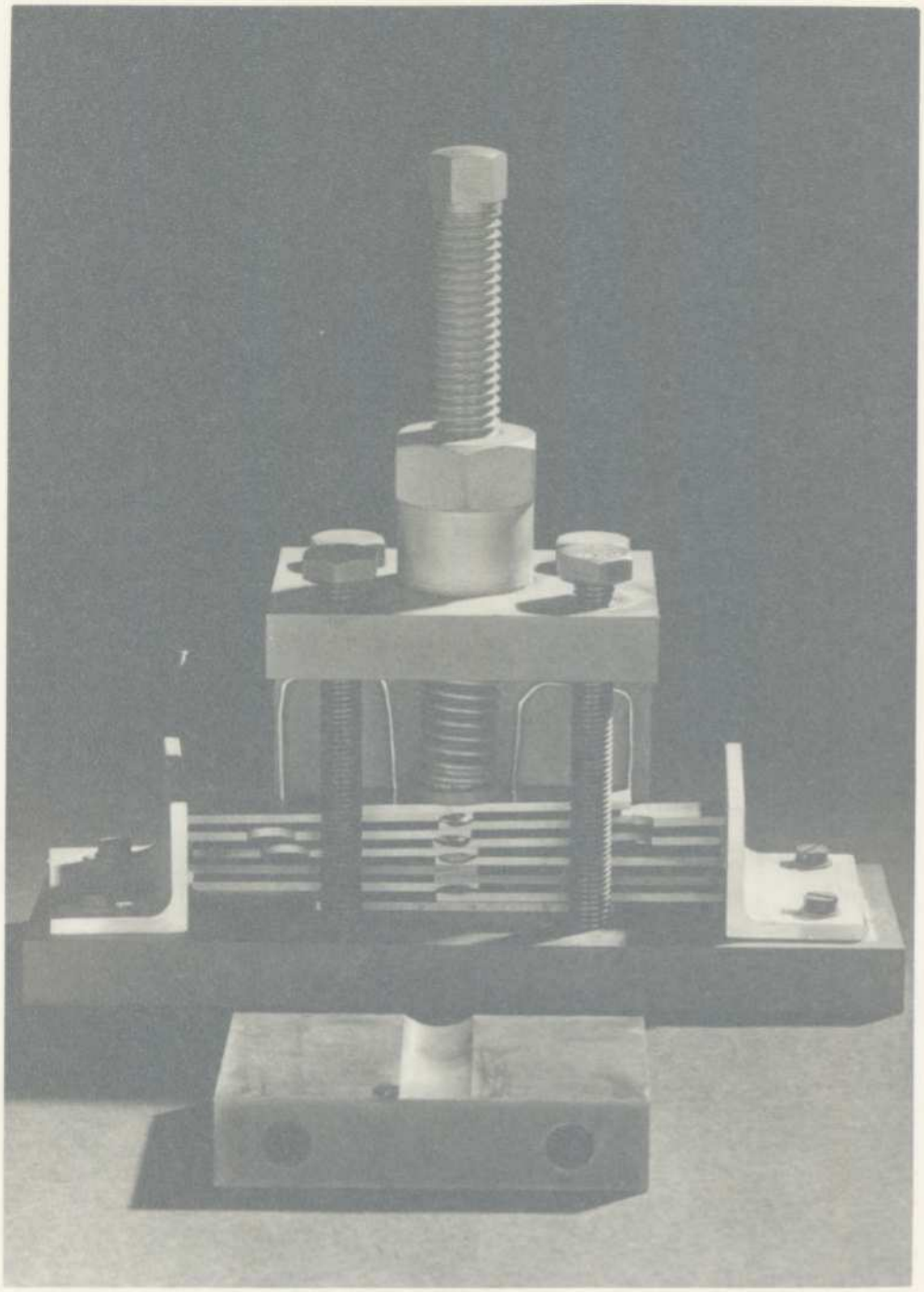
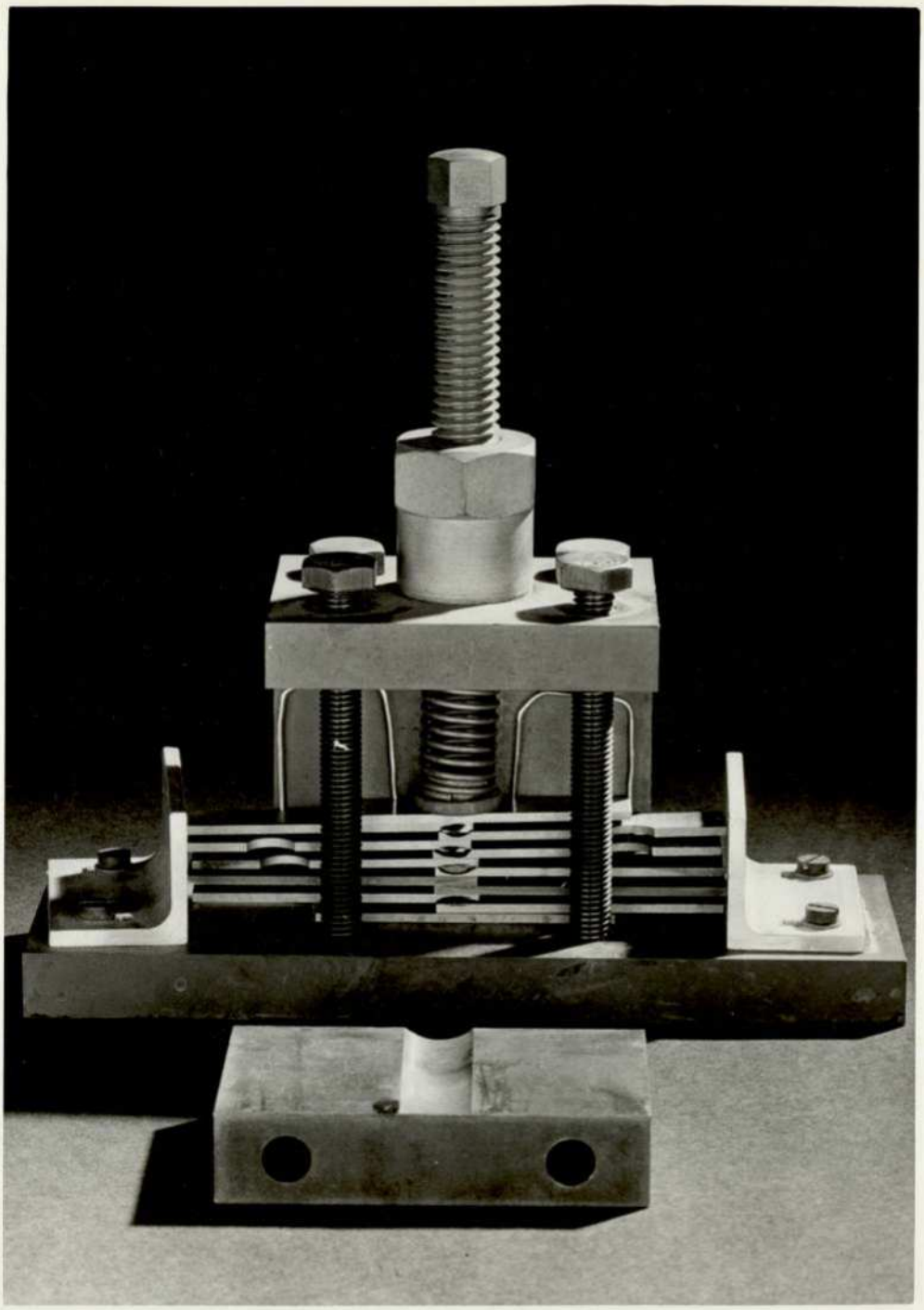


Figure 5.1 : Exposed view of the jig employed in section 5.4.1. One side has been removed to show the arrangement of laps and compression spring.



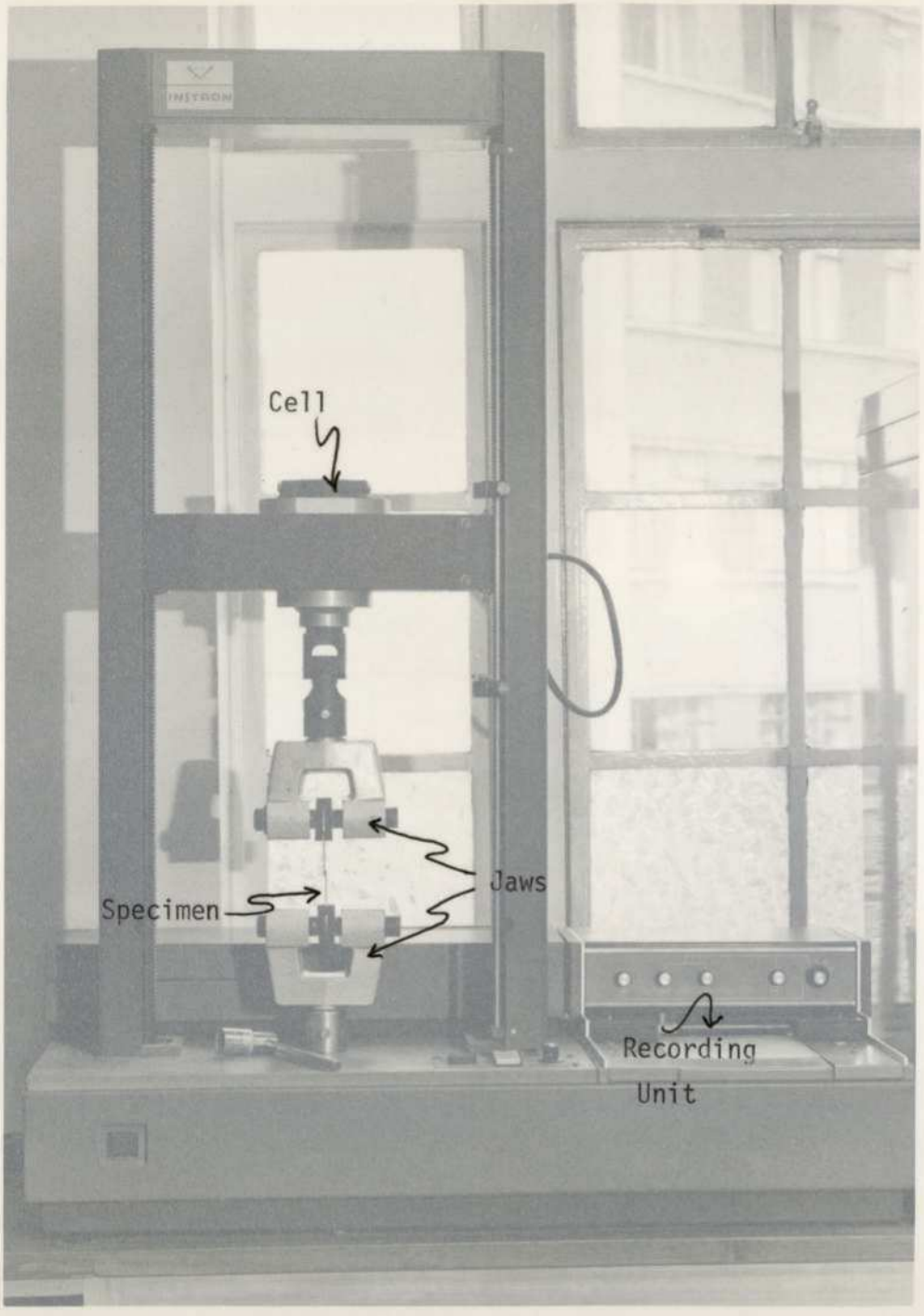
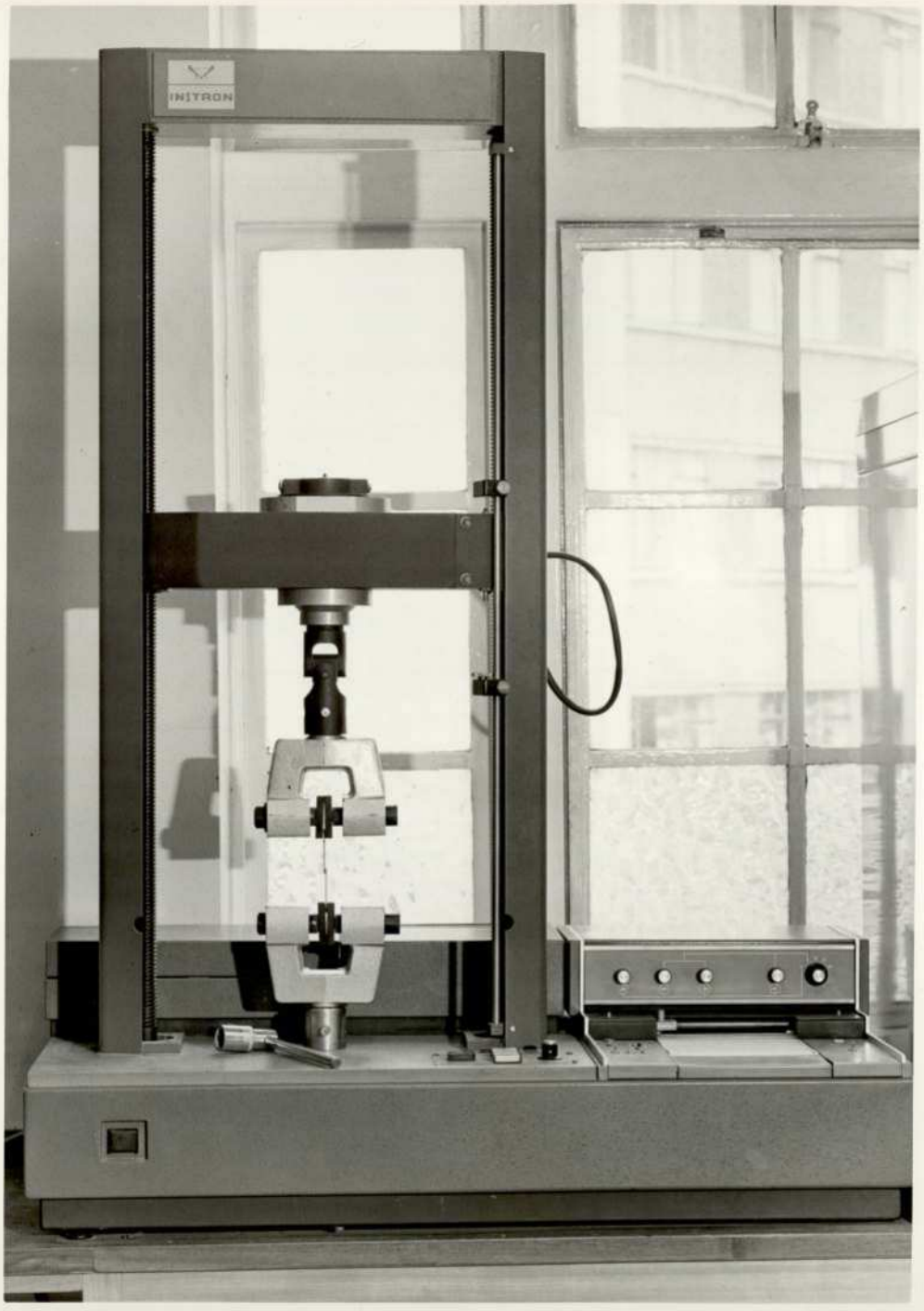


Figure 5.1a : The Instron tensile test machine model 1026.


INSTRON

5.42 Effect of pressure and temperature during curing on bond strength

In order to ensure that all laps have similar surfaces, they were etched for one minute in aqueous hydrofluoric acid 4% (w/v). The results obtained are shown in Table 5.2

From the results, the following analysis of variance table was calculated. The units used in calculations are c.g.s. as the ratio of variance is not affected these are not converted to SI units.

Source of Variance	Sums of Squares	Degrees of Freedom	Mean Squares	Components of Variance
Between temperatures (T)	24592.5	3	8197.5	$\eta_2\eta_3\sigma_1^2 + \eta_3\sigma_{12}^2 + \sigma_o$
Between pressures (P)	586.1	2	283	$\eta_1\eta_3\sigma_2^2 + \eta_3\sigma_{12}^2 + \sigma_o$
Interaction (P x T)	8274	6	1379	$\eta_3\sigma_{12}^2 + \sigma_o^2$
Residual	28972.5	12	2414.4	σ_o^2
Total	62425	23		

Where η_1 = number of temperature levels used in the experiment.

η_2 = number of pressure levels used in the experiment.

σ_1^2 = variance due to differences between temperatures.

σ_2^2 = variance due to differences between pressures.

σ_{12}^2 = (P x T) interaction.

σ_o^2 = residual error.

Since the mean squares ascribed to the pressure effect 283, is much less than the residual, the effect of pressure is not real, i.e. pressure has no effect on bond strength over the range investigated.

Adhesive bond thickness $X10^{-3}$cm	Curing temperature ^{o}C	Pressure applied kg/cm^2	Tensile shear stress in MN/m^2	
7.6	160	2	48	
7.6	160	2	53	
6.3	160	5	47	Mean = 48.50
6.3	160	5	48	
5.1	160	10	46	S.E.M = 0.99
5.1	160	10	49	
6.4	170	2	53	
5.6	170	2	52	
5.1	170	5	54	Mean = 51.50
3.3	170	5	49	
3.1	170	10	52	S.E.M = 0.85
3.8	170	10	49	
6.6	181	2	56	
5.6	181	2	46	
5.3	181	5	53	Mean = 51.50
5.7	181	5	50	
5.8	181	10	60	S.E.M = 2.47
7.1	181	10	44	
5.8	193	2	57	
6.6	193	2	48	
3.6	193	5	62	Mean = 57.33
4.3	193	5	59	
3.3	193	10	62	S.E.M = 2.12
4.1	193	10	56	

TABLE 5.2- (IMI-318 alloy/BSL-308 adhesive)

Effect of temperatures and pressures during curing on bond strength.

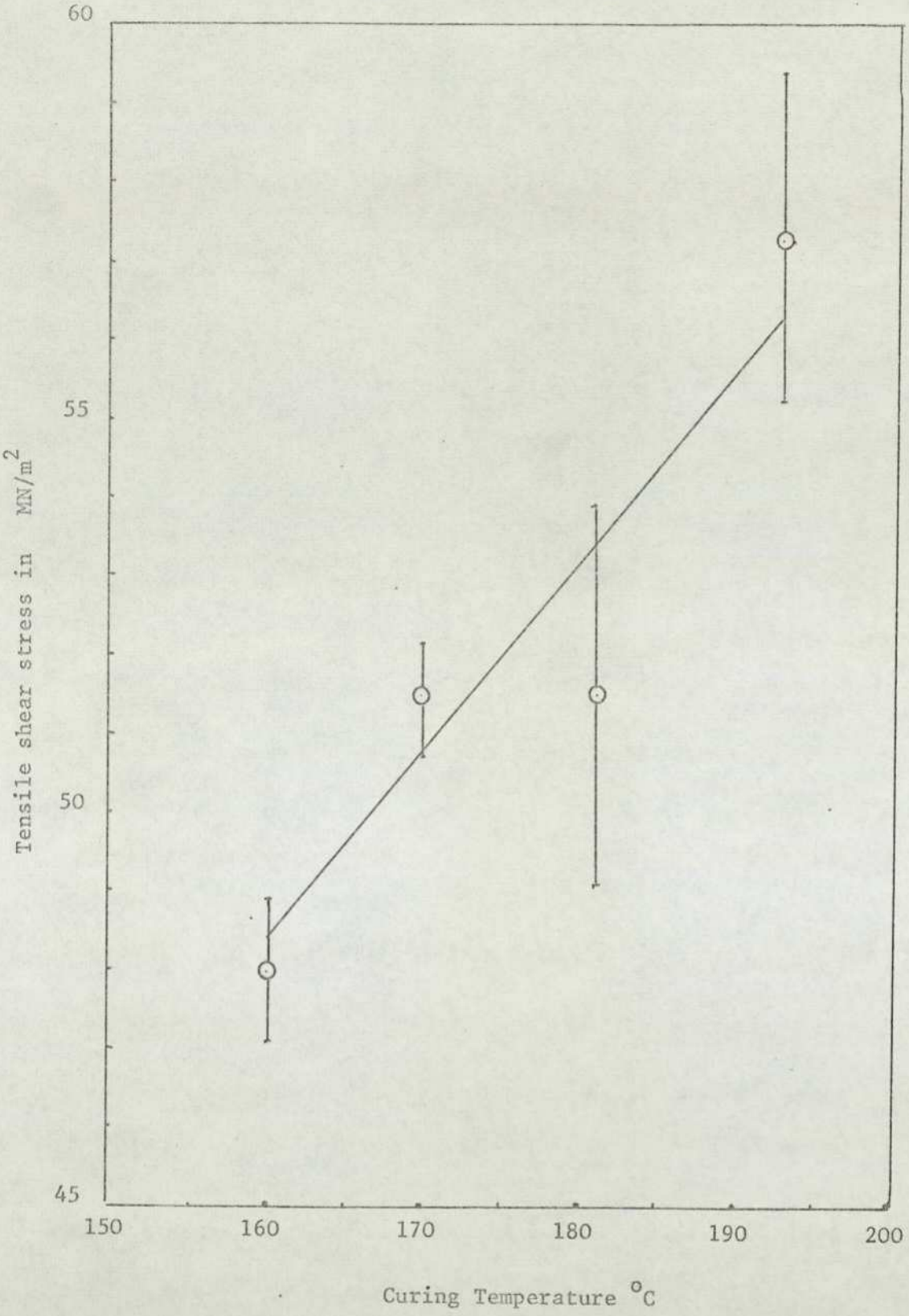


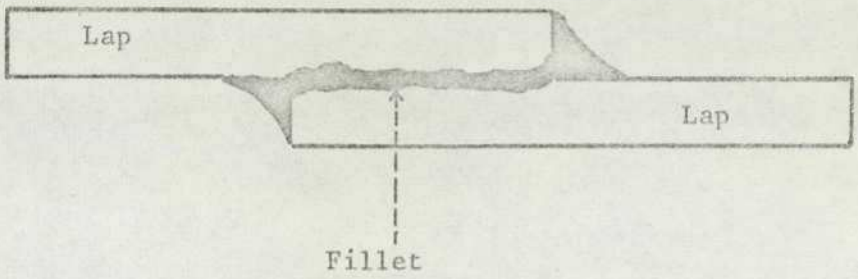
Figure 5.2 - (IMI-318 alloy/BSL-308 adhesive)

Effect of curing temperature on bond strength

Again since the mean squares of P x T interaction is less than the residual, the term $n_3\sigma^2_{12}$ is unreal, i.e. pressure and temperature do not interact over the range investigated.

Accordingly the residual sums of squares should include those ascribed to pressure and P x T interaction and thus the total number of degrees of freedom involved becomes 20; hence the mean square ascribed to experimental error (σ^2_o) = 37832 ÷ 20 = 1892. This figure can be used as a base against which to assess the significance of temperature by the well-known F - ratio test. In this case F = 4.33 whereas the tables give, at the 2.5% level with degrees of freedom 3 and 20, F = 3.86 implying that the temperature effect is real and as seen from figure 5.2 bond strength is roughly proportional to curing temperature over the range 160 - 192°C. These results are in line with the manufacturers recommendations. A pressure of 3 ∿ 3.5 kgf/cm^2(0.029-0.034 MN/m^2) and a temperature of 175° ± 2°C were adopted, and all future experiments were carried out under these conditions.

Because of the small overlap used in these experiments it was thought that the cured adhesive present on the sides of joints, as illustrated in the diagram below, contribute towards the observed scatter in bond strength. An experiment was designed to investigate this effect.



21 lap joints were prepared with the fillets either untouched, removed completely, or scratched around the edges. These were tested and the scatter of the results from each set compared and illustrated in Table 5.3 .

The adhesive on the sides of bonds evidently increases bond strength but produces larger scatter. (S.E.M. 1.99 greater than either of the other techniques. Scratching reduces scatter (S.E.M. 1.11) but not as much as complete removal of the surplus adhesive from the sides of the joints (S.E.M. 0.720). As a check on previously reported work and confirmation that no scatter was arising from thickness variation, the correlation between thickness and strength was calculated and found non-significant. This technique was therefore adopted for later experiments.

Adhesive bond thickness $X10^{-3}$ cm	Tensile shear stress in MN/m^2	Treatment
4.1	57	
5.8	53	
5.1	56	
7.9	49	Fillet left untouched
5.1	55	Mean bond strength = 56
6.4	50	Standard error of the
5.8	64	mean = 1.99
4.1	64	
4.6	53	
13.2	52	
7.3	56	Fillet was removed
5.8	53	from sides only.
10.7	51	Mean bond strength = 53
7.6	56	Standard error of the
7.6	52	mean = 0.72
10.2	51	
13.9	58	
17.3	53	Fillet was scratched
8.2	54	all round.
10.7	56	Mean bond strength = 56
11.4	58	Standard error of the
		mean = 1.11

TABLE 5.3- (IMI-318 alloy/BSL-308 adhesive)

The effect of "fillet" on bond strength and on their scatter.

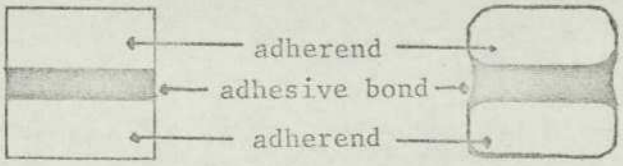
5.5 Effect of etching IMI-318 alloy on bond strength

Optimum conditions were determined by etching the adherends for different times. Since temperature increases the rate of reaction between titanium and hydrofluoric acid, and because the reaction is exothermic, etching was carried out using 250 ml solution each time in a beaker immersed in a large volume of water at 25°C. Etching times were controlled to an accuracy of ± 2 seconds.

the effect of aqueous hydrofluoric acid (4% w/v) and hydrofluoric acid (4% w/v) in saturated oxalic acid solution were investigated. The results obtained from both experiments are shown in tables 5.4 and 5.5 , and are illustrated graphically in Figure 5.3 after the tables .

Despite the large scatter in both experiments the results do indicate that etching increases bond strength and that etching with aqueous hydrofluoric acid leads to stronger bonds.

The mode of failure was followed using the conventional optical microscope. Plain polished specimens failed mainly at the interface with on physical damage to the substrate. The amount of interfacial failure decreased rapidly upon etching , all bonds made with etched adherends for ½ to 1½ minutes failed cohesively within the adhesive. Further etching caused substrate failure. The two phases of the alloy were clearly visible on the adhesive in some parts. In each case, bonds failed with the adhesive equally distributed between the adherends. Etching for longer than three minutes dissolved the sharp edge around the areas to be bonded as illustrated in the following diagram:



Before etching After prolonged etching

Adhesive bond thickness $X10^{-3}$cm	Etching time in minutes	Tensile shear stress in MN/m^2	Mean bond strength	Standard error of the mean
15.2	0	50		
12.7	0	50		
8.9	0	55	49.33	1.60
20.3	0	44		
12.7	0	46		
13.9	0	51		
11.4	0.25	58		
15.2	0.25	52	55.67	1.66
10.2	0.25	57		
7.6	0.75	63		
5.1	0.75	62	61.67	0.79
7.6	0.75	60		
7.6	1.00	56		
7.6	1.00	52		
10.2	1.00	51	52.17	1.68
7.8	1.00	49		
5.1	1.00	55		
6.3	1.00	50		
6.8	1.50	54		
11.4	1.50	51	56.33	3.92
9.2	1.50	64		
7.6	2.00	61		
7.6	2.00	54	59.00	2.38
7.6	2.00	62		
13.4	2.50	49		
14.5	2.50	59	56.67	4.07
7.1	2.50	62		
10.2	3.00	59		
7.6	3.00	57	57.00	1.05
15.2	3.00	55		
11.9	5.00	57		
17.3	5.00	57	59.67	2.58
12.5	5.00	65		
22.8	10.00	60		
25.4	10.00	52	56.33	2.45
17.8	10.00	57		

TABLE 5.4: (IMI-318 alloy/BSL-308 adhesive)
Effect of etching with aqueous hydrofluoric acid (4% w/v) for various times on bond strength.

Adhesive bond thickness $X10^{-3}$cm	Etching time in minutes	Tensile shear stress in MN/m^2	Mean bond strength	Standard error of the mean
8.9	0.50	59		
12.7	0.50	59	56.67	2.26
13.9	0.50	52		
17.7	0.75	54		
10.2	0.75	59	58.33	2.15
7.6	0.75	62		
7.6	1.00	49		
6.3	1.00	59	54.67	3.18
6.3	1.00	56		
10.2	1.50	61		
10.2	1.50	52	57.33	2.61
8.9	1.50	59		
7.6	2.00	51		
6.3	2.00	53	54.00	2.00
6.3	2.00	58		
7.6	2.50	59		
7.6	2.50	60	57.67	1.84
7.6	2.50	54		
7.2	5.00	54		
7.6	5.00	53	53.67	0.16
7.2	5.00	54		

TABLE 5.5 - (IMI-318 alloy/BSL-308 adhesive)
Effect of etching with hydrofluoric acid (4% w/v) in saturated oxalic acid aqueous solution for various times on bond strength.

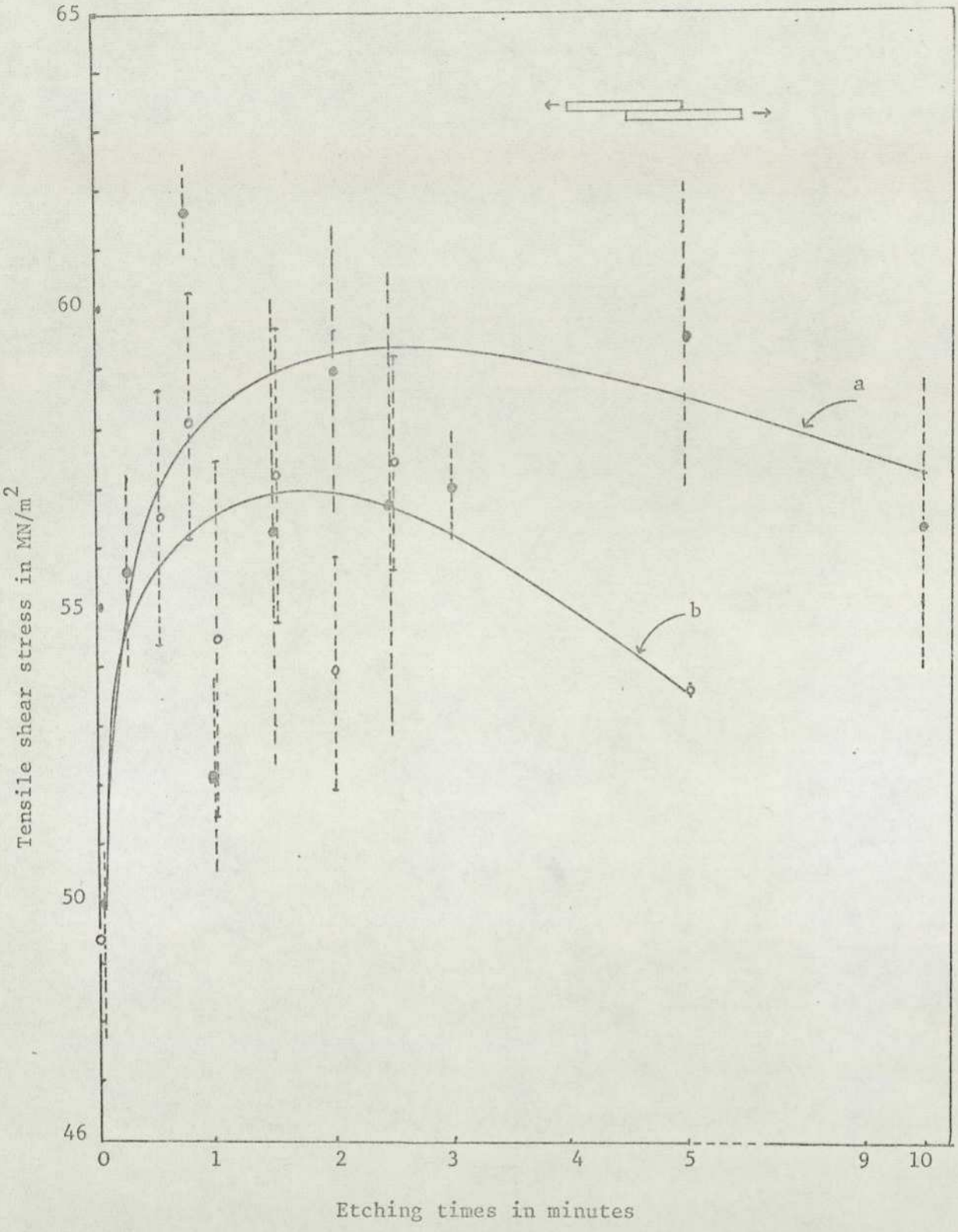


Figure 5.3 - Effect of etching with aqueous hydrofluoric acid (4% w/v) (● - curve a) and hydrofluoric acid (4% w/v) in saturated oxalic acid aqueous solution (o - curve b) for various times on bond strength.

Because of the nominal areas bonded ca. 0.65 cm^2 the presence of "adhesive wedge" around the bonded areas is beleived to have contributed to the observed decrease in bond strength obtained with specimens etched for longer than three minutes, presumably by changing stress distribution.

It is interesting to note that when fractured surfaces were soaked in formamide, the cured adhesive was released from polished specimens within half an hour at room temperature, but it required boiling for several hours before the adhesive was freed from the etched specimens. This is undoubtedly due to mechanical interlocking of the cured adhesive with the rough surface of the etched specimen.

The effect on bond strength by addition of nitric acid to aqueous solution of hydrofluoric acid (4% w/v) was investigated by bonding laps etched for two minutes . The results are shown in table 5.6 . Again large scatter was obtained. The correlation between bond strength and nitric acid concentration was examined and a non-significant value of the correlation coefficient (-0.437), with 12 degrees of freedom was obtained. This means that no correlation between bond strength and concentration of nitric acid exists.

The mode of failure changed from cohesive within the adhesive at low concentrations of nitric acid to interfacial at high concentration.

The large scatter observed in these experiments is believed to be mainly due to different surface roughness produced by the etchant. As has been illustrated previously , the roughness obtained is dictated by the volume of each titanium phase present at the surface. A real correlation between nitric acid added and bond strength could well have been obscured by this effect.

Adhesive bond thickness $X10^{-3}$cm	Concentration of HNO_3 %(w/v) in 4% (w/v)HF	Tensile shear stress in MN/m^2	Mean bond strength
7.6	0.75	61.61	62.78
6.8	0.75	64.01	
8.9	1.50	57.07	55.03
12.9	1.50	52.97	
5.8	2.25	61.31	59.19
5.2	2.25	57.07	
5.1	3.00	64.05	65.47
4.2	3.00	66.88	
6.3	3.75	63.45	62.85
6.3	3.75	62.26	
7.1	7.50	62.39	61.89
10.2	7.50	61.40	
10.2	11.25	54.34	55.28
12.7	11.25	56.21	
7.6	12.00	55.43	59.44
7.4	12.00	63.37	
7.6	15.00	54.84	51.96
7.4	15.00	49.05	
9.8	18.00	51.40	46.50
12.9	18.00	41.59	
11.4	22.50	54.41	56.60
8.9	22.50	58.86	
9.3	24.00	62.39	61.21
6.3	24.00	59.94	
11.9	30.00	50.12	52.32
12.7	30.00	54.54	

TABLE 5.6 - (IMI-318 alloy/BSL-308 adhesive)

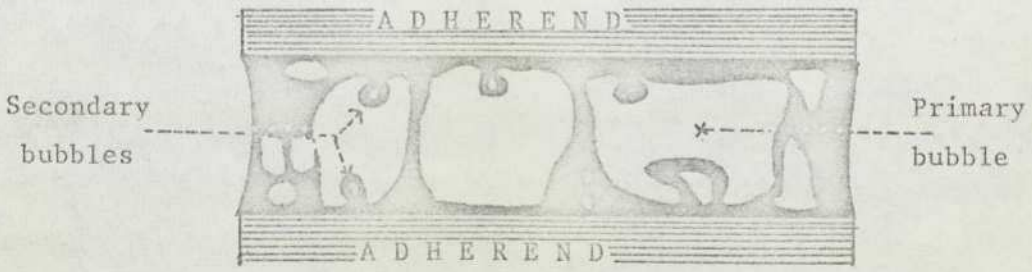
Effect of addition of nitric acid to 4%(w/v) hydrofluoric acid on bond strength.

5.6 Oxidation in alkaline hydrogen peroxide and bond strength using IMI-318 and BSL-308

An experiment was designed to find the best oxide layer leading to strong bonds. Laps were oxidised in hydrogen peroxide/ sodium hydroxide solutions at 20°C for 72 hours, washed with acidified water, water alone and finally acetone. Their colour was recorded after the specimens had been dried at 100°C for one hour. The specimens were grouped according to their oxide colour. The results obtained are shown in Tables

The fractured surfaces were examined by optical microscopy and the following observations were noted:

All joints (except those of group A - Table 5.7) had large bubbles within the adhesive. The size and number of these bubbles varied not only within each group but also between groups. Bubbles as large as 3 x 2 mm were seen in some bonds. Figure 5.4 is an actual photograph showing these bubbles. Their source was traced to entrapped gases within the adherend surface. Expansion of these gases during curing led to the formation of bubbles within the adhesive. Some secondary bubbles were seen within the primary ones as illustrated in the following diagram:



The absence of these bubbles near the edges of bonded areas and the formation of secondary bubbles indicated that their source was the adherend. Presence of these bubbles obviously affected the measured bond strength.

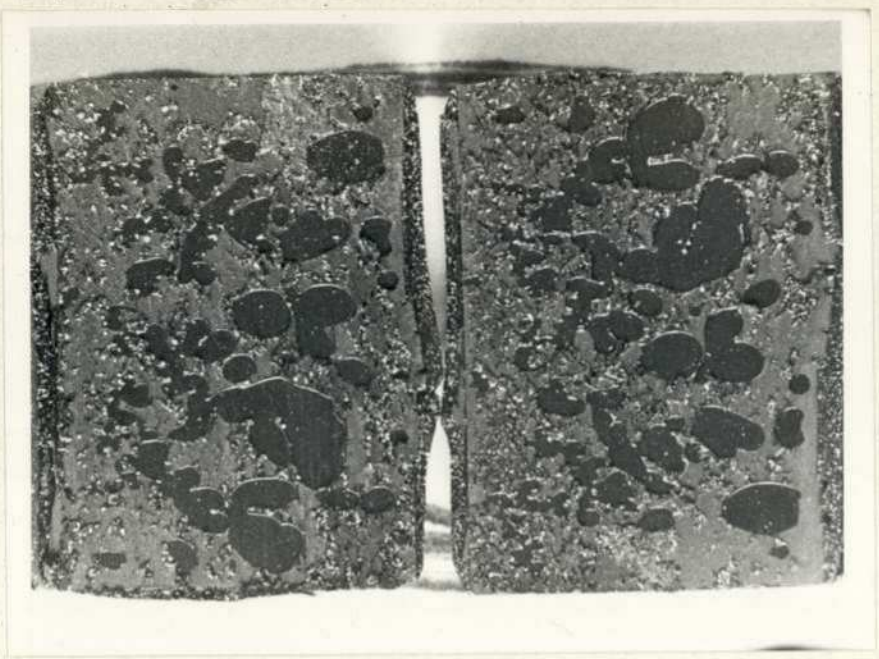


Figure 5.4 : Photograph of a complete fractured joint (1cm.x0.75cm) showing the large air bubbles mentioned in section 5.6 and formed as a result of expantion of entrapped gases within the adherend surface.

	Adhesive bond thickness $X10^{-3}$ cm	Tensile shear stress in MN/m^2	
Group A	17.7	40	
	15.2	43	
	15.2	43	Mean bond strength = 47
	11.4	52	Standard error of the
	10.2	46	mean = 1.41
	7.6	50	
	7.6	52	(Joints made with laps)
	8.9	46	(coated with yellow oxide)
	10.2	50	
Group B	3.8	43	
	10.2	59	Mean bond strength = 43
	6.3	39	Standard error of the
	3.8	57	mean = 4.11
	11.4	24	
	12.7	33	(Joints made with laps)
	12.7	47	(coated with mauve oxide)
	13.9	46	
Group C	15.2	27	
	10.2	30	
	14.0	28	Mean bond strength = 25
	8.9	26	Standard error of the
	12.7	27	mean = 1.25
	8.8	29	
	7.6	23	(Joints made with laps)
	10.6	25	(coated with black oxide)
	12.9	17	
	17.9	21	
Group D	7.6	46	
	10.2	51	Mean bond strength = 44
	15.2	48	Standard error of the
	10.2	57	mean = 3.30
	7.6	45	
	12.7	38	(Joints made with laps)
	7.6	33	(partially corroded, covered)
	7.6	32	(with coherent "black-grey"oxide)

CONTINUED ON NEXT PAGE

Table 5.7 : (IMI-318 alloy / BSL-308 adhesive)

Joints made with various coloured laps , oxidised in hydrogen peroxide/ sodium hydroxide solutions.

	Adhesive bond thickness $X10^{-3}$cm	Tensile shear stress in MN/m^2	
Group E	12.7	21	
	7.6	20	
	7.6	24	Mean bond strength = 18
	12.7	16	Standard error of the mean = 1.12
	12.7	10	(Joints made with laps
	10.2	20	partially corroded, covered
	10.2	15	with grey-white oxide)
	17.7	14	
	15.2	18	
	8.9	19	
	5.1	21	
	10.2	17	
Group F	12.9	36	
	11.8	25	
	15.2	36	
	8.8	42	
	7.7	28	Mean bond strength = 30
	7.0	30	Standard error of the mean = 1.94
	6.3	27	(Joints made with laps
	6.3	17	covered with grey oxide)
	12.8	29	
	10.2	46	
	10.2	18	
	10.2	24	
	7.6	25	
	8.8	30	
	5.8	28	
	7.6	28	

TABLE 5.7 -(IMI-318 alloy/BSL-308 adhesive)

Joints made with various coloured laps, oxidised in hydrogen peroxide/ sodium hydroxide solutions.

Careful examination of the adherends showed that they were very rough and had grooves which could have resulted from dissolution of one phase and/or the oxide formed deposited on one phase more than the other.

The yellow oxide (group A) of Table 5.7 had a matt finish and no such grooves were seen, bonds made with such laps had no air bubbles at all, a fact which supports the above conclusion regarding their source. In this group, failure always was cohesive within the adhesive.

An attempt was made to investigate the roughest surfaces, namely, those covered with a black oxide,but this time instead of bonding the cold adherends, they were preheated to about 70°-80°C. and bonded while hot. This was an attempt to expel most of the gases present in their crevices. The results of this attempt are shown below.

Adhesive bond thickness X 10^{-3} cm	Tensile shear stress in MN/m^2	
9.8	57	
10.2	57	
8.8	56	
10.2	58	Mean bond strength = 56.33 MN/m^2
11.8	54	
8.9	56	

As seen, much stronger bonds (cf. group C of Table 5.7 with a mean of 25) were obtained by this method, and although bubbles were present their number and size was diminished. This method of preheating the adherends was adopted to examine the effect of oxidation time on bond strength in the black oxide region.

Oxidation was carried out at 20°C for various times. The oxidised lap adherends were prepared in three separate batches and the results obtained are listed in Table 5.8 and represented graphically in Figure 5.5 .

Clearly, this oxide provides strong joints. Specimens oxidised for 48 hours and longer failed mainly within the substrate, as illustrated in Figure 5.6 , leading to a nearly constant bond strength, while an apparently interfacial or a cohesive failure was observed with laps oxidised for shorter times.

The relationship between oxidation time (x) and bond strength (y) was examined and found to be of the type

$$y = \frac{A}{x} + B \quad \text{where } (x > 0) \text{ and A and B are constants.}$$

A plot of xy against x is shown in Figure 5.7 to be a reasonable straight line from which the constants A and B can be deduced. The apparently large scatter of points in Figure 5.5 compared with Figure 5.7 is a scaling artefact.

This experiment indicates that in order to obtain stronger bonds a thin oxide film is required. Whether the relationship between bond strength and oxidation time originates from different oxide layer thicknesses or due to various roughnesses this is not clear. Most probably it is a combination of the two factors, but one thing is definitely clear and that is substrate failure dominated with thick oxide layers.

The scatter observed here is believed to have originated from the different roughness of the adherends and the presence of air bubbles within the bond. These were seen to form with most of the specimens oxidised for more than nine hours.

Electron microscope examination revealed (as has been discussed before) that very rough surfaces are produced on specimens oxidised for short times and this roughness seems to decrease with oxidation

Adhesive bond thickness $X10^{-3}$cm	Oxidisation time in hours	Tensile shear stress in MN/m^2	Mean bond strength
5.1	4	63.27	61.90
5.6	4	60.53	
3.8	8	72.89	69.65
4.0	8	66.41	
10.2	9	67.10	67.15
8.5	9	67.20	
3.8	12	66.02	66.10
3.8	12	66.18	
7.6	14	63.86	63.77
12.2	14	63.67	
5.6	21.5	67.59	63.13
7.3	21.5	58.66	
6.3	24	58.04	60.12
7.6	24	62.19	
7.1	29	62.88	62.19
12.7	29	61.51	
5.8	32	59.64	62.69
5.8	32	65.73	
6.0	40	57.98	57.93
6.2	40	57.88	
5.6	48	62.26	61.37
5.1	48	60.49	
5.1	56	67.20	67.35
5.6	56	67.49	
5.3	72	55.23	56.80
5.1	72	58.37	
5.8	80	57.29	57.24
6.0	80	57.19	
6.0	96	55.92	56.36
6.2	96	56.80	

TABLE 5.8 - (IMI-318 alloy/BSL-308 adhesive)
Effect of oxidisation for various times in hydrogen peroxide (0.04M)/ Sodium hydroxide (0.24M) solution (Black Oxide Region) on bond strength.

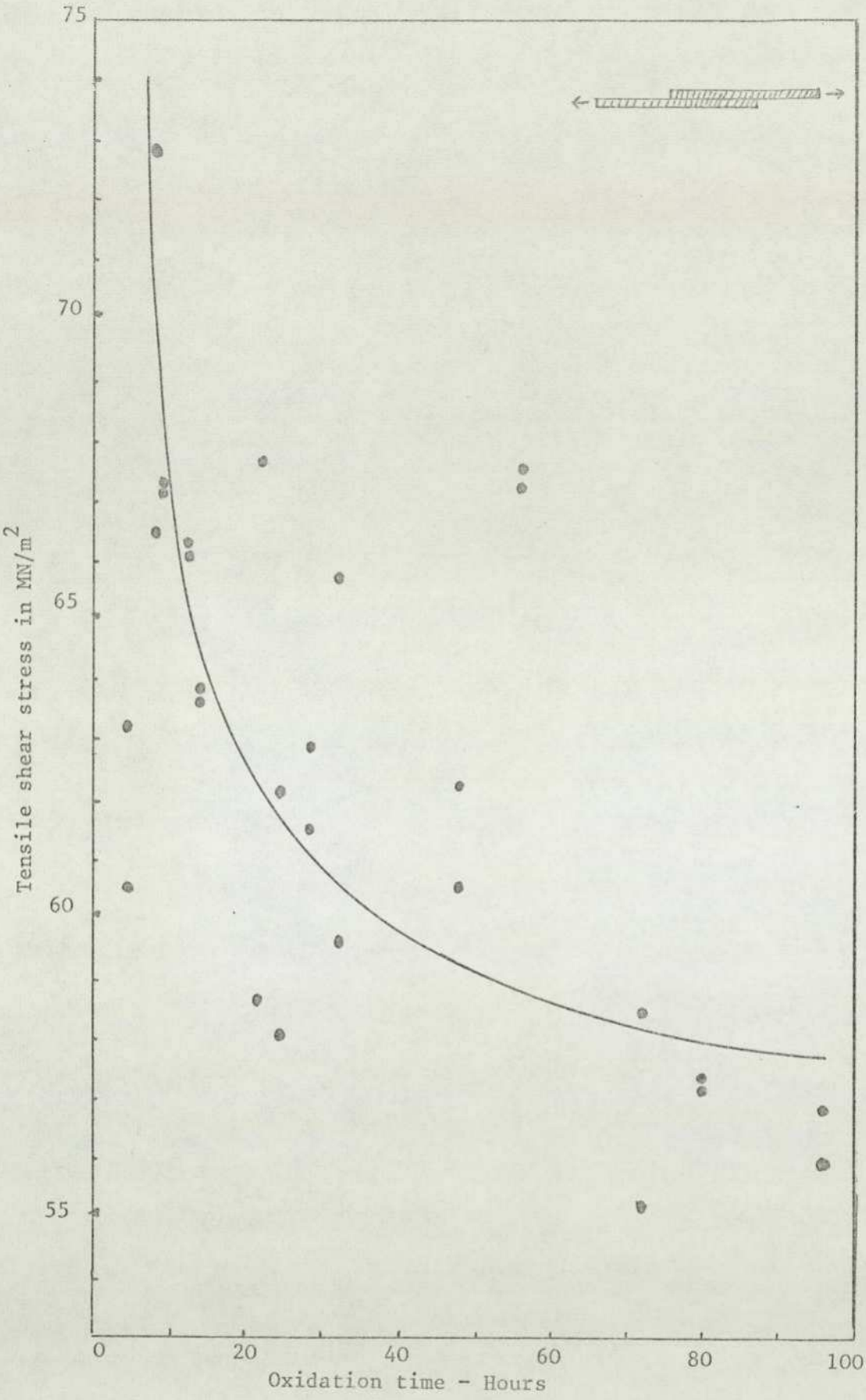
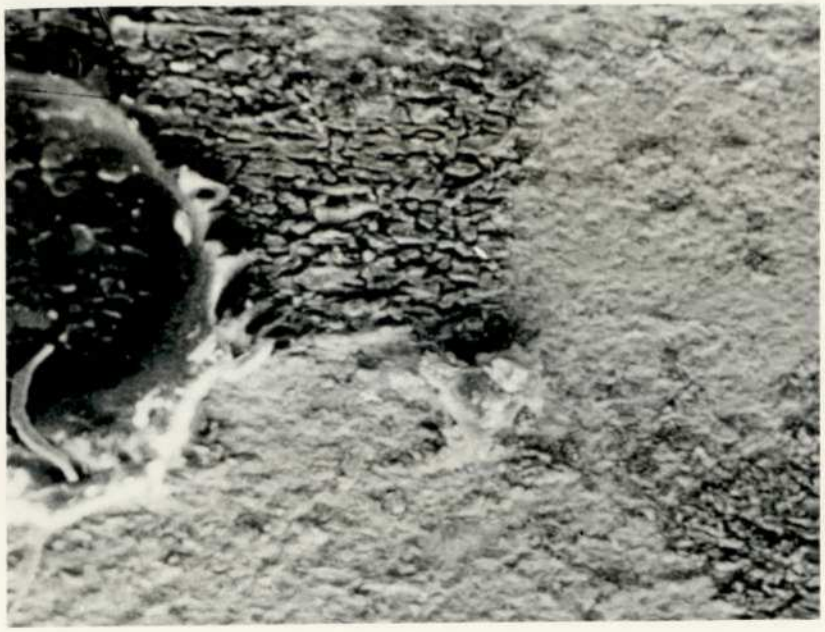


Figure 5.5 - (IMI-318 alloy/BSL-308 adhesive)
Effect of oxidation for various times in hydrogen peroxide (0.04M)/ Sodium hydroxide (0.24M) solution (Black Oxide Region) on bond strength.



(Magnification is 1cm = 40 μm)

Figure 5.6 : Stereo electron micrograph of IMI-318 alloy lap oxidised for 48 hours at room temperature in H_2O_2(0.04M)/ NaOH (0.24M) ,and bonded with BSL-308 adhesive.The areas seen covered with fine structure are in fact substrate and they show clearly the alpha phases separated by crevices. The large area appearing in the middle left part of the micrograph is part of an air bubble.

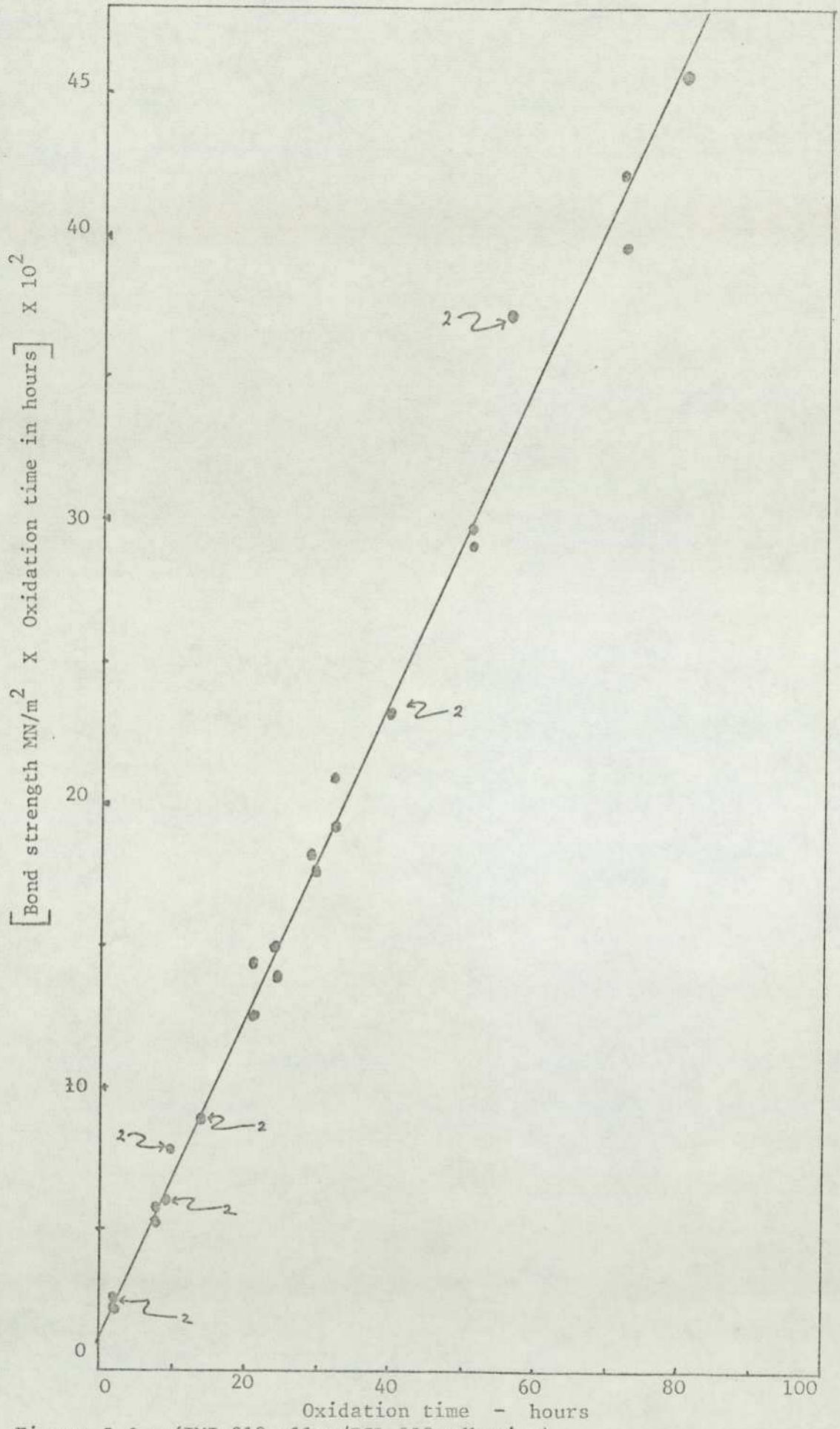


Figure 5.6 - (IMI-318 alloy/BSL-308 adhesive)

Effect of oxidation for various times in hydrogen peroxide (0.04M)/ Sodium hydroxide (0.24M) solution (Black Oxide Region) on bond strength.

time. In addition a new type of roughness begins to form, namely crevices mainly around the alpha phase of the alloy. The pits formed by oxidation for short periods are shallow and small in size, (ca. 0.1 - 0.25 μm in diameter) which can be filled easily with adhesive, unlike the deep crevices which inevitably will trap some gases and form stress concentrations, which may initiate failure. Therefore it is expected that adherends oxidised for short periods form stronger bonds.

Reflection electron diffraction studies indicated that the oxides formed after short oxidation times were more crystalline than those formed after long oxidation times. Adsorption of polymer molecules on the adherends will be affected by this and in turn the bond strength may be influenced.

CHAPTER 6

TORSIONAL SHEAR TESTING OF JOINTS

		Page
6.1	Description of apparatus used.	143
6.2	Calculation of bond strength.	145
6.3	Procedure for making the joints.	147
6.4	Heating and cooling the joints.	147
6.5	Effect of temperature on bond strength using IMI-205 alloy and BSL-308 adhesive.	148
6.5.1	Discussion of results.	157
6.6	Effect of temperature on bond strength using IMI-318 alloy and BSL-308 adhesive	165
6.6.1	Discussion of results.	169
6.7	Bonding IMI-318 alloy with Hidux 1198C adhesive.	171
6.8	Effect of etching IMI-318 alloy with aqueous hydrofluoric acid on bond strength.	171
6.9	Effect of temperature on bond strength using IMI-318 alloy and Hidux 1197C adhesive.	182
6.9.1	Discussion of results.	193

6.1 Torsional shear testing of joints

Description of the torsional shear adhesive test apparatus[135]

Experiments with lap joints were discontinued when a torsional test machine became available. Figure 6.1 shows the actual test machine. It consists of a driving motor coupled through a system of pulleys to a main pulley of radius 12.70 cm fixed to a bar through a universal joint. This bar can be coupled to the torque bar by inserting a specimen. The torque bar is fixed at the lower end. Any torsional movement in the torque bar is magnified through a system of levers ending with a pointer moving across a scale which enables one to read its position. When the motor is switched on, power is transmitted to the main pulley which sets up a torque against the torque bar, the magnitude of which can be calculated from the position of the pointer. The pointer system is designed in such a way that a sudden release of the torque causes no shift of the pointer. The apparatus includes a heater capable of heating the joints up to 400^{o}C. The temperature is controlled by a thermocouple. Three torque bars were supplied capable of exerting torques in the following ranges.

Torque bar No.1 from 0 to 500 kg.cm.
Torque bar No.2 from 0 to 750 kg.cm.
Torque bar No.3 from 0 to 1600 kg.cm

Each torsional bar was calibrated by dead load method.

Specimens commonly known as napkin rings for this machine were in the form of pairs of annular rings. The napkin surfaces were carefully machined and polished and then stuck together with the adhesive under test. In the following experiments the napkin rings used had the following basic dimensions:

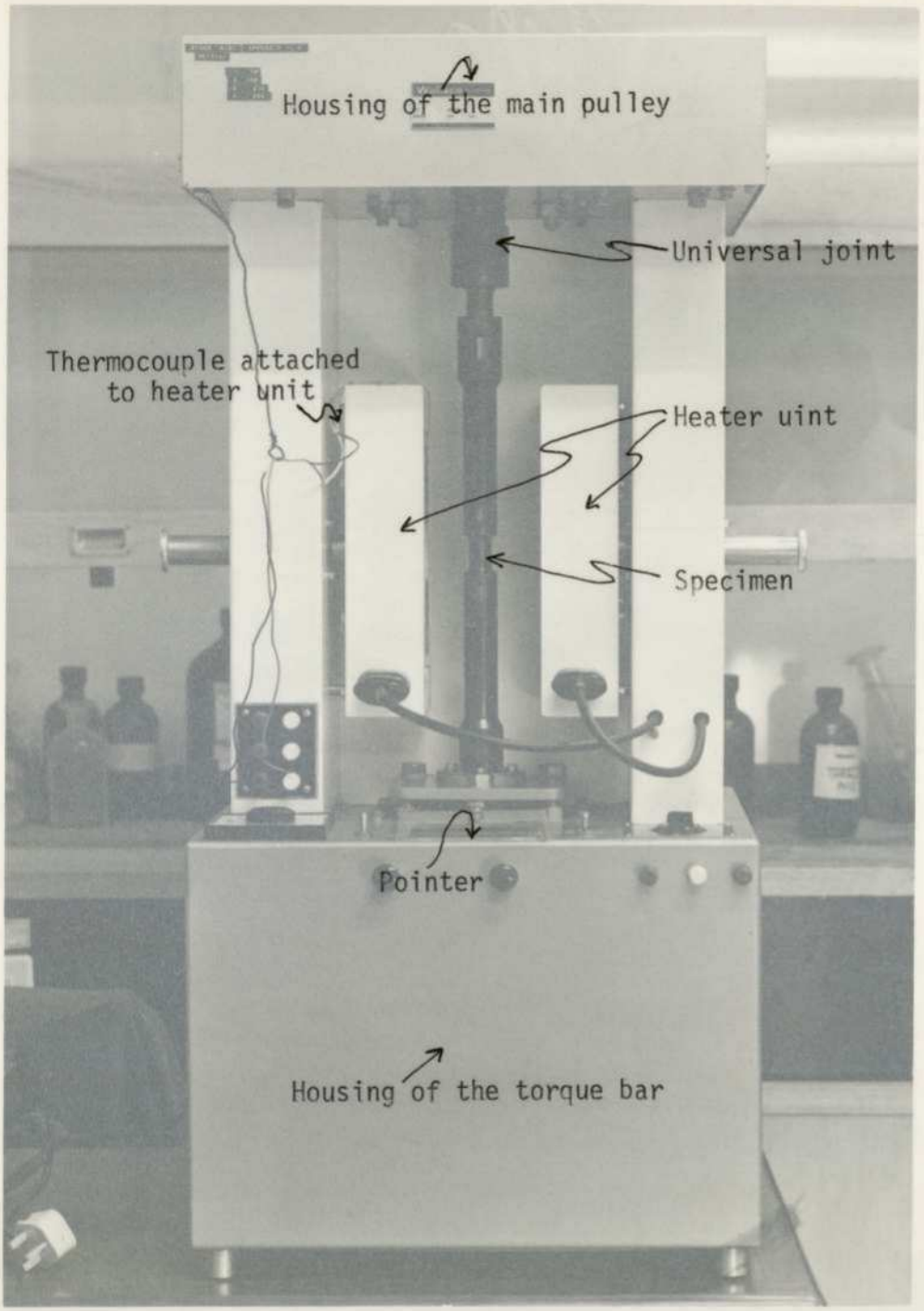


Figure 6.1 : The torsional test machine completely assembled.

Alloy IMI-205

r_o = 0.825 cm; r_i = 0.635 cm

Bonding area = 0.875 cm^2

Alloy IMI-318

r_o = 0.793 cm; r_i = 0.635 cm

Bonding area = 0.707 cm^2

A jig was supplied for assembling and curing joints, six at one time. In this jig pressure is applied to the joints by compression springs. These, too, were calibrated. A special tool for polishing by lapping was also supplied.

Figure 6.2 shows the actual jig used together with the napkin rings in these experiments.

6.2 Calculation of bond strengths

In the present work all calculations assumed elastic failure, although at elevated temperatures this is unlikely. The error is of no consequence as absolute stress values are not discussed in the present work only relative values are discussed. Therefore, as was shown earlier (Page 38) torsional shear S is given by

$$S = \frac{T}{2\pi R^2 (r_o - r_i)}$$

where T = torque applied

$R = (r_o + r_i)/2$

r_o = outer radius of annulus

r_i = inner radius of annulus

The above equation can be reduced to:

S = constant x T.

The magnitude of the constant depends on the radii of the rings used. For IMI-205 napkin rings used it is 1.571 and for IMI-318 it is 1.983. T is obtained from the calibration of the torque bar.

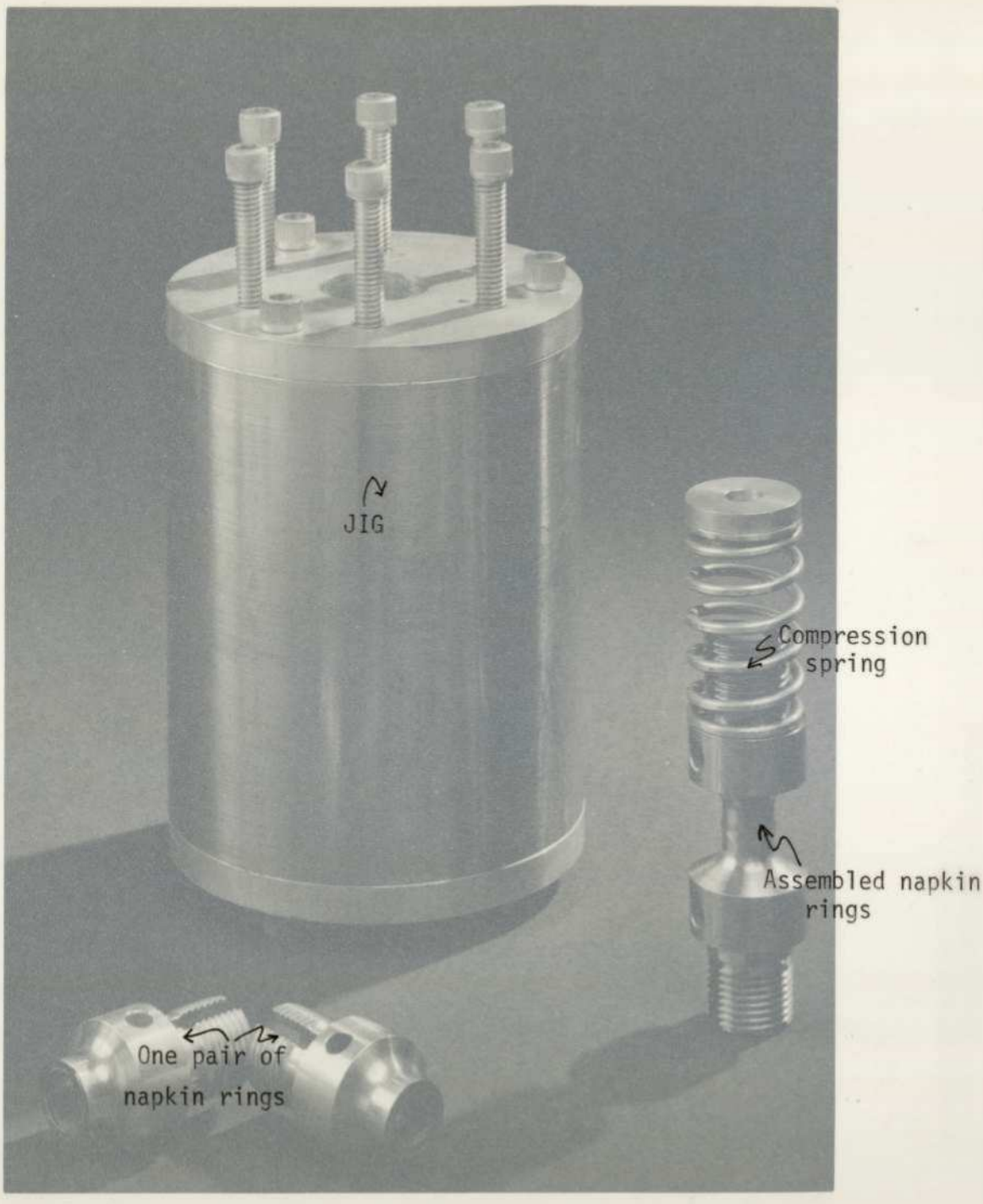


Figure 6.2 : The actual jig used to cure assembled napkin rings.



6.3 Procedure for making the joints

The napkin rings were polished by lapping to 6μm smoothness, using water as a lubricant, rinsed with acetone and dried at temperatures ca. 75°C for ½ hour. Before bonding the napkin rings, they were allowed to cool to room temperature and were either bonded in this condition or were subjected to a chemical pretreatment.

The joint was assembled by putting a ring of adhesive between the faces of two napkin rings and placed in the jig. A pressure (3.5 - 4.5 kg/cm^2) was then applied and the assembled jig placed in an oven at 178° ± 2°C for 2¼ hours to cure the adhesive (BSL-308).

The jig was then removed and allowed to cool to room temperature while the joints were still under pressure. Joints were allowed to stand for at least 24 hours after removal from the jig before testing.

Adhesive bond thickness was taken to be the difference between the total thickness of adherends and adherends plus the adhesive bond. The thickness represented in the following experiments with napkin rings is the mean of at least three measurements made with a vernier calliper.

6.4 Heating and cooling the joints

Using the built in heater, the joint under test was heated to the desired temperature. The actual temperature of the joint was recorded by a thermocouple attached directly to the alloy/adhesive region from inside. A condition in which the temperature difference across the ring was never greater than 2°C was achieved by eliminating air currents.

Cooling of the joints was carried out by circulating through a special jacket cold air obtained by passing nitrogen gas

through a coil immersed in dry ice-acetone or liquid nitrogen. The desired temperature was obtained by controlling the rate of flow.

The joints were tested in each case when a steady temperature was achieved.

6.5 Effect of temperature on bond strength using IMI-205 alloy and BSL-308 adhesive

Having established conditions under which bond strengths values are reproducible, the work on the effect of temperature on bond strength was started using adherends prepared by different methods. The following pretreatments were investigated:

1. Plain polished to 6 μm.
2. First order mauve oxide produced electrolytically in 1% H_2O_2, at 35 volts.
3. First order blue oxide produced electrolytically in 0.IN H_2SO_4, at 30 volts.
4. Second order yellow oxide produced electrolytically in 0.IN H_2SO_4 at 50 volts.
5. Bronze oxide produced electrolytically in 0.IN H_2SO_4 at 55 volts.
6. Etching with aqueous hydrofluoric acid (4% w/v) for 1½ minutes.
7. Black oxide produced by oxidation in H_2O_2 (0.05M)/NaOH(0.4M) (Black oxide region) for 2 hours at 20°C.

The results obtained from these experiments are shown graphically in Figures 6.3, 6.4, and 6.5 and the actual data given in Tables 6.1, 6.2, 6.3, 6.4, 6.5, 6.6, and 6.7 immediately after the figure to which they refer. The mode of failure in each experiment was followed by examination of fractured surfaces with an optical microscope as well as by the Nomarski's interference method. In some cases two-stage replicas for electron microscopy were prepared and photographed.

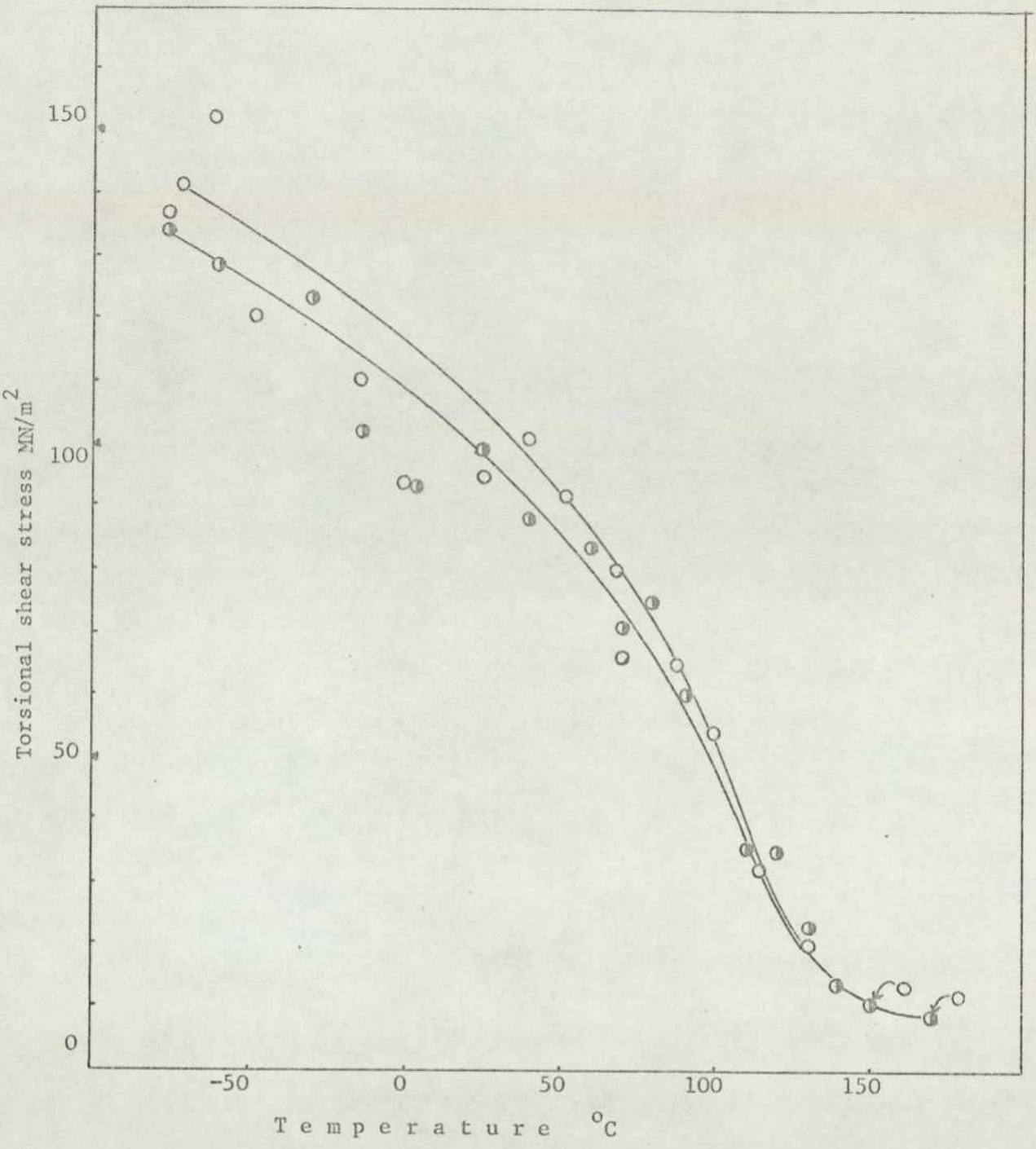


Figure 6.3 - Strength - temperature profile of BSL-308 adhesive on titanium alloy IMI-205

(●) Plain polished adherends.
(○) First order mauve oxide produced electrolytically in 1% H_2O_2 at 35 Volts.

Adhesive bond Thickness X10^{-3}cm	Torsional shear stress in MN/m^2	Temperature of Test in ^{o}C
6	134	-76
6	129	-60
6	123	-30
7	102	-14
6	93	4
5	99	25
8	88	40
5	83	60
7	71	70
6	75	80
6	60	90
6	35	110
7	35	120
6	23	130
8	14	140
7	11	150
6	9	170

TABLE 6.1 - (IMI-205 alloy/BSL-308 adhesive)
Plain polished

Adhesive bond Thickness X10^{-3}cm	Torsional shear Stress in MN/m^2	Temperature of Test in ^{o}C
7	137	-78
6	141	-72
6	152	-61
8	120	-48
5	110	-15
6	94	0
5	95	25
7	101	40
7	92	52
7	80	68
6	66	70
5	65	88
7	54	100
6	32	115
6	20	130
5	11	150
7	9	170

TABLE 6.2 - (IMI-205 alloy/BSL-308 adhesive)
First order mauve oxide produced electrolytically in 1% H_2O_2, at 35 volts.

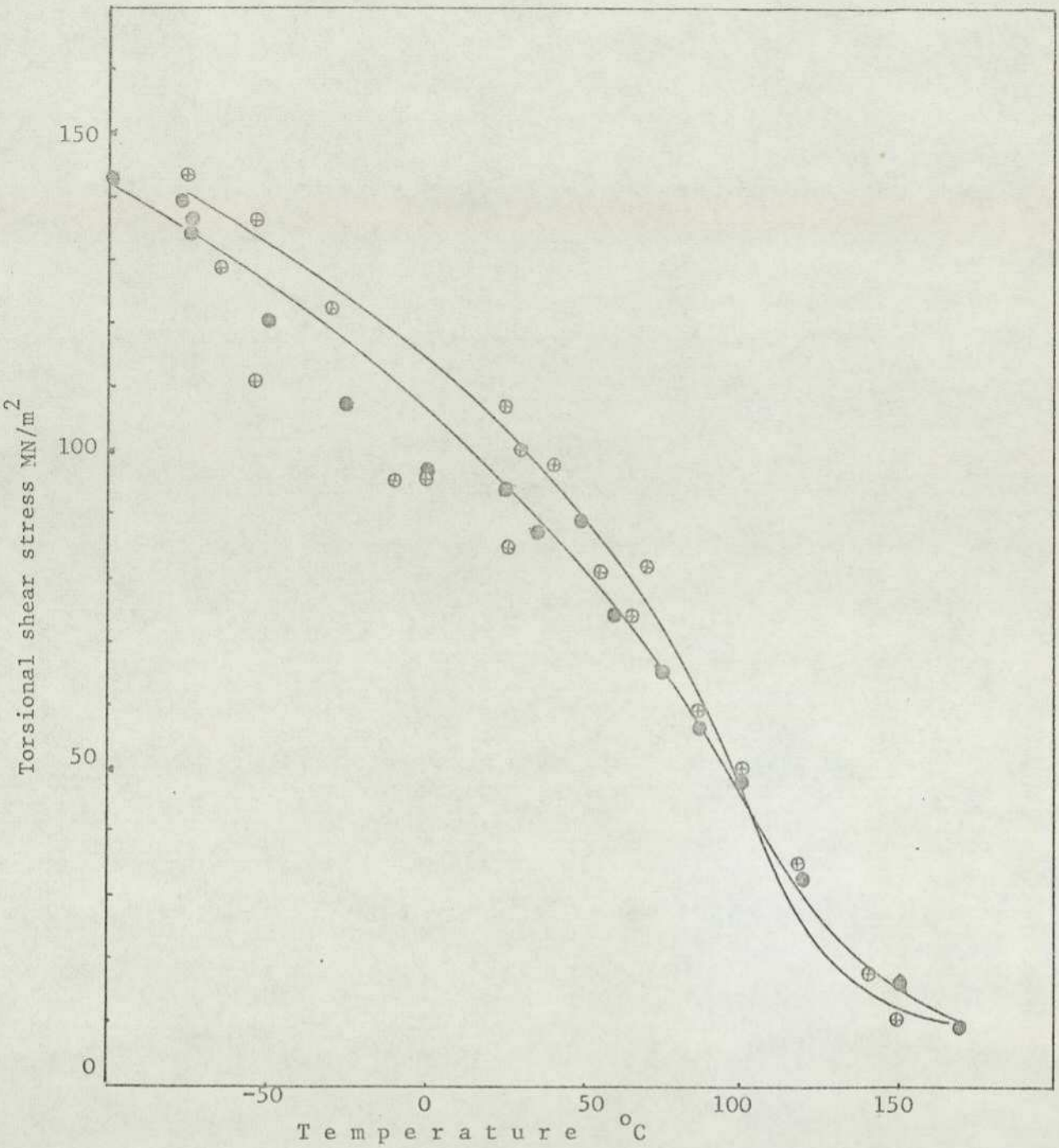


Figure 6.4 - Strength - temperature profile of BSL-308 adhesive on titanium alloy IMI-205.

(●) First order blue oxide produced electrolytically in 0.1N sulphuric acid at 30 Volts.
(●) Second order yellow oxide produced electrolytically in 0.1N sulphuric acid at 50 Volts.

Adhesive bond Thickness X10^{-3}cm	Torsional shear stress in MN/m^2	Temperature of Test in ^{o}C
7	143	-100
6	139	- 78
7	136	- 75
6	134	- 75
7	120	- 50
6	107	- 25
7	97	0
7	94	25
5	87	35
6	89	50
7	74	60
7	65	75
7	56	87
6	48	100
6	32	120
6	16	150
7	9	170

TABLE 6.3 - (IMI-205 alloy/BSL-308 adhesive)
First order blue oxide produced electrolytically in 0.1N H_2SO_4 at 30 volts.

Adhesive bond Thickness X10^{-3}cm	Torsional shear Stress in MN/m^2	Temperature of Test in ^{o}C
6	143	-76
7	129	-65
6	136	-55
7	111	-55
6	122	-30
6	95	-10
8	96	0
7	107	25
6	85	25
6	100	30
6	98	40
6	81	55
7	74	65
8	82	70
7	59	85
7	50	100
7	35	118
6	17	140
6	11	150

TABLE 6.4 - (IMI-205 alloy/BSL-308 adhesive)
Second order yellow oxide produced electrolytically in 0.1N H_2 SO_4 at 50 volts.

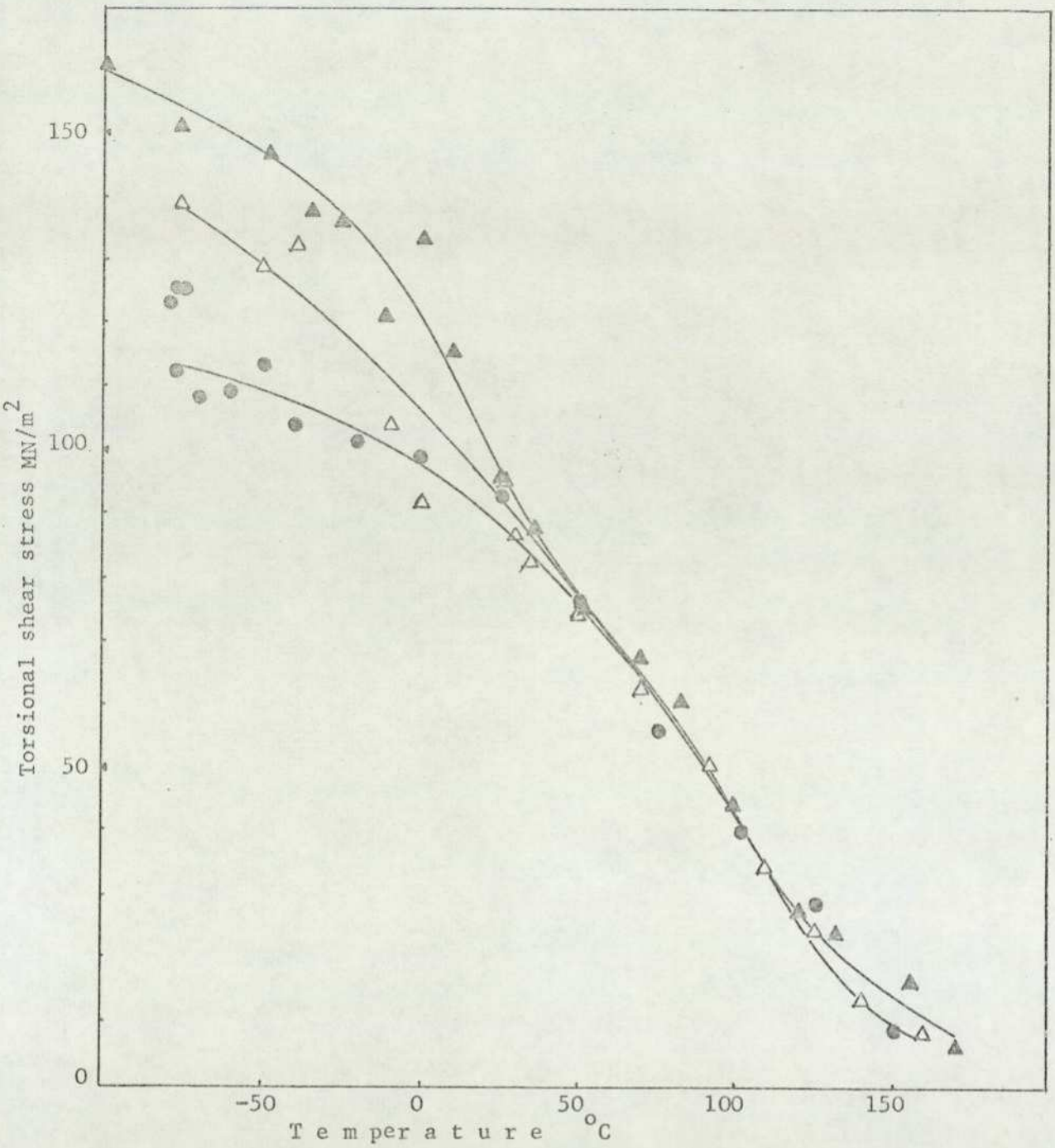


Figure 6.5 - Strength - temperature profile of BSL-308 adhesive on titanium alloy IMI-205.

(●) Surface etched with hydrofluoric acid (4%w/v) for 1½ minutes.
(△) 'Bronze' oxide produced electrolytically in 0.1N sulphuric acid at 55Volts.
(▲) Surface oxidised in hydrogen peroxide (0.05M)/sodium hydroxide (0.4M) at 20°C for two hours.

Adhesive bond Thickness X10^{-3}cm	Torsional shear stress in MN/m^2	Temperature of Test in ^{o}C
6	186	- 95
7	138	- 76
7	129	- 50
7	132	- 40
6	104	- 10
7	92	0
7	95	25
7	87	30
6	83	35
6	74	50
6	63	70
6	51	92
7	35	110
5	25	125
6	14	140
5	9	160

TABLE 6.5 - (IMI-205 alloy/BSL-308 adhesive)
Bronze coloured oxide produced electrolytically in 0.1N H_2SO_4 at 55 volts.

Adhesive bond Thickness X10^{-3}cm	Torsional shear Stress in MN/m^2	Temperature of Test in ^{o}C
7	123	- 80
6	125	- 78
7	112	- 78
7	125	- 76
7	108	- 70
5	109	- 60
6	113	- 50
7	104	- 40
6	101	- 20
7	99	0
6	93	25
6	76	50
6	56	75
7	41	102
7	29	125
6	9	150

TABLE 6.6 - (IMI-205 alloy/BSL-308 adhesive)
Adherends etched in 4% w/v hydrofluoric acid for 1½ minutes.

Adhesive bond Thickness $X10^{-3}$ cm	Torsional shear stress in MN/m^2	Temperature of Test in ^{o}C
6	161	-100
5	152	- 76
6	147	- 48
6	138	- 35
6	137	- 25
7	122	- 11
6	134	0
7	116	10
7	96	25
7	88	35
7	75	52
6	68	70
6	61	83
6	45	100
5	28	120
5	25	132
6	17	156
5	7	170

TABLE 6.7 - (IMI-205 alloy/BSL-308 adhesive)
Adherends oxidised for two hours at room temperature in hydrogen peroxide (0.05M)/Sodium hydroxide (0.4M) (Black oxide region).

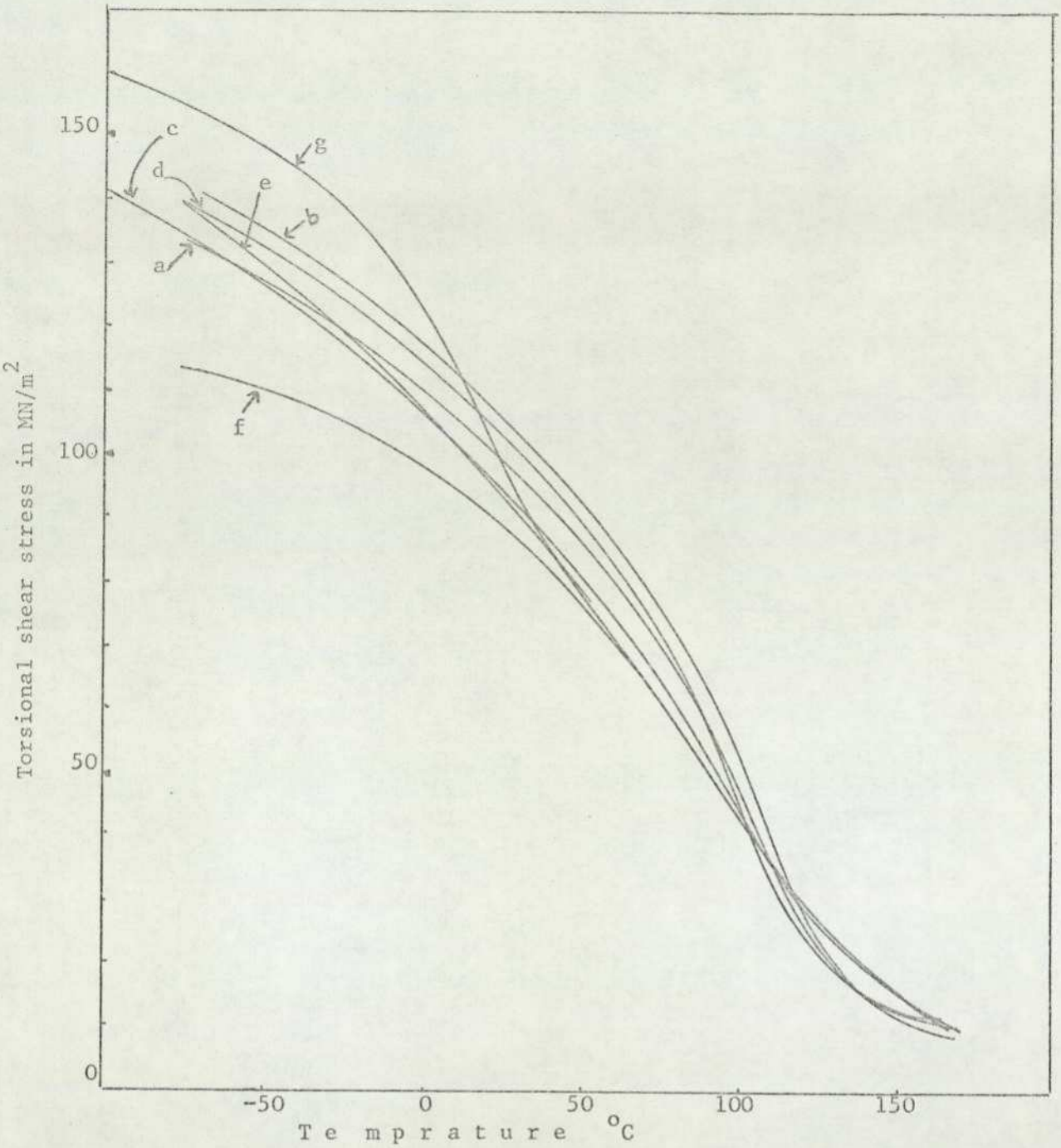


Figure 6.6 - Strength - temperature profile of BSL-308 adhesive on titanium alloy IMI-318.

(a) Plain polished adherends.
(b) First order mauve oxide produced electrolytically in 1% hydrogen peroxide at 35 Volts.
(c) First order blue oxide produced electrolytically in 0.1N sulphuric acid at 30 Volts.
(d) As in (c) Second order yellow oxide - at 50 Volts.
(e) As in (c) 'Bronze' oxide - at 55 Volts.
(f) Surface etched with HF (4%w/v) for 1½ minutes.
(g) Surface oxidised in H_2O_2 (0.05M)/NaOH (0.4M) at 20°C for two hours.

" Composite of previous three figures "

6.5.1 Discussion of the results

Figures 6.3,6.4,and 6.5 are summarised in the composite Figure 6.6 . It shows clearly that the temperature profiles of BSL-308 adhesive do depend on the pretreatment substrates at least at the lower temperatures. At temperatures lower than 25°C, different levels of bond strength were obtained with different substrate treatments. Moreover, the strength-temperature curves were by no means level at these temperatures although for some of the surface treatments there is less temperature dependence than for others. The highest strengths are given by oxidation for two hours by hydrogen peroxide/sodium hydroxide at room temperature and the lowest strengths by etching with aqueous hydrofluoric acid for 1½ minutes. At temperatures above 25°C there is no significant difference in bond strengths arising from pretreatments of the substrates.

The appearance of the broken test pieces remained unchanged over the entire temperature range for each treatment. The adhesive appeared irregularly broken at the interface and across the thickness of the adhesive. Neither brittle nor ductile failure was obvious in any of the treatments. All the joints tested at temperatures lower than 120°C had areas which appeared to be bare metal and some interfacial failure was suspected. Contact angle measurements using doubly distilled water on these areas gave very similar values as seen in Table 6.8 . Contact angle values were recorded after 45 seconds in each case. For comparison, attempts were made to measure contact angles similarly on freshly prepared metal surfaces which had not been bonded and were certainly bare in this context. For these surfaces, values were usually very small, the largest ever obtained was 10°. The values obtained indicate that all areas examined were not bare but were covered with

Adherend	Temperature of test °C	Contact angle measurement on four different areas of "bare" metal areas					Actual adhesive				
		1	2	3	4	Mean	1	2	3	4	Mean
Plain polished	-78	34.5	31.4	32.3	30.6	32.2	28.9	31.0	28.3	30.2	29.6
Blue oxide	-78	31.2	31.3	28.9	30.1	30.4	35.0	36.0	33.9	34.7	34.9
Etched in HF/H_2O	-20	31.0	33.5	30.9	31.6	31.8	31.1	35.0	31.8	33.9	33.4
Plain polished	10	32.5	33.7	30.7	32.1	32.3	35.3	34.0	34.0	32.8	34.0
"Bronze" oxide	20	32.8	34.3	31.6	31.9	32.7	32.8	34.5	31.6	32.8	32.9
Yellow oxide	75	32.7	35.2	31.6	33.7	33.3	35.1	33.2	34.3	32.4	33.8
Oxidised in $H_2O_2/NaOH$	0	31.7	31.9	33.0	30.8	31.9	32.3	33.5	30.7	32.5	32.3
Oxidised in $H_2O_2/NaOH$	-50	30.8	33.4	32.1	29.9	31.6	32.7	30.8	32.0	31.8	31.8

TABLE 6.8 - (IMI-205 alloy/BSL-308 adhesive).

Contact angles of water on fractured joints tested at various temperatures.

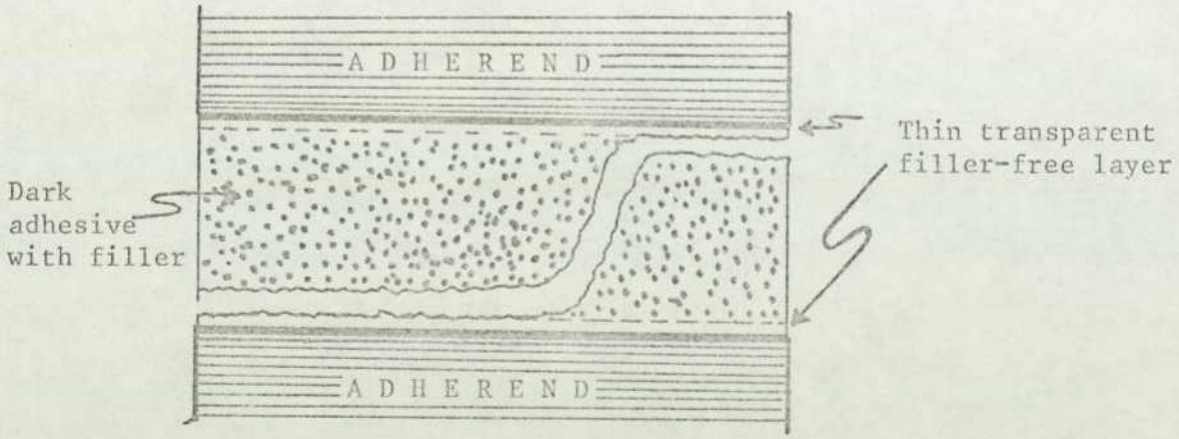
similar material. This is a situation which can be achieved if failure is always cohesive within the adhesive.

Further examination of bare metal areas with phase contrast interference microscopy (Nomarski's method) revealed the presence of a thin layer of adhesive on these areas. Figure 6.7 is an actual photograph of such an area. The bright blue areas represent true bare metal areas, and all other colours are due to various thicknesses of the thin film at the surface.

A two stage replication method was used to replicate bare areas for examination with the electron microscope. Figures 6.8, 6.9, 6.10, 6.11 and 6.12 are of such areas. They show clearly that a thin film does exist on the surface and also in some cases truly bare metal areas are seen.

Furthermore, no trace of any filler particles could be seen in this thin film.

From this evidence, it seems that failure is almost entirely cohesive within the adhesive at a position very close to the interface, leaving a thin and transparent film on the substrate. The position of the break is shown diagramatically below:



An attempt was made to measure the refractive index of the thin transparent film mentioned above by flooding with liquids of different refractive indices. It appeared that the film was not entirely homogeneous as the reflection from some areas disappeared in a liquid of refractive index 1.598 and other areas in a liquid

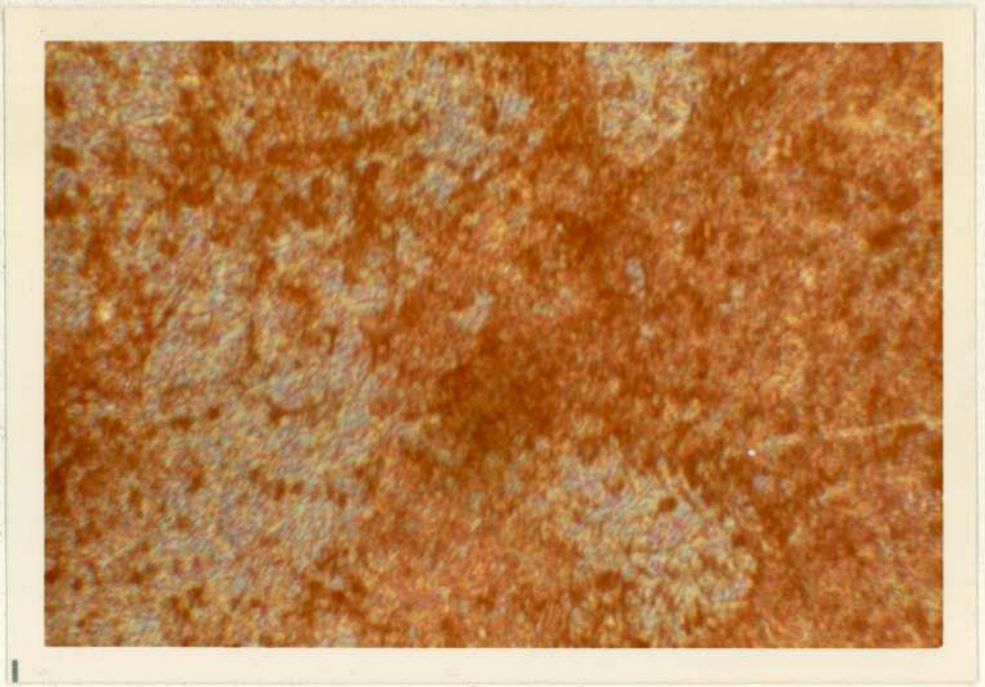
of 1.585. (The refractive index of an epoxy resin based on bis phenol-A is about 1.55, increasing with cross-linking and depending on the nature of the curing agent[136].

It appears therefore that some component of the adhesive migrates during curing to the interface and failure of the bond is close to or at the boundary of this migrated layer although this does not imply that a sharp boundary exists. Material of low molecular weight would be expected to migrate preferentially from a broadly dispersed polymer. Obviously the substrate surface is influencing the breaking of the bond in some way at lower temperatures by initiating the failure process differently. At higher temperatures this is not so and failure may be assumed to be wholly initiated within the adhesive.

Bonds made with specimens oxidised in hydrogen peroxide/sodium hydroxide and tested at temperatures lower than $-50^{\circ}C$ showed some substrate failure on a microscopic scale.

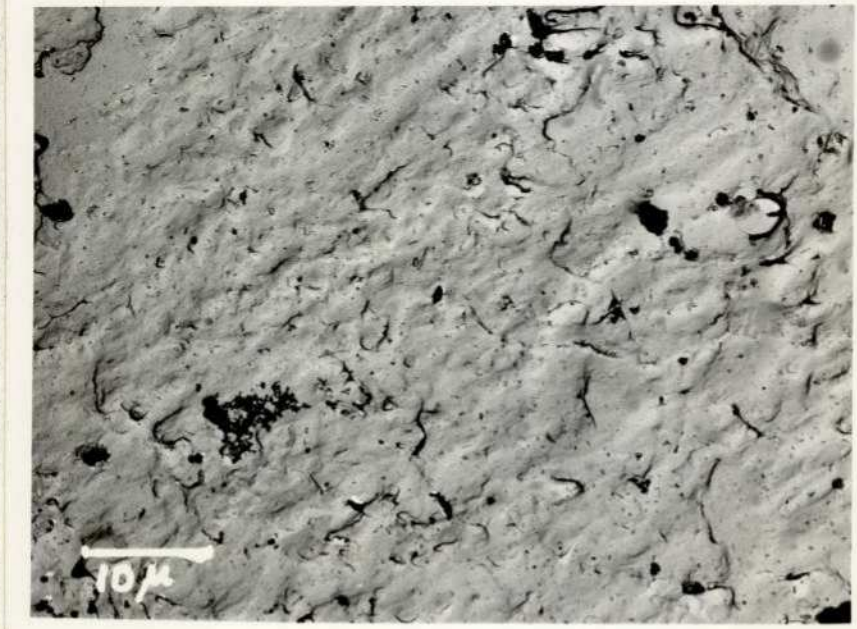
The low strength values obtained with adherends etched with hydrofluoric acid are mainly due to formation of a black and rather loose material on the surface which has been shown by X-ray diffraction (page102) to be molybdenum oxide(s). Clear interfacial failure as well as substrate failure was observed in these joints over the whole range of temperatures. Substrate failure in this case was either entirely within the black powder or at the interface between the black oxide(s) and the bulk of the alloy.

When IMI-318 alloy napkin rings became available the work on IMI-205 was stopped. Further experiments with BSL-308 adhesive were carried out using IMI-318 alloy napkin rings.



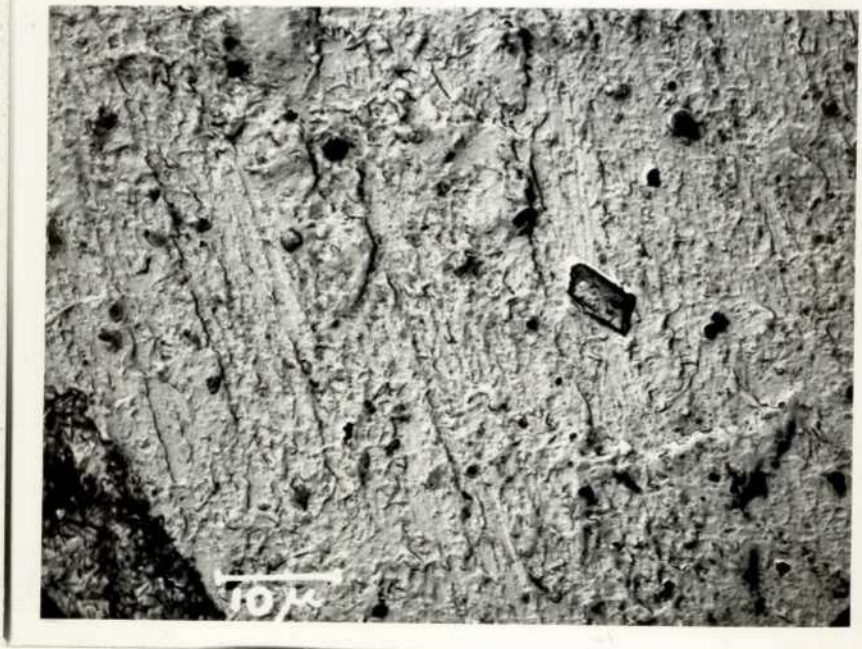
(Original mag.200X)

Figure 6.7 : Photo micrograph of a fracured joint tested at $-78^{o}C$. Dark blue areas represent bare metal areas while other colours are due to different thicknesses of the thin film of adhesive. Initially the surface was electrolytically oxidised in 0.1N sulphuric acid at 30 volts (blue oxide coating) and bonded with BSL-308 adhesive.



(Original mag.1,000X)

Figure 6.8 : Electron micrograph (indirect replication) of IMI-205 alloy surface bonded with BSL-308 adhesive, showing the thin film of adhesive on the adherend . Initially the surface was electrolytically oxidised at 35 volts in 0.1%H_2O_2 and the joint tested at -78°C.



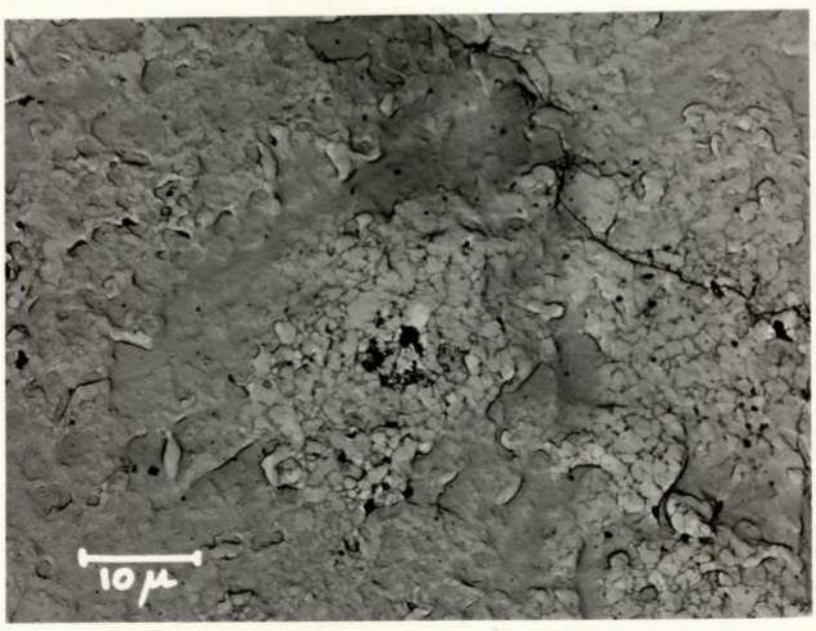
(Original mag. 1,000X)

Figure 6.9 : Electron micrograph (indirect replication) of IMI-205 alloy surface bonded with BSL-308 adhesive, showing the thin film of adhesive on the adherend. Initially the surface was oxidised in H_2O_2(0.05M)/NaOH (0.4M) at 20°C for two hours. The joint was tested at -50°C.



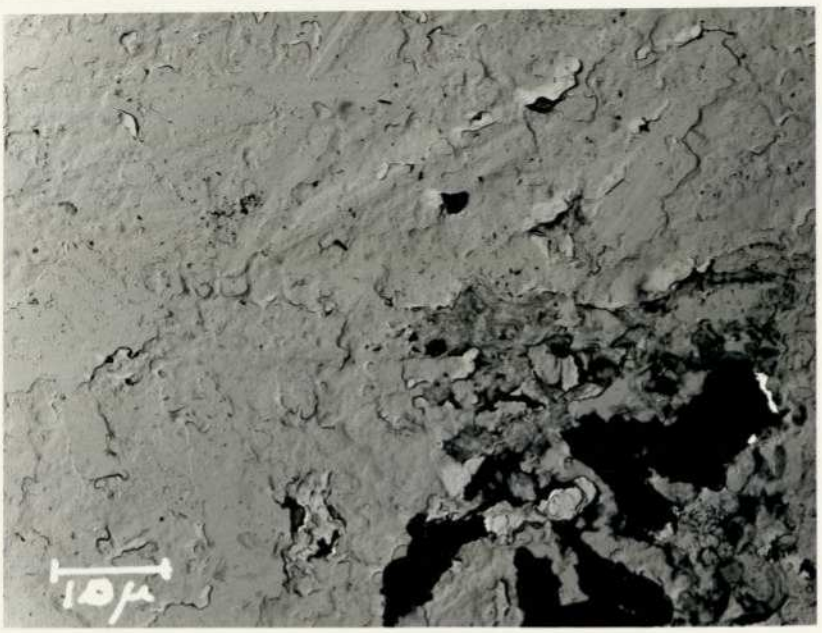
(Original mag. 1,000X)

Figure 6.10 : Electron micrograph (indirect replication) of IMI-205 alloy surface bonded with BSL-308 adhesive, showing the thin film of adhesive on the adherend. Initially the surface was polished to 6 μm smoothness and the joint tested at 100°C.



(Original mag. 1,000X)

Figure 6.11 : Electron micrograph (indirect replication) of IMI-205 alloy surface bonded with BSL-308 adhesive, showing the thin film of adhesive on the adherend. Initially the surface was electrolytically oxidised at 30 volts in 0.1 sulphuric acid (1st.order blue oxide) and tested at -20°C .



(Original mag. 1,000X)

Figure 6.12 : Electron micrograph (indirect replication) of IMI-205 alloy surface bonded with BSL-308 adhesive , showing the thin film of adhesive on the adherend. Initially the surface was electrolytically oxidised at 55 volts in 0.1N sulphuric acid (bronze oxide) and the joint was tested at 22°C.

6.6 Effect of temperature on bond strength using IMI-318 alloy and BSL-308 adhesive

The following pretreatments were investigated :

1. Plain polished to 6 μm smoothness.
2. Etching with aqueous hydrofluoric acid (4% w/v) for 1 minute at 25°C.
3. First order blue oxide produced electrolytically in 0.1N sulphuric acid at 24 volts.
4. Oxidation for one hour at 21°C in hydrogen peroxide (0.05M)/ sodium hydroxide (0.4M) .

The results obtained from these experiments are shown graphically in Figure 6.13 and the actual data are given in tables 6.9, 6.10, 6.11 and 6.12 immediately after the figure.

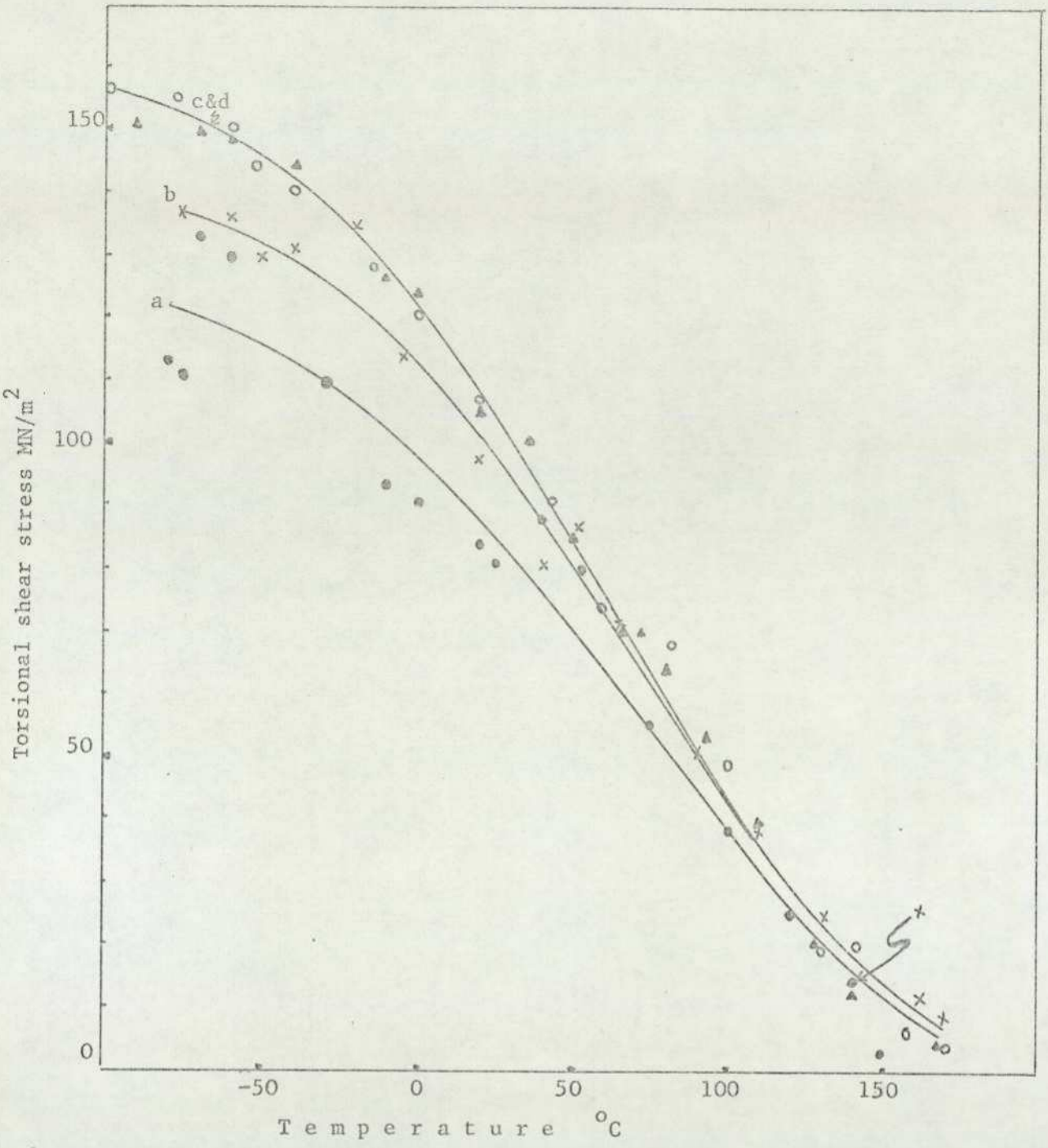


Figure 6.13- Strength - temperature profile of BSL-308 adhesive on titanium alloy IMI-318.

(●) Plain polished surface -a-
(x) Surface etched with HF (4%w/v) for 1 minute.-b-
(o) First order blue oxide produced electrolytically in 0.1N sulphuric acid at 30 Volts. -c-
(▲) Surface oxidised for hour in hydrogen peroxide (0.05M)/ sodium hydroxide (0.4M) at 21 ^{o}C. -d-

Adhesive bond Thickness $X10^{-3}$cm	Torsional shear Stress in MN/m^2	Temperature of Test in ^{o}C
6	113	- 80
7	110	- 76
6	133	- 70
7	130	- 60
7	110	- 30
6	94	- 10
5	91	0
6	84	20
6	81	25
7	88	40
5	80	52
7	55	75
6	38	100
6	25	120
6	14	140
5	3	150

TABLE 6.9 - (IMI-318 alloy/BSL-308 adhesive)
Plain polished (6 μm)

Adhesive bond Thickness $X10^{-3}$cm	Torsional shear Stress in MN/m^2	Temperature of Test in ^{o}C
6	137	- 76
7	136	- 60
7	130	- 50
6	132	- 40
7	135	- 20
5	114	- 5
6	98	20
8	81	40
6	87	52
6	71	65
7	51	90
7	38	110
5	25	131
5	14	140
6	12	162
8	9	170

TABLE 6.10- (IMI-318 alloy/BSL-308 adhesive)
Adherends etched in 4% w/v hydrofluoric acid for 1 minute.

Adhesive bond Thickness X10^{-3}cm	Torsional shear Stress in MN/m^2	Temperature of Test in ^{o}C
5	157	-100
6	155	- 78
8	150	- 60
6	144	- 52
6	140	- 40
6	128	- 15
6	120	0
7	107	20
6	91	43
7	74	61
5	68	82
6	49	100
7	19	130
7	20	141
6	6	158
5	4	170

TABLE 6.11- (IMI-318 alloy/BSL-308 adhesive)
First order blue oxide produced electrolytically in 0.1N H_2SO_4 at 30 volts.

Adhesive bond Thickness X10^{-3}cm	Torsional shear Stress in MN/m^2	Temperature of Test in ^{o}C
6	152	- 90
7	149	- 70
7	148	- 60
7	144	- 40
6	126	- 10
5	124	0
5	105	20
6	100	36
6	85	50
8	71	67
6	70	72
5	64	80
7	53	93
7	39	110
6	20	128
7	12	140
6	4	170

TABLE 6.12- (IMI-318 alloy/BSL-308 adhesive)
Adherends oxidised for one hour in hydrogen peroxide(0.05M)/ sodium hydroxide (0.4M) at 21^{o}C.

6.6.1 Discussion of the results

The appearance of fractured surfaces of the adhesive bond was similar to that observed with IMI-205, but there were some differences. First, substrate failure was noticed over larger areas with adherends oxidised electrolytically (blue oxide) or in alkaline hydrogen peroxide, while the etched adherends showed considerably less substrate failure. Second, the results obtained with IMI-318 alloy generally show less scatter than those obtained with IMI-205 alloy.

The existance of the filler free thin layer near the interface on IMI-318 alloy was confirmed by Nomarski's interference contrast method as well as by electron microscopy.

From Figure 6.13 it seems strongest joints are obtained by two treatments, electrolytic oxidation and oxidation in alkaline hydrogen peroxide.

The present work was extended to cover Hidux 1197C adhesive, which has been mentioned earlier in this thesis contains a glass cloth in addition to aluminium powder. Quantitative measurement which involved dissolving known areas of the two adhesives in acetone and N.N.dimethylformamide indicated that Hidux 1197C adhesive contains more aluminium per unit area than BSL-308 adhesive and that it is also less uniformally distributed.

The work started by investigating the pressures and temperatures leading to optimum joint strength. Napkin rings of IMI-205 alloy polished to 6μm were employed in this experiment. All joints were cured for $2\frac{1}{2}$ hours. The results obtained are contained in Table 6.13.

The results were examined statistically as in section 5.4.2 (page 119) and they indicate that once the temperature is high enough for cure, neither temperature nor pressure has any significant effect

Adhesive bond thickness $X10^{-3}$cm	Curing temperature ^{o}C	Pressure applied kg/cm^2	Torsional shear stress in MN/m^2
18	102	1.6	0 *
20	102	1.6	12 *
15	102	3.5	14 *
15	102	3.5	14 *
19	102	6.0	14 *
16	102	6.0	14 *
21	135	1.6	43
20	135	1.6	46
19	135	3.5	59
22	135	3.5	49
14	135	6.0	54
17	135	6.0	57
14	155	1.6	57
14	155	1.6	52
23	155	3.5	47
15	155	3.5	57
15	155	6.0	50
15	155	6.0	49
18	200	1.6	55
22	200	1.6	52
21	200	3.5	54
18	200	3.5	57
20	200	6.0	63
23	200	6.0	52

* all these bonds were under cured.

TABLE 6.13 - (IMI-205 alloy/Hidux 1197C adhesive)

Effect of temperature and pressure during curing on bond strength.

on bond strength. These results are in line with the manufacturers recommendations, and a pressure of ca. 4.5 - 5 kg/cm^2 and curing temperature of 166 $\pm$ 2^{o}C for 2½ hours were chosen for bonding Hidux 1197C adhesive film. These conditions were maintained throughout the following work.

6.7 Bonding IMI-318 alloy with Hidux 1197C adhesive

The work started by investigating the effect of etching on bond strength using hydrofluoric acid with and without nitric acid.

6.8 Effect on bond strength of etching IMI-318 alloy napkin rings with aqueous hydrofluoric acid (4% w/v) for various times

The napkin rings used were polished each time to 6 μm smoothness before they were etched. Each pair of rings were etched in a beaker containing 100 ml of etchant immersed in a large volume of water. This was necessary in order to maintain constant temperature of the etchant as the reaction between titanium and hydrofluoric acid is exthothermic. Etching times were controlled to an accuracy of $\pm$ 1 second. The etched specimens were rinsed with water and acetone before they were dried at ca.100^{o}C for half an hour. They were allowed to attain room temperature before they were bonded.

Testing of joints was carried out at temperatures 21 ∿ 23^{o}C and the bond strength results obtained are contained in Table 6.14 and shown graphically in figures 6.14 and 6.15. The second of these figures serves to substantiate that the relation between bond strength and etching time follows an equation of the type

$$y = B - \frac{A}{x} \qquad (x > o)$$

where
y = bond strength
x = etching time
A and B are constants.

A plot of xy against x is shown in figure 6.15. The values of A and B as calculated by the least square method are 108.7 and 316.7 respectively.

Adhesive Bond Thickness X 10^{-3}cm	Etching times in seconds	Torsional shear stress in MN/m^2
20	0	69
20	15	85
21	20	87
23	30	92
20	35	99
20	45	106
20	50	104
18	60	106
20	75	107
20	90	106
19	100	101
21	105	107
21	120	107
18	135	106
17	150	106
23	165	107
19	180	107

TABLE 6.14 -(IMI-318 alloy/Hidux 1197C adhesive)
Effect of etching with aqueous hydrofluoric acid (4% w/v) for various times on bond strength.

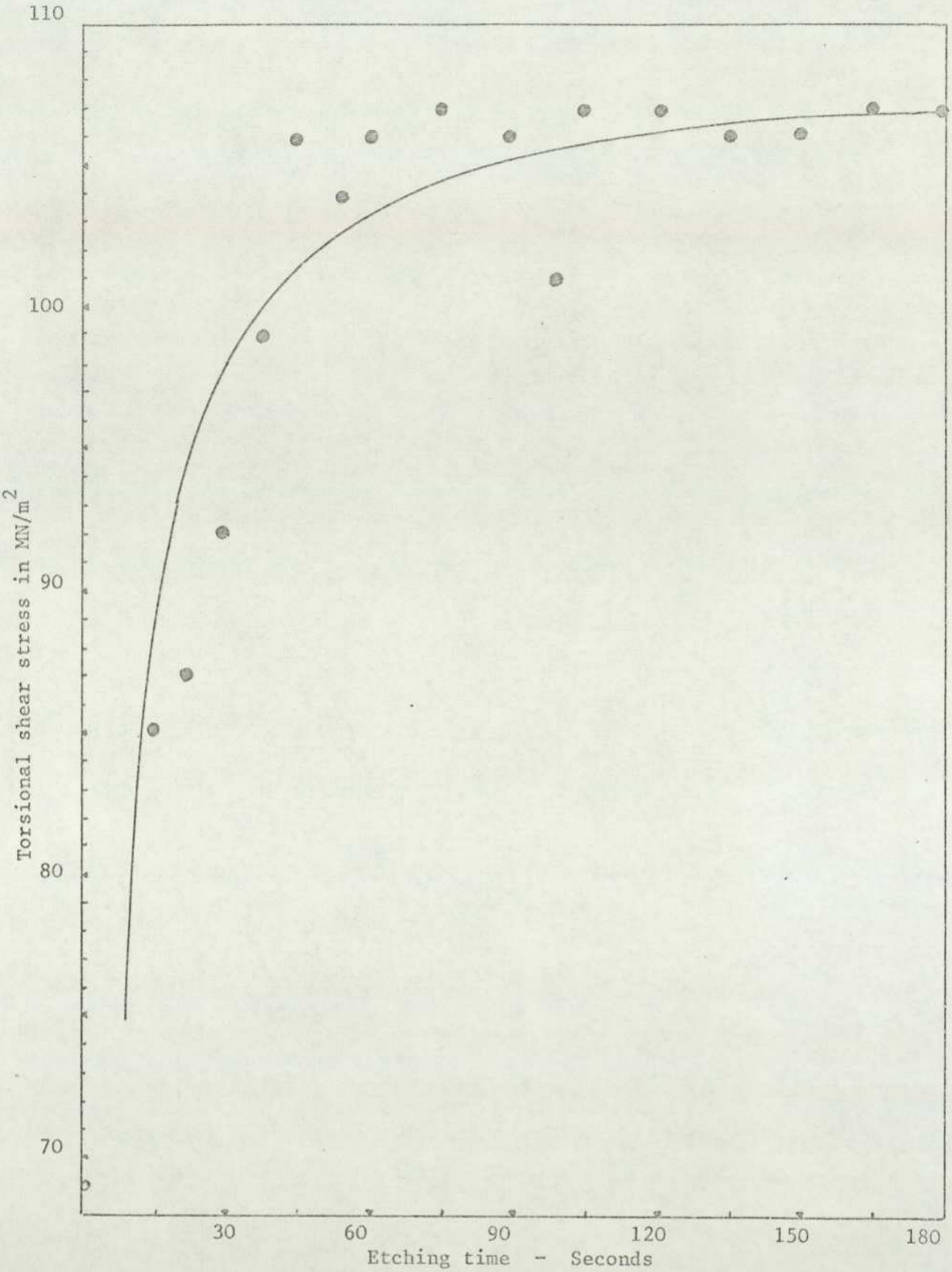


Figure 6.14 - (IMI-318 alloy/Hidux 1197C adhesive)
Effect of etching with aqueous hydrofluoric acid (4%w/v) for various times on bond strength.

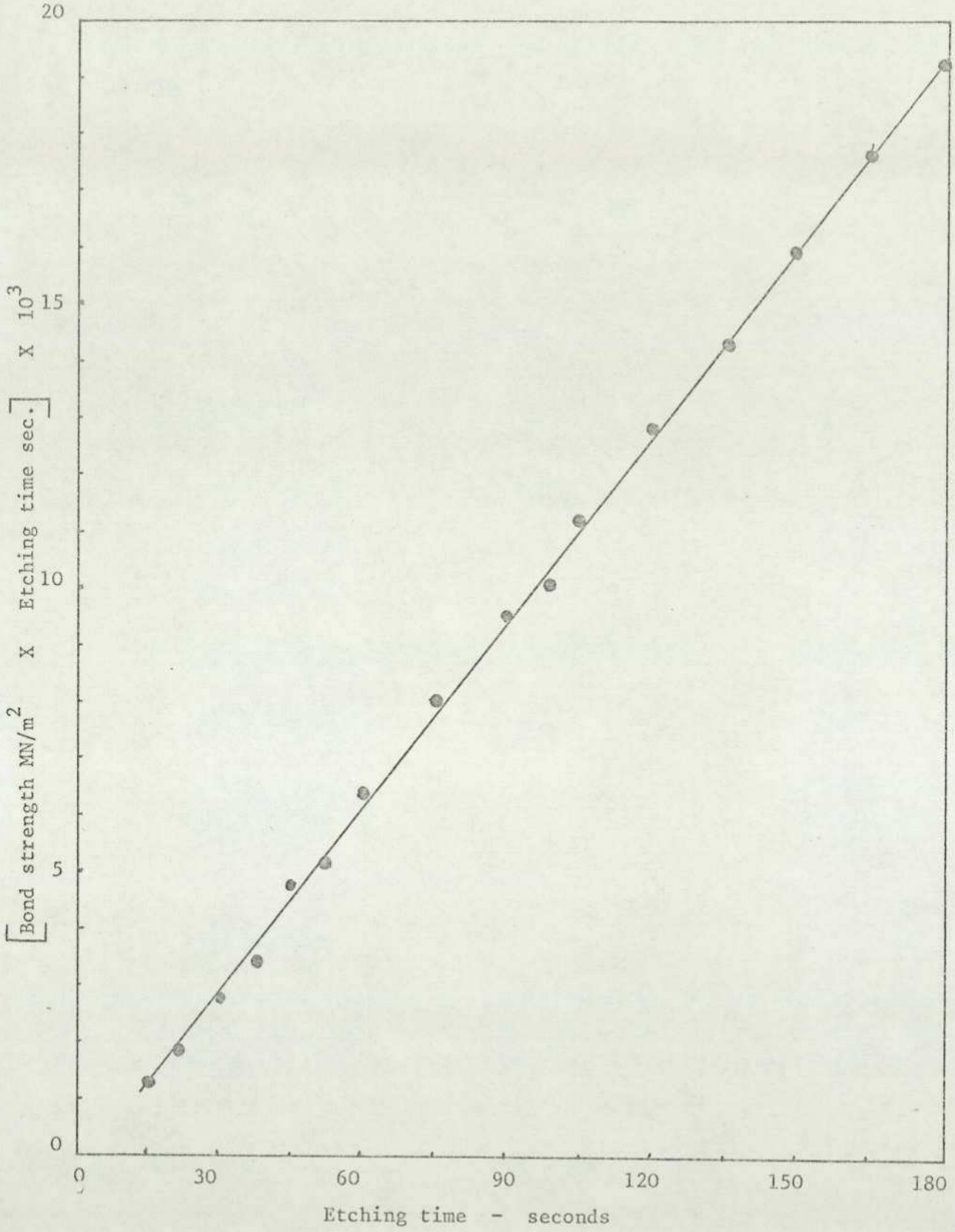


Figure 6.15 - (IMI-318 alloy/Hidux 1197C adhesive)
Effect of etching with aqueous hydrofluoric acid (4% w/v) for various times on bond strength.

It seems that etching in hydrofluoric acid (4% w/v) for longer than one minute produces no change in joint strength. This could be due to the fact that maximum roughness is reached after etching for one minute. The increase in roughness between 15 - 60 seconds etch, was followed by preparing stereoelectron micrographs of etched specimens in this region. Clearly they show that surface roughness does increase to a maximum after etching for one minute. Furthermore, the height of rutile needles formed on the alpha phases also increased with increasing etching times and reached a maximum height at about the same time when maximum roughness is obtained.

The mode of failure was followed by using both Nomarski's interference contrast optical method and two stage replication technique for examination with the electron microscope. Failure changes from nearly 100% interfacial to cohesive within the adhesive as well as substrate failure was noticed with specimens etched longer than 1½ minutes. The plain polished adherends appear superficially clean and the high finish of the metal is reflected in the surface of the separated adhesive as if no true wetting had occurred. Electron micrographs of such surfaces showed that most of the adherend surface was bare metal, i.e. interfacial failure was taking place. This kind of failure persists up to etching for 40 seconds, beyond which cohesive failure within the adhesive becomes obvious and further etching leads to more of the cohesive failure. A situation was reached when failure was entirely close to the supporting glass cloth and in no case did the fracture cross the glass cloth. "Bare" areas, forming about 1% of the total bonded areas were seen on rings etched for longer than one minute. Careful examination of these areas with optical microscope showed that a yellow/orange filler-free film was present next to the dark adhesive and in some cases broken beta phases were seen on the corresponding part on the second ring. The following diagram illustrates these points:

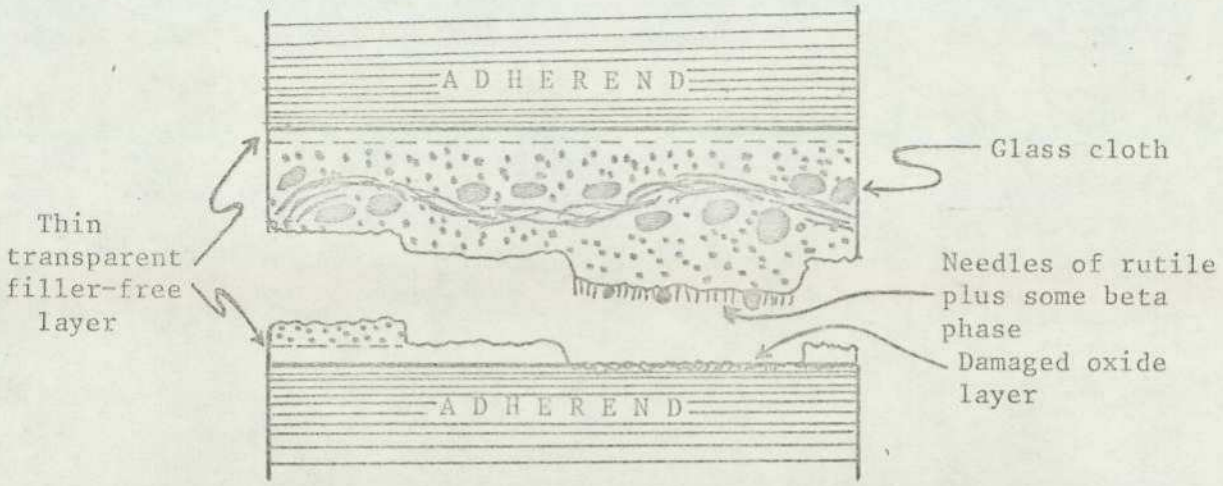


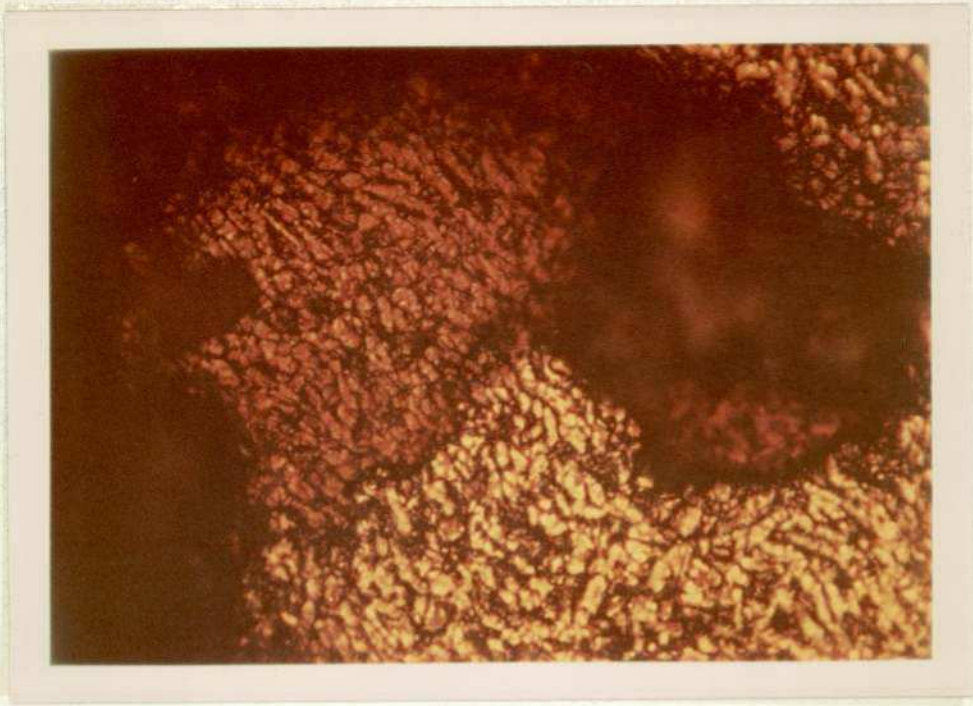
Figure 6.16 is an actual photograph of a typical area.

Figure 6.17 is an electronmicrograph of an area where substrate failure was suspected. It shows clearly the oxide needles protruding from the adhesive layer.

The relationship between bond strength and time of etching is believed to be due to an increase in surface roughness alone, which was seen to reach its maximum after etching for one minute. There are no other significant changes taking place during the process apart from formation of rutile needles on alpha phase areas, which undoubtedly will contribute towards the measured bond strength in the form of mechanical interlocking.

Another possibility which cannot be excluded is that the adherend surface (TiO_2-rutile) may be somehow affecting polymerisation of the adhesive. The depth of this effect will be a function of the height of asperities and once the latter reaches a maximum this too reaches its maximum. This could account for the observed results as cohesive failure within the adhesive dominating almost the entire range.

In an attempt to understand the factor(s) leading to the existence of such a relationship between etching for various times and bond strength, an experiment was designed to affect the roughness. As mentioned earlier, addition of nitric acid slows down the rate as well as preferential attack on the various phases of the alloy by hydrofluoric acid. Joints were made using adherends etched for one and a half minutes



(Original mag. 250 X)

Figure 6.16 : Photomicrograph of an area where substrate failure took place. It also shows the thin yellow - orange film which is believed to have separated during curing. The surface of adherends was etched with HF before bonding with Hidux 1197C.



(Original mag. 50,000X)

Figure 6.17 : Electron micrograph (indirect replication) of an adhesive area opposite an area where substrate failure took place and showing oxide needles embeded in the adhesive.

in solutions containing 4% hydrofluoric acid to which amounts (0-30% w/v) of nitric acid were added. Such solutions are known to leave rutile on the alloy.

The results obtained are listed in Table 6.15 together with other relevant information and represented graphically in Figure 6.18. All joints were tested at temperatures (20 $\sim$ 23^{o}C).

Figure 6.18 shows that addition of nitric acid leads to weaker joints which tend to a limiting value ca.71 MN/m^{2}, at concentrations greater than 20% w/v of nitric acid. The mode of failure changed from about 100% cohesive within the adhesive at low concentrations of nitric acid, to almost complete interfacial at high concentrations as far as can be detected by electronmicroscopy, with a progressive change from the former type to the latter, with increase in concentrations of nitric acid. The position of failure within the adhesive bond depended on the concentration of nitric acid. The distance of the fracture from the interface decreased with increase in nitric acid concentration. Some substrate failure was observed and it was confined to adherends etched in solutions containing less than 3% w/v nitric acid. The magnitude of the substrate failure was of the same order to that observed with adherends etched in aqueous hydrofluoric acid for longer than one minute.

The relationship between joint strength and concentration of nitric acid seems to be of the type:

$$y_c = m \log C$$

where y_c = bond strength at concentration = C
C = concentration of nitric acid added
m = constant

and as seen in Figure 6.19 a plot of y against log C shows a good linear relationship between bond strength and concentration of nitric acid. The value of m as calculated from Figure 6.19 is 24.

Adhesive Bond Thickness X 10^{-3}cm	Torsional shear stress in MN/m^2	Concentration of HNO_3 %(w/v) in 4%(w/v) hydrofluoric acid
18	107	0
21	104	1
18	95	2
24	93	3
17	88	4
21	87	5
21	87	6
20	84	7
20	83	8
22	82	10
22	78	11
22	77	12
20	72	15
20	73	16
17	74	18
19	71	20
19	71	22
20	71	25
18	72	30

TABLE 6.15 (IMI-318 alloy/Hidux 1197C adhesive)

Effect of addition of nitric acid to 4% (w/v) hydrofluoric acid on joint strength.

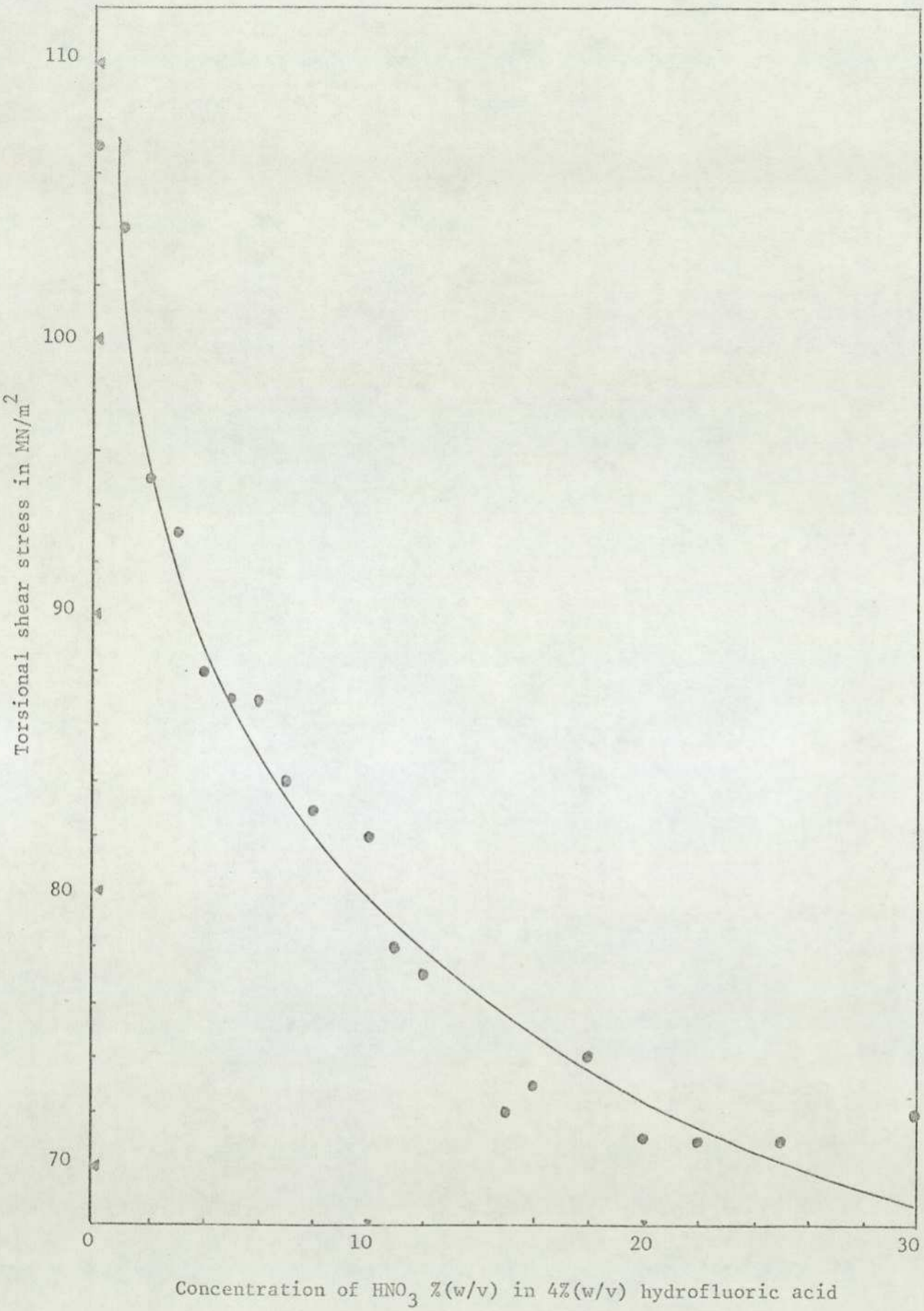


Figure6.18 - (IMI-318 alloy/Hidux 1197C adhesive)

Effect of addition of nitric acid to 4% (w/v) hydrofluoric acid on joint strength.

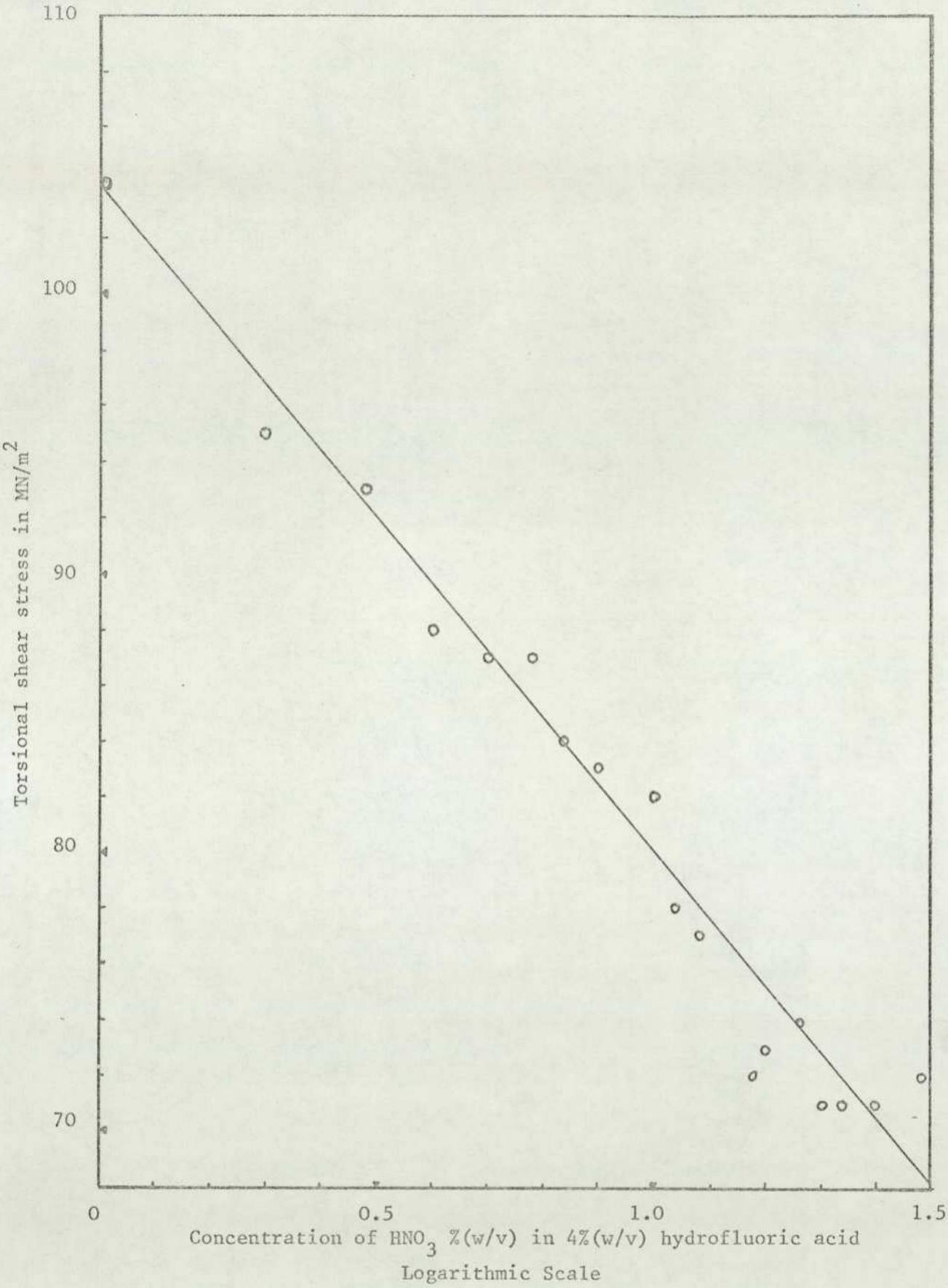


Figure 6.19 - (IMI-318 alloy/Hidux 1197C adhesive)

Effect of addition of nitric acid to 4% (w/v) hydrofluoric acid on joint strength.

The results from the previous two experiments seem to indicate that surface roughness makes the larger contribution towards the relationship between etching time and bond strength. This is supported by the evidence collected from observations on the position of fracture. Such a situation can arise if fracture is taking place very near the asperities each time. The height of the asperities decreased progressively with increasing nitric acid concentration.

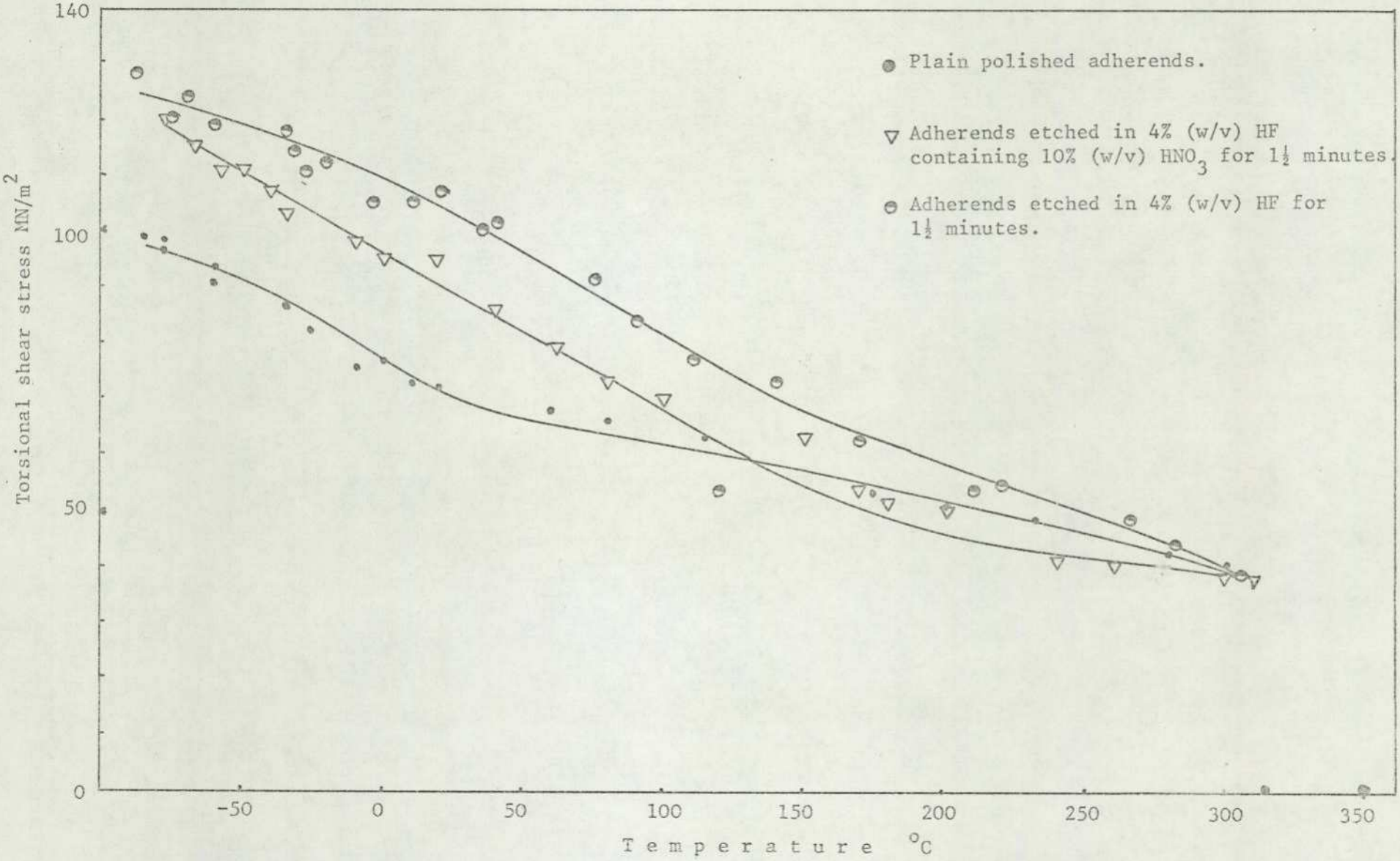
6.9 Effect of temperature on bond strength using IMI-318 alloy and Hidux 1197C adhesive

The following pretreatments were investigated:

1. Plain polished to 6 μm.
2. Etching with aqueous hydrofluoric acid (4% w/v) for 1½ minutes at room temperature.
3. Etching with aqueous hydrofluoric avid (4% w/v) containing 10% (w/v) nitric acid for 1½ minutes at room temperature.
4. First order yellow/brown oxide produced electrolytically in 0.1N sulphuric acid at 12 volts.
5. First order blue oxide produced electrolytically in 0.1N sulphuric acid at 24 volts.
6. Second order yellow oxide produced electrolytically in 0.1N sulphuric acid at 45 volts.
7. Oxidation for one hour in hydrogen peroxide (0.05M)/sodium hydroxide (0.4M) (Black oxide region) at 22°C.

The results obtained from these experiments are shown graphically in Figures 6.20 and 6.21, and the actual data given in Tables 6.16, 6.17, 6.18, 6.19, 6.20, 6.21 and 6.22 immediately after the figures to which they refer. The mode of failure in each experiment was followed by examination of fractured surfaces by optical microscopy as well as Nomarski's interference method and in some cases two stage replication techniques were used for examination by electron microscopy.

Figure 6.20 - Strength - temperature profile of Hidux 1197C adhesive on IMI-318 alloy.



Adhesive Bond Thickness X 10^{-3} cm	Torsional shear stress in MN/m^2	Temperature of Test ^{o}C
18	99	-85
21	98	-78
18	97	-78
21	91	-60
20	93	-60
18	86	-35
21	82	-25
22	76	-10
18	77	0
18	73	10
20	72	20
17	68	60
20	66	80
19	63	115
25	54	175
18	51	200
20	49	232
19	43	280
20	41	300
18	0	315
23	0	350

TABLE 6.16 - (IMI-318 alloy/Hidux 1197C adhesive)
Plain polished adherends.

Adhesive Bond Thickness X 10^{-3}cm	Torsional shear stress in MN/m^2	Temperature of Test ^{o}C
22	128	-88
21	120	-76
21	124	-70
21	119	-60
18	118	-35
18	114	-32
24	110	-28
18	112	-20
20	105	- 4
22	105	10
19	107	20
19	100	35
18	101	40
19	91	75
20	84	90
23	77	110
21	54	120
18	73	140
18	63	170
18	54	210
19	55	220
19	49	265
20	44	282
20	39	305

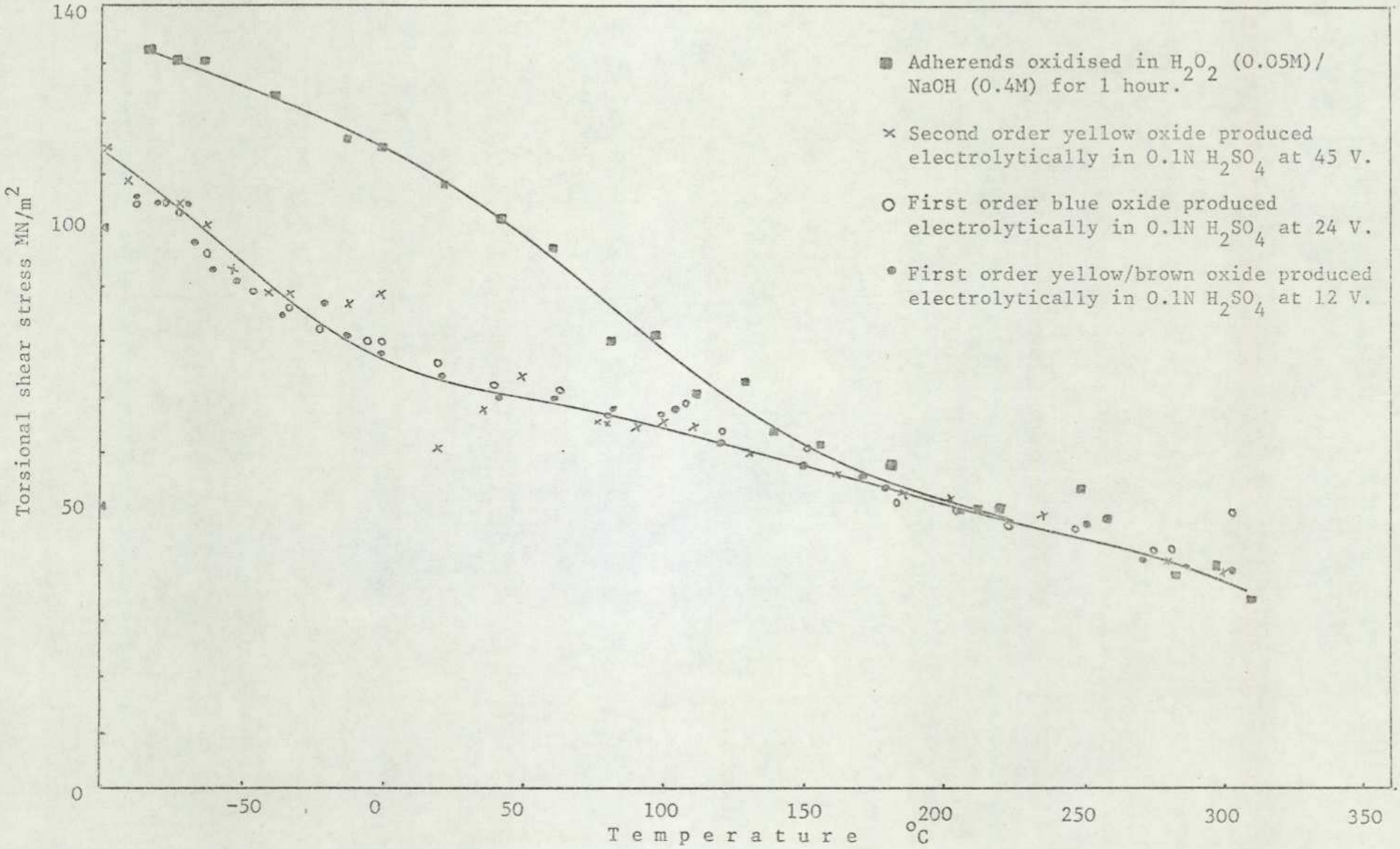
TABLE 6.17 - (IMI-318 alloy/Hidux 1197C)

Adherends etched in 4% (w/v) hydrofluoric acid for 1½ minutes at room temperature.

Adhesive Bond Thickness X 10^{-3}cm	Torsional shear stress in MN/m^2	Temperature of Test ^{o}C
18	118	-78
21	120	-78
17	120	-78
20	115	-68
22	112	-58
19	112	-50
20	107	-40
21	103	-35
17	98	-10
21	95	0
22	95	20
22	96	20
23	86	40
18	79	61
19	73	80
20	70	100
19	63	150
19	54	170
20	52	180
20	50	200
19	41	240
19	41	260
17	39	300
17	38	310

TABLE 6.18 - (IMI-318 alloy/Hidux 1197C adhesive)
Adherends etched in 4% (w/v) hydrofluoric acid containing 10% (w/v) nitric acid for 1½ minutes at room temperature.

Figure 6.21 - Strength - temperature profile of Hidux 1197C adhesive on IMI-318 alloy.



Adhesive Bond Thickness X 10^{-3}cm	Torsional shear stress in MN/m^2	Temperature of Test ^{o}C
19	106	-86
20	105	-80
19	105	-70
19	97	-67
21	93	-60
17	91	-51
22	85	-35
23	87	-20
18	81	-12
21	78	0
17	74	21
21	70	42
22	70	62
22	68	83
18	68	105
18	62	121
20	58	150
19	56	172
20	54	180
21	50	205
18	47	250
18	41	272
22	40	287
21	39	303

TABLE 6.19-(IMI-318 alloy/Hidux 1197C adhesive)
First order yellow/brown oxide produced electrolytically in 0.1N H_2SO_4 at 12 volts.

Adhesive Bond Thickness X 10^{-3}cm	Torsional shear stress in MN/m^2	Temperature of Test ^{o}C
22	105	-87
20	105	-78
20	103	-72
20	96	-62
20	89	-45
20	86	-33
22	82	-21
21	80	- 5
17	80	0
21	76	20
18	72	40
18	71	63
21	68	82
23	67	100
21	69	109
23	64	121
19	61	152
21	51	183
20	50	203
18	47	223
22	47	247
17	43	276
19	43	281
22	50	303

TABLE 6.20 -(IMI-318 alloy/Hidux 1197C adhesive)
First order blue oxide produced electrolytically in 0.1N H_2SO_4 at 24 volts.

Adhesive Bond Thickness X 10^{-3}cm	Torsional shear stress in MN/m^2	Temperature of Test ^{o}C
21	115	-98
20	109	-80
18	105	-71
22	101	-62
20	93	-53
22	89	-40
22	89	-32
20	87	-11
21	89	0
23	61	20
23	68	36
20	74	50
18	66	80
18	65	91
20	66	100
19	65	111
20	60	131
18	58	149
19	56	162
20	53	185
18	52	202
19	49	235
19	41	280
21	39	300

TABLE 6.21- (IMI-318 alloy/Hidux 1197C)

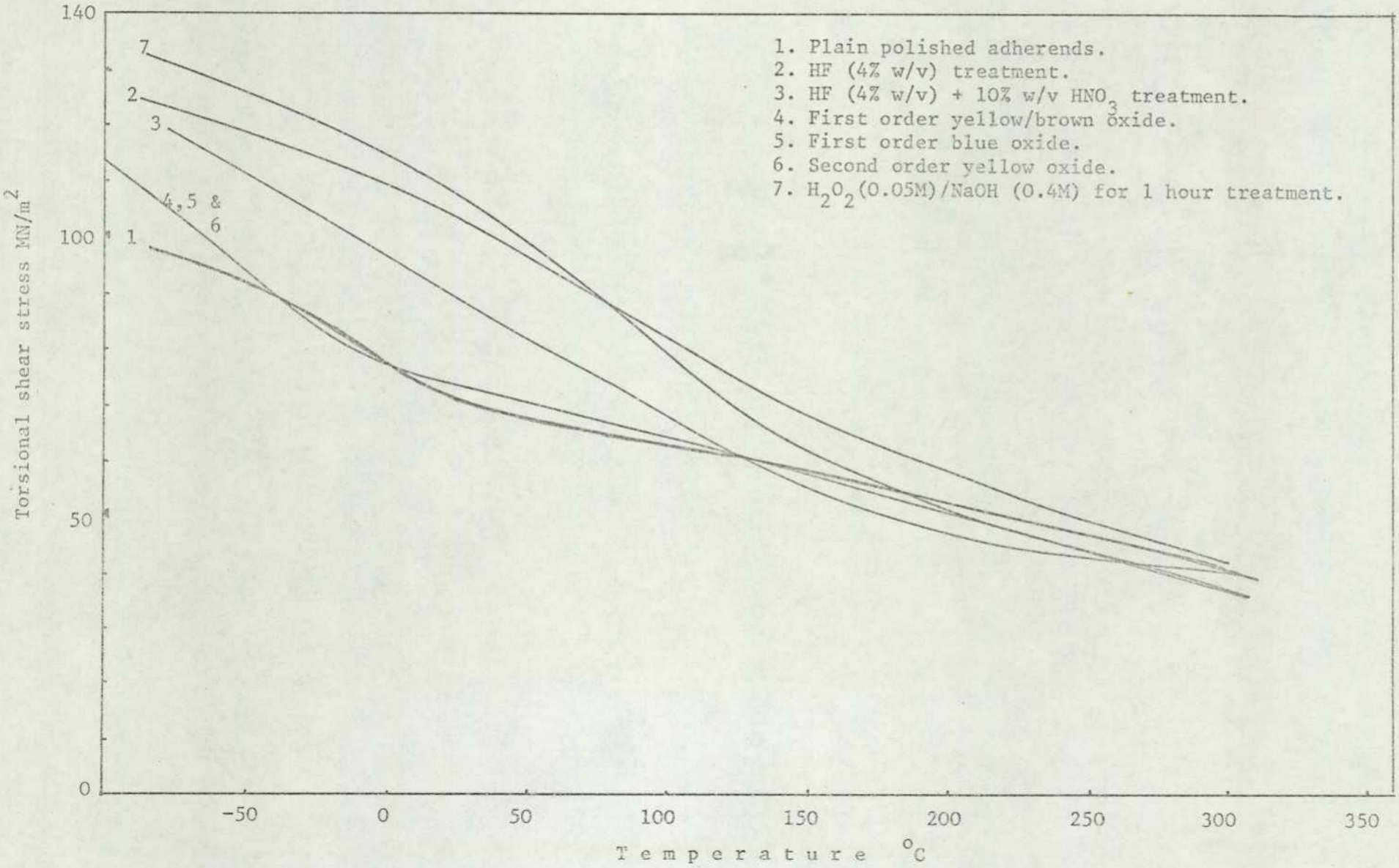
Second order yellow oxide produced electrolytically in 0.1N H_2SO_4 at 45 volts.

Adhesive Bond Thickness X 10^{-3} cm	Torsional shear stress in MN/m^2	Temperature of Test ^{o}C
17	132	-82
21	130	-73
20	130	-72
22	130	-63
21	124	-38
21	116	-12
20	115	0
22	108	22
21	102	42
20	97	61
19	80	82
21	81	98
19	70	112
18	73	130
20	64	140
23	62	157
20	58	181
21	50	212
18	50	220
22	54	249
21	48	258
18	38	283
20	40	298
18	34	310

TABLE 6.22- (IMI-318 alloy/Hidux 1197C adhesive)

Adherends were oxidised in hydrogen peroxide (0.05M)/Sodium hydroxide(0.4M) for one hour at $22^{o}C$.

Figure 6.22- Strength - temperature profile of Hidux 1197C adhesive on IMI-318 alloy.

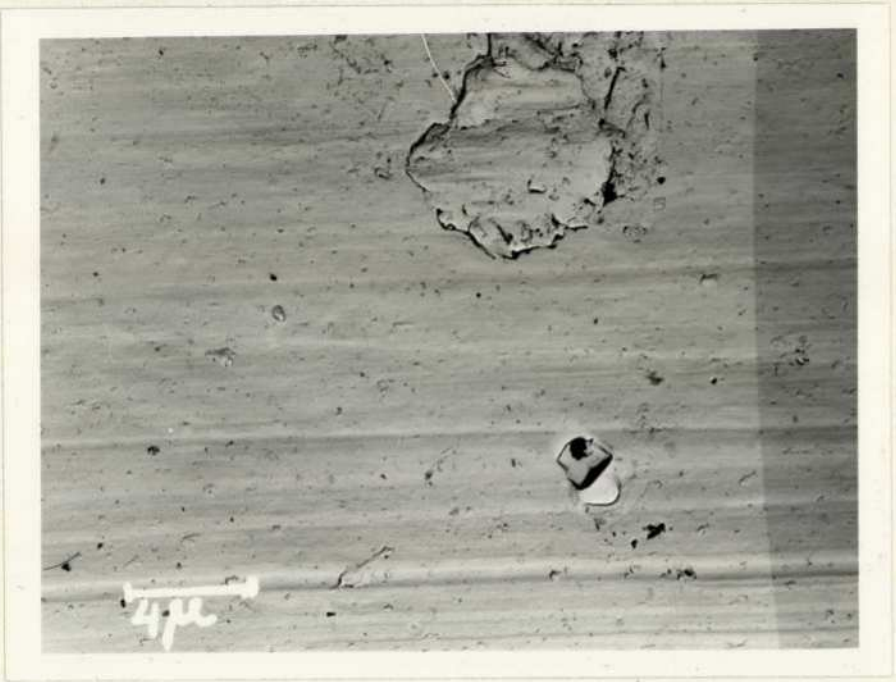


6.9.1 Discussion of results

Figures 6.20 and 6.21 are summarised in the composite Figure 6.22. It can be clearly seen from Figure 6.22 that the various pretreatments studied affect strength-temperature profiles. These profiles are different in general form, and as might be expected with an adhesive reinforced by glass cloth, failure was at (or near) the interface. In all these pretreatments, bonds failed on one side of the glass cloth and the fracture never crossed the glass cloth.

In treatments 1, 4, 5 and 6 the adherend surface appears superficially clean and the high finish of the metal is reflected in the surface appearance of the separated adhesive as if no true wetting had occurred. Further examination with optical and electron microscopy revealed the absence of any adhesive on about 98% of the total area of the adherend. Figures 6.23, 6.24, and 6.25 are electron micrographs of adherend surface after bond fracture and as can be seen very little adhesive is present on the substrate and interfacial failure was concluded to be the main type which is taking place. Contact angles of water on these surfaces confirm this impression. The actual values obtained are contained in Table 6.23. The large differences which exist between contact angle values on "bare" metal areas and adhesive indicate that the two surfaces are different. The bare metal before bonding showed various contact angles, all less than 10^{o}.

The appearance of broken joints remained the same over the entire range of temperatures investigated and up to $300^{o}C$; beyond which decomposition of the adhesive became apparent.



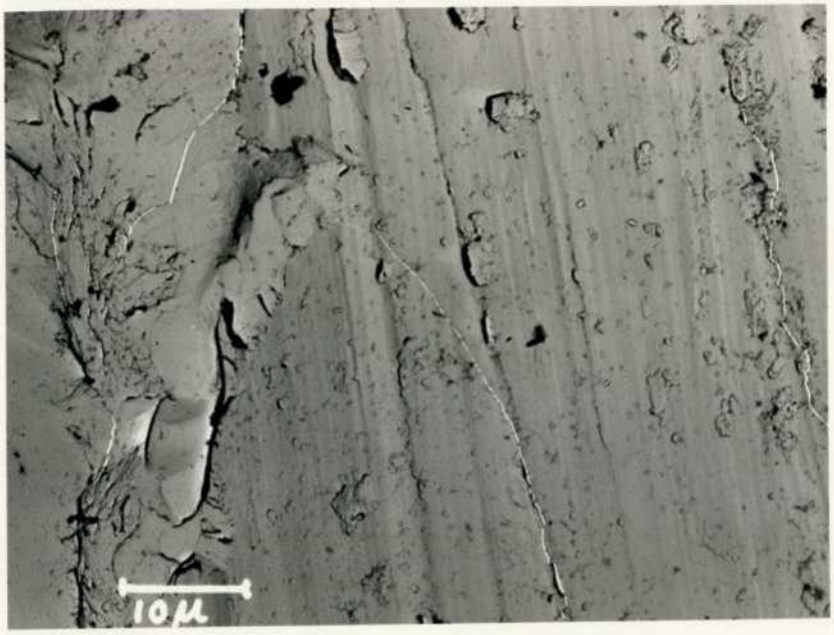
(Original mag. 1,000X)

Figure 6.23 : Electron micrograph (indirect replication) of IMI-318 alloy polished to 6 μm , bonded with Hiduxl197C and tested at -78°C. It shows clearly that most of the surface is bare. The broad lines seen are polishing marks.



(Original mag. 1,000X)

Figure 6.24 : Electron micrograph (indirect replication) of IMI—318 alloy electrolytically oxidised (1st.order blue oxide) in 0.1N sulphuric acid, bonded with Hidux 1197C and tested at -21°C. It shows an area where some adhesive remained on the adherend.



(Original mag. 1,000X)

Figure 6.25 : Electron micrograph (indirect replication) of IMI-318 alloy electrolytically oxidised (1st. order yellow/brown oxide) in 0.1N sulphuric acid, bonded with Hidux 1197C and tested at $0^{o}C$. It shows an area where some adhesive remained on the adherend and where interfacial failure has taken place.

Adherend	Temperature of test °C	Contact angle measurement on four different areas of bare metal after bonding					actual adhesive				
		1	2	3	4	Mean	1	2	3	4	Mean
Plain polished	-78	15.3	16.7	14.9	14.8	15.4	38.6	37.8	38.1	38.5	38.2
Plain polished	-10	14.7	15.0	14.3	15.1	14.8	37.1	38.2	38.0	37.7	37.7
First order yellow brown oxide	-51	15.1	15.5	13.9	14.7	14.8	36.8	38.1	37.8	37.6	37.6
Blue oxide	0	14.8	15.0	14.6	15.2	14.9	36.5	37.0	38.5	38.1	37.5
Blue oxide	100	15.7	16.0	14.8	14.1	15.2	36.9	38.2	37.5	36.6	37.3
Second order yellow oxide	50	14.8	15.2	14.7	14.3	14.7	38.3	37.8	37.8	36.9	37.7

Table 6.23 : Contact angles of water on fractured joints made with IMI-318 alloy and Hidux 1197C .

The previous mode of failure changed from interfacial to cohesive within the adhesive with adherends pretreated chemically (pretreatments 2, 3 and 7). The exact position varied from one pretreatment to another. In treatment (3) the position of failure was nearest to the interface while in (7) it was the furthest. Again this type of failure was dominant over the whole temperature range. The position of failure in these pretreatments was similar to that shown diagramatically on page 176 .

Towards the lower end of the temperature range in about 1 to 2% of the total areas, the fracture did reach the substrate and careful examination by optical microscopy revealed that not only was substrate failure taking place, but also a thin and filler-free (yellow-orange) film was present, around the bare metal areas. (See Figure 6.16). A two stage replication method was employed to examine the opposite areas on adherends etched with hydrofluoric acid (pretreatment 2). This showed clearly oxide needles embedded in the adhesive (similar to those in Figure 6.17). Unfortunately, the roughness of the fractured joints in these pretreatments (2,3 and 7) prevented examination of these small areas in greater detail but an attempt was made to collect these oxide needles for identification by X-ray powder analysis. The results obtained are shown in Table 6.24 confirming the presence of rutile. The few extra lines are due to beta phase of titanium. This result confirms that substrate failure was taking place.

Similar behaviour was observed with pretreatments 3 and 7, but because of the very small areas showing substrate failure, it was not possible to collect enough material for X-ray powder analysis.

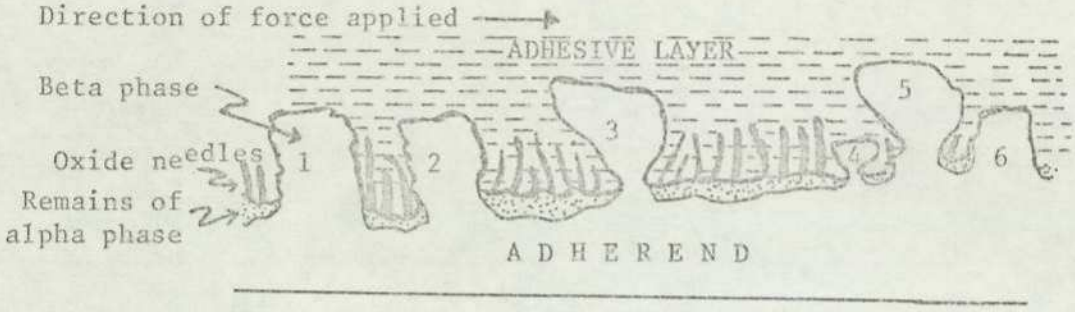
No obvious transition from ductile to brittle failure was noted even with alkaline hydrogen peroxide pretreatment. Neither drawn ductile edges nor complete cohesive failure was seen in all the pretreatments investigated.

Experimental results X-ray powder diffraction method		Calculated d-values for beta phase Ti		ASTM data for TiO_2 - rutile	
dÅ	Intensity	dÅ	hkl values	dÅ	Intensity
3.244	vst	-	-	3.245	100
2.490	m	-	-	2.489	41
2.332	st	2.338	110	-	-
2.293	w	-	-	2.297	7
2.183	m	-	-	2.188	22
2.050	w	-	-	2.054	9
1.688	st	-	-	1.687	50
1.648	m/st	1.653	200	-	-
1.621	w	-	-	1.624	16
1.480	w	-	-	1.480	8
1.360	m	-	-	1.360	16
1.352	m	1.349	211	-	-
1.341	w	-	-	1.347	7
(1.170-1.168)	m	1.169	220	1.170	4
1.148	w	-	-	1.148	4
1.090	w	-	-	1.093	4
1.078	w	-	-	1.081	4
(1.046-1.040)	w	1.046	310	1.042	5
		0.954	222		
		0.884	321		
		0.826	400		

v = very ; st = strong ; m = medium ; w = weak

Table 6.24 : X-ray powder diffraction of material recovered from Hidux 1197C adhesive from areas where substrate failure took place. Adherends were etched with HF 4%w/v for 1½ minutes .The beta phase d-values were calculated based on a body centered cubic cell with lattice dimension 3.3065 Å [137].

It may be asked why is cohesive failure obtained within the adhesive when the substrate is pretreated chemically? The situation at the interface on such substrates is very similar and although the following diagram illustrates a surface etched with hydrofluoric acid, it applies equally to the other surfaces.



As seen, it is impossible to load the interface because of the presence of these asperities which undoubtedly, in such cases, assume a large fraction of the load in the interfacial plane. Therefore, fracture away from the interface is promoted. These asperities tend to form stress concentrations and possibly initiate a fracture which can propagate in one of two places depending on the point of initiation. If the crack begins on top of an asperity, then it will tend to propagate away from the interface. This will be assisted by the fact that the adhesive above these asperities is usually more sheared than that within the asperities. But if one of the asperities like that numbered 3 on the diagram breaks off, then the crack may propagate along the interface removing some of the oxide needles and any loosely held beta phase, like those numbered 4 and 5. This mechanism is justified by the presence of rutile needles and fragments of beta phase from the alloy on the adhesive after breaking the bond. The crack will move away from the interface when it reaches a firm asperity like that numbered 6.

The position of failure was seen to depend on the various pretreatments and generally the smoother the surface, the nearer to the interface the failure. This accounts for the identical type of failure observed with all electrolytically oxidised adherends. Furthermore, electron microscopy examination of these substrates showed that they were very similar, if not the same. It should be remembered that electrolytic oxidation employed in this work did not lead to change in the topography of surfaces as far as can be detected with the available techniques.

CHAPTER 7

GENERAL CONCLUSIONS AND DISCUSSION

GENERAL CONCLUSIONS AND DISCUSSION

Surface Chemistry

Despite the numerous pretreatments investigated, it seems the only coating which is produced and is stable at room temperatures is TiO_2-rutile. The degree of crystallinity of this oxide varies from one pretreatment to another. Neither a hydride nor a fluoride was found on either alloy. The compounds are said to be formed on titanium when etched in hydrofluoric (or sulphuric) acid[43] or fluoride-phosphate etch[62] respectively. All the various etchants reported in literature seem to be based on no more than trial and error and the nature of the coatings formed by the various etching solution has received little attention. Likewise, the mode of attack on multiple-phase titanium alloys or the final roughness obtained has received almost no attention.

The present work indicates that the etching methods employed in surface pretreatment give different topographical features. The maximum roughness obtained was by etching in boiling 10%(w/v) hydrochloric or sulphuric acid for longer than two hours, and it is most unfortunate that lapjoints ca. 0.6 cm^2 overlap made with adherends after such pretreatment could not be tested as they exceeded the limits of the available testing machines. The appearance of such coatings indicate that they are composed of very coherent and rough oxide layers. (This treatment was not used on torsional shear test pieces because of the danger of uneven dissolution of the ring).

Oxidation in alkaline hydrogen peroxide leads to different roughnesses depending on the concentrations employed. The maximum roughness was formed by oxidation within the black oxide region, but prolonged oxidation in any region had the undesirable effect

of either entrapping gasses in the porous surface or producing a thick weak oxide layer. The experimental results obtained from oxidation within the black oxide region, indicate that oxidation for about one hour at room temperature gives an excellent substrate for bonding.

Very rough surfaces were obtained by etching with aqueous hydrofluoric acid alone. Such surfaces were shown to form strong bonds and although some substrate failure with IMI-318 alloy did occur it was over small areas only.

Etching IMI-205 alloy with aqueous hydrofluoric acid left a black and rather loose amorphous oxide of molybdenum on the surface which hindered a detailed examination of such surfaces before and after bonding. The only way to remove this oxide was by addition of nitric acid (ca. 30% w/v), but solutions with such high concentration of nitric acid leave very smooth surfaces and therefore the effect of roughness on IMI-205 surfaces and bond strength could not be compared with those of IMI-318 alloy.

Presence of oxidising agents with hydrofluoric acid reduced the roughness on both alloys considerably. This is believed to be due to the protective action of a film of oxide extending over all phases of the alloy. Hence preferential attack of one or more of the phases is markedly decreased.

Electrolytic oxidation leads to no change in the topography of surfaces, any oxide formed merely replicates the substrate. Production of such oxides on titanium alloys has received very little attention. The effect of pH or temperature has never been investigated. Thicker oxide layers can be produced by increasing the applied potential. No attempt was made here to investigate the possibility of electrolytic formation of porous oxide layers on titanium but it is believed that

such oxides can be obtained. If this could be achieved, then because of the coherence of such oxides coupled with their porosity they would provide a very good coating for bonding.

It has been reported by Caprido and Turris[62], and Breshears[65] that blue coatings formed by anodic oxidation are the least favourable coatings for bonding titanium or its alloys but they did not mention the evidence on which their conclusions are based. The present work shows that very strong bonds can be obtained with blue coatings and they are as good as any other coloured oxide coating formed by this method. It should be remembered that these coloured coatings owe their colours not to excess metal as suggested by Bianchi et al[50] but to interference due to various thicknesses of the rutile coating.

Effect of substrate surface on bond strength

The present work confirms that surface pretreatments do affect joint strength and although only TiO_2-rutile is formed on the surface, different oxidation methods produced different strength-temperature profiles. This arises from one or more of the following ways:

1. Different roughnesses of adherends.
2. Different mechanical properties of oxides produced.
3. Specific interaction of substrate with adhesive.

These possibilities are expanded below:

1. With rough surfaces mechanical interlocking may take place and this is usually accepted as the cause of improved adhesion rather than the increased surface area which naturally accompanies this process. Unfortunately, the roughest surfaces obtained in this work could not be investigated in the same detail as the other surfaces, but it is interesting to note that with both adhesives the roughest surfaces investigated lead to strongest joints over a wide

range of temperatures. This is despite the fact that with rough surfaces complete wetting can only be obtained with difficulty and in many joints specially those oxidised in alkaline hydrogen peroxide for long times, entrapped gases were noticed, which inevitably lead to stress concentration points.

2. X-ray powder diffraction, together with transmission and reflection electron diffractions, indicate that the TiO_2 produced in the majority of cases was of low crystallinity with the exception of the oxide needles which form on the alpha phases in IMI-318 alloy when etched in hydrofluoric acid solutions. The crystallinity of the oxide will affect bond strength directly through the mechanical properties of the oxide layer and possibly indirectly by selective adsorption of the polymer. Substrate failure at lower temperatures was observed with all oxides. Whether this failure is due to weak mechanical properties of the oxide or due to the stresses within the oxide layer arising from the coexistence of multiple oxides of titanium and those of the alloying elements, was not clear. However, as examination by transmission electron diffraction of stripped oxide coatings did not show the existence of oxides other than TiO_2-rutile, the weak mechanical properties seem to be the most likely cause.

3. Differences in the strength of the bonded joints even when all failure is cohesive in nature suggest that the surface formed by the various treatments influences the properties of the adhesive. The surface of the adherend may affect the process of hardening, since it is known that many metals and oxides catalyse or inhibit the crosslinking of polymers and alter the strength of the joints. Refractive index measurements described on page 159 showed that near the interface different degrees of crosslinking were present

which could be due to catalytic action of the adherend surface. Crosslinking can be modified near the interface if selective adsorption is taking place, which limit the mobility of polymer chains. Adherends could also affect the degree of crystallinity of the polymer particularly with the very thin adhesive bonds employed here.

Another possibility which could affect joint strength is that if the adherend surface is dissolving in the adhesive. This can be ruled out in the present work as no damage of this kind was seen on all adherends examined.

Mode of failure and locus

Surface pretreatments affected the mode of failure in addition to their effect on joint strength.

There seems to be a different mechanism for initiating failure at higher temperatures than at lower temperatures, although with the adhesives studied it is not simply a case of brittle fracture at low and ductile failure at higher temperatures. The appearance of the broken adhesive does not differ sharply over the temperature range. BSL-308 adhesive shows more breaks through the adhesive from one interface to the other at lower temperatures but there are no signs of drawn ductile edges at high temperatures as was reported for Redux 775[114]. Breaks through the adhesive suggest a form of brittle fracture. This is prevented by the glass reinforcement of Hidux 1197C which throws the process towards the interface with the metal, in fact to the very thin adhesive layer between the glass cloth and the metal. This entails a higher rate of straining of adhesive near the interface than for unsupported adhesive where the shear is distributed across the total thickness, constant rate of angular movement is imposed by the test apparatus.

A further differentiation in the properties of the adhesive near to the metal is that it is free of any filler caused by migration. Whether the material is intrinsically different in constitution or molecular weight or not, makes little difference since freedom from filler will alone suffice to change the fracture properties. There exists therefore an extreme case of the situation postulated by Good[138] in which variations in fracture, and perhaps molecular, properties are a function of distance from the interface leading to failure close to but not at the interface.

The metal surface after pretreatment is very rough and the exact interface is difficult to define. It is reasonable to expect concentration of stresses at the tips of asperities and hence failure at this level. On the other hand if the adhesive is sufficiently strong it may be that the whole of the outer layer of the oxide will be removed when fracture occurs. Where fracture occurs more easily through the bulk of the adhesive, the temperature profile tends to level off at lower temperatures as was clearly demonstrated by Foulkes et al[114] but where reinforcement interferes with bulk fracture this feature of the temperature-joint strength profile is absent. Evidence has been presented (see page159) that the material near the interface differs from that in the bulk of the adhesive. This will give different mechanical properties.

Substrate failure was observed with both alloys. IMI-205 etched with hydrofluoric acid failed mainly within the oxide coating due to the presence of the loose molybdenum oxide, IMI-318 alloy when etched with hydrofluoric acid is rather more complicated. However, it can be explained by fracture reaching the substrate breaking off some of the beta phase and oxide needles as has been indicated earlier, (page 199).

Also with IMI-318, alkaline hydrogen peroxide oxidation gives thick black oxide layers which failed mainly because they are weakly-coherent.

Plain polished adherends in each case produced largest scatter and weakest joints (apart from IMI-205 alloy etched with hydrofluoric acid, which is a special case). This may be the result of contamination as well as of a"Bikerman weak boundary layer" in the form of hydrated oxide. Actually, all the previously mentioned modes of failure can be regarded similarly as forms of Bikerman's weak layer whether within the substrate or the adhesive.

Finally, the indications in the present work are that of a coherent, rough surface of rutile provides the best substrate on the two alloys studied for adhesive bonding. This is betst obtained by short period oxidation by alkaline hydrogen peroxide. This, coupled with the information on the nature of failure in the adherend suggests that at low temperatures there is a mechanical interaction which modifies adhesive behaviour.

POSSIBLE FUTURE WORK

The foregoing suggests that the following possibilities for further work on the subject matter in this field are:

(a) The large scatter observed from bonding adherends containing different ratios of alpha to beta phases is attributed to different roughness as obtained by various pretreatments. Since the final roughness is a function of volume of the various phases present, it would be worthwhile to see if the alpha/beta phase ratio at the surface has any appreciable effect.

(b) Since thick anodic oxides can be obtained on titanium alloy, it is possible that under certain conditions of pH or temperature a porous oxide (similar to that which can form on aluminium and its alloys) could be obtained. These would undoubtedly be advantageous for bonding because of the mechanical element contributed by pore penetration.

(c) Anodic oxides are very coherent and might be used to reinforce rough surfaces produced by other treatments.

APPENDIX 1

Glossary Of Terms Used In Titanium Metallography

Acicular alpha: Alpha phase formed by the transformation from beta along preferred planes of the beta lattice appearing as needles or plates in the microstructure.

Acicular alpha-beta structure: A two phase alpha-beta structure wherein the alpha phase is acicular in appearance.

Alpha (α) : The low-temperature hexagonal-close-packed allotrope of titanium.

Alpha martensite structure: A structure composed of primary alpha and martensite formed by quenching an alpha-beta alloy from a temperature where the composition of the beta-phase component is less than the composition where the M_s temperature is at room temperature.

Alpha prime (α'): A super saturated solution of alpha formed by quenching alpha-beta alloys from the beta field or alpha-beta field where the composition of the beta phase is less than the composition of the M_s at room temperature. (Also called martensite).

Alpha transus: The temperature which designates the phase boundary between the alpha and alpha plus beta fields for a given alloy composition.

Beta (β): The high-temperature, body-centered cubic allotrope of titanium.

Beta isomorphous: A term used to describe an alloying element which forms a system in which there is a complete solubility between the alloying element and beta titanium.

Beta transus: The temperature which designates the phase boundary between the alpha-plus-beta and beta fields for a given alloy composition.

Elongated alpha: A term used to describe the elongated shape of alpha phase in an alpha-beta alloy that has been formed as a result of fabrication in one direction.

Equiaxed alpha: Alpha phase in alpha or alpha-beta alloys which has an equiaxed appearance. It is used to describe structures obtained by fabrication and annealing in the alpha or alpha-beta fields.

Martensite: The product of the diffusionless transformation of beta to alpha in titanium alloys which results in an acicular (alpha-prime) structure with well defined needles or plates. It is often difficult to distinguish from acicular alpha formed by nucleation and growth although the latter is usually less well defined with curved rather than straight sides. Sometimes called alpha prime.

M_s temperature: The temperature at which martensite starts to form during cooling.

Omega phase: A transition phase that forms during the nucleation and growth transformation of beta to alpha. It is coherent with the beta lattice and cannot be seen under the light microscopy. Omega phase can be seen by using the electron microscope.

Primary alpha: Alpha phase which was present prior to a heat treatment as distinct from the alpha phase formed during the heat treatment.

Retained beta: Beta phase which is present in the microstructure as a result of quenching. No transformation of the beta has taken place.

Transformed alpha: A term sometimes used to designate alpha formed by the transformation from beta. More commonly called transformed beta.

Transformed beta: Alpha phase which is formed by transformation from beta, also called acicular alpha.

Widmanstatten alpha: Alpha phase formed by transformation from beta in a Widmanstatten pattern.

Widmanstatten pattern: A geometrical pattern resulting from the formation of a new phase along certain crystallographic planes of the parent phase.

REFERENCES

1. Imperial Metal Industries (Kynoch) ltd., New metals division, Birmingham 6, IMI-318,2 ed/MK 140/23/Nov.1969 ,page 3.

2. ibid , page 5.

3. J.J. Rausch, F.A. Crossley, and H.D. Kessler, Transactions of AIME, J.of metals,206,211,(1956).

4. J.C. Williams and M.J. Blackburn, Transactions Quaterly, Trans. American Soc. for Metals, 60 (3),373,(1967).

5. H.L. Gegel and S. Fujishiro, J. Less-Common Metals, 17 ,305,(1969).

6. H. Margolin and H. Portisch , Trans. Metallurgical Soc. of AIME, 242, 1901,(Sept. 1968).

7. H.R. Ogden, D.J. Maykuth, W.L. Finlay and R.I. Jaffee, Trans. Am. Inst. Min(Metall). Engrs., 191, 1150, (1951).

8. A.D. McQuillan, J. Inst. Met., 80,433, (1951 - 54).

9. P.J. Fopiano, M.B.Bever and B.L. Averbach, Trans. of the ASM.,62(2), 324, (1969).

10. Imperial Metal Industries (Kynoch) ltd., New metals division, Birmingham 6, IMI-205 , R1/MK 60/ Sept.1965 , page 1.

11. H. Ikawa, S. Shin, and M. Morikawa , Technology Reports - Osaka University, 19, 449, (1969) .(In English).

12 M. Hansen, E.L. Kamen, H.D. Kessler, and D.J. McPherson, Trans. Amer. Inst. Min.(Metall). Engrs., 191, 881, (1951).

13. C.M. Graighead, O.W. Simmons, and L.W. Eastwood, Trans. Amer. Inst. Min.(Metall). Engrs., 188,485, (1950).

14. W.J.Z. Kroll, Metallk. 29, 189, (1937). Cited by A.D. McQuillan and M.K. McQuillan in Titanium, Butterworths, London 1956, page 232.

15. E.I. Larsen, E.F. Swazy, L.S. Busch, and R.H. Freyer, Metal Progr., 55, 785, (1950).

16. M. Hansen, E.L. Kamen, H.D. Kessler, and D.J. McPherson, Trans. Inst. Min.(Metall.). Engrs., 191, 881, (1951).

17. S. Andersson and L. Jahnberg, Arkiv för Kemi, Band 21(nr.39), 413, (Oct. 1963).

17a. Phase diagrams for ceramists, Ed.and published by the American Ceram. Soc., 2nd. Edition, 1969, page 41.

18. J.M. Ferguson, Battle Memorial Institute, Columbus,Ohio, DMIC No.238, part 13, 2, (1968).

19. ibid

20. D.I. Lainer, E.N. Slesareva, M.I. Tsypin, and A.S. Bai, Zashchita Metallov, 2 (6), 692,(Nov.-Dec., 1966). (In Russian).

21. V.V. Glazova, Izv. Akad. Nauk. SSR. Metal, 219, (1967).(In Russian)

22. N.N. Kornilov, and V.V. Glazova, Novye Issledovaniia Titanovykh Splavov Trudy, Akad. Nauk. SSSR, 3, (1965). (In Russian)

23. I.S. Anitov and S.A. Gorbunov, Zhur. Prik. Khim., 34 , 725,(1961). (In Russian).

24. R.C. Weast (Ed.), Handbook of Chemistry and Physics, 52nd. Ed., The Chemical Rubber Co., Ohio,(1971 - 1972), page B-152.

25. J.M. Ferguson, Battle Memorial Institute, Columbus, Ohio, DMIC No.238, part 13, 8, (1968).

26. J. Stringer, G. Metcalf, and M.L. Nicholson, J. Less-Common Metals, 4 , 69, (1962).

27. R.C. Weast (Ed.), Handbook of Chemistry and Physics,52nd. Ed., The Chemical Rubber Co., Ohio, (1971 - 1972), pages B-64, B-111, B-150, and B- 152.

28. D.M. Vasilev, A.I. Melker, and V.V. Trofimov, Zavodskaya Laboratoriya, 33(12), 1539,(Dec.1967). (In Russian).

29. R.J. Kotfia and E.F. Erbin, Metal Progr., 66(4),128, (1954).

30. A.D. McQuillan and M.K. McQuillan, Titanium , Butterworths Sci. Pub., London (1956), page 396.

31. H.R. Ogden and F.C. Holden, Metallography of Titanium alloys,TML-Report No.103, (1958), page 37.

32. H. Margolin and H. Pertisch, Trans. AIME, 242 , 1901, (1968).

33. H.L. Gegel and S. Fujishiro, J. Less-Common Metals, 17 , 305, (1969).

34. H.B. Bomberger, M.B. Vordahl, and W.L. Finlay. Cited by McQuillan and McQuillan in Titanium, Butterworths Sc. Pub., London,(1956), page 397.

35. A.D. McQuillan and M.K. McQuillan, Titanium,Butterworths Sc. Pub., London,(1956), page 242.

36. ibid , page 439.

37. E.R. Scheffer in Treatise on Analytical Chemistry, 5(II), Edited by I.M. Kolthoff and P.J. Elving, Interscience, New York, (1961), page 15.

38. F.A. Cotton and G. Wilkinson, Advanced Inorganic Chemistry, 2nd.Ed., Interscience, (1967), page 803.

39. G.C. Kieffer, Iron Age, 170 , 170, (Dec.1952).

40. I.P. Sorokin and D.D. Babich, Khim. Tekhnologya RESP Mezhveal Naukhnor Tech. Sbornik, 14 , 65, (1968). (In Russian).

41. L.L. Neroslavskaya and V.E. Artemev, Zhur. Priklad. Khim., 42(7), 1650, (1969). (In Russian).

42. T. Koizumi and T. Nakayama, Corrosion Science, 8 , 195, (1968).

43. E.S. Chiganova and K.P. Batashev, Zhur. Prik. Khim., XLI, 521, (March 1968). (In Russian).

44. L.B. Golden, I.R. Lane, and W.L. Acherman, Indust. Engng. Chem., 44 , 1930, (1952).

45. J. Beukankamp and K.D. Herrington, J.Am. Chem. Soc., 82, 3025,(1960).

46. U.R. Evans, The Corrosion and Oxidation of Metals, Edward Arnold ltd., (1961),page 344.

47. S.H. Weiman, Corrosion - Nat. Assoc. of Corrosion Engineers, 22 , 98, (1966).

48. T. Koizumi and T. Nakayama, Proc. of 3rd. Int. Cong. on Metallic Corrosion, 1 , MIR ,Moscow, (1969), page 451.

49. S. Ogawa and D. Watanabe, J. Japan Inst. Met., 18 , 523, (1954).

50. G. Bianchi, F. Mazza, and S. Trasatti, Proc. 2nd. Int. Cong. on Metallic Corrosion,(New York 1963),Pub. by Nat. Assoc. of Corrosion Eng., Texas, page 905.

51. G. Caprioglio, F. Mazza, and F. Mussini, Cited by Bianchi et.al.(ref.50).

52. L. Young, Anodic Oxide Films, Academic press, London,(1961),page 253.

53. S. Yamaguchi, J. Electrochem. Soc., 108 , 302, (1961).

54. B. Rivolta, Met. Ital., 50,173 and 255, (1958).

55. W.C. Wake , in Adhesion - Fundamentals and Practice, Maclaren and Sons ltd., London (1969), page 111.

56. N.A. de Bruyne, The extend of contact between glue and adherend, Bull. No.168, Aero-Research ltd., Cambridge, (1956).

57. C.W. Jennings, Amer. Chem. Soc. Div. of Organic coatings and plastics Chem., Washington meeting, 3(2), 184, (1971).

58. A.D.McQuillan and M.K. McQuillan, Titanium , Butterworths Sci. Pub., London, (1956), page 450.

59. D.F. Neal, IMI-Kynoch Report No. 690/DFN/LGH/ (20th.April 1970)

60. W.H. Guttmann , Coincise Guide to Structural Adhesives, Reinhold Pub. Corp., New York, (1961), page 23.

61. C.V. Cagle, Adhesive Bonding, McGraw-Hill, New York,(1968), page 98.

62. I. Capriolo and F. Turris, Paper presented at "Titanium Symposium", Milano, (1969). Translated by R.L. Preece of IMI-Kynoch ,Birmingham.

63. P.F.A. Bijlmer, Metal Finish, 68(11), 64, (1970).

64. R. Houwink and G. Salomon (Editors), Adhesion and Adhesives, 1 , 108, Elsevier, (1965).

65. S.R. Breshears,Lectures given on titanium at Norair Symposium, March 28-29/1966), DMIC-Memo No.215, AD.801280, page 86.

66. N.K. Benson in Adhesion and Adhesives, (Ed. R. Houwink and G. Salomon), Elsevier,(1965) , 2 , page 490.

67. L. Greenwood in Adhesion ,(Ed. D.D. Eley), Oxford University Press, (1961), page 260.

68. L. Greenwood in Aspects of Adhesion , (Ed.D.J. Alner), 5 , University of London Press, (1969), page 40.

69. J.J. Bikerman , The Science of Adhesive Joints ,2nd. Ed., Academic Press, New York,(1968), page 215.

70. I.N. Sneddon in Adhesion ,(Ed.D.D. Eley), Oxford University Press, (1961), page 207.

71. N.A. de Bruyne, cited by L. Greenwood in Aspects of Adhesion , 5, (Ed.D.J. Alner), University of London Press,(1969), page 40.

72. R.W. Bryant , Nature , 202 (4937), 1087, (1964).

73. N.A. de Bruyne in Adhesion and Adhesives, (Ed. N.A. de Bruyne and R. Houwink), Elsevier,(1951), page 92.

74. T. Gillespie and E.K. Rideal , J. Coll. Sci., 11 , 732, (1956).

75. W.C. Wake in Adhesion ,(Ed.D.D. Eley), Oxford University Press, (1961), page 191.

76. H. Foulkes, J. Shield, and W.C. Wake, J. of Adhesion, 2 , 254,(Oct.1970).

77. R.W. Bryant, and W.A. dukes, Brit.J. Appl. Phys., 16, 101, (1965).

78. W.H. Guttmann, Coincise Guide to Structural Adhesives , Reinhold Publishing Corp., New York,(1961), pp(1-9) and (42-117).

79. C.V. Cagle, Adhesive Bonding, McGraw-Hill Book Co., New York,(1968) pp (17 - 36).

80. H. Lee and K. Neville, Handbook of Epoxy resins, McGraw-Hill Book Co., (1967), Chapters 4-16.

81. J. Hurd, Adhesive Guide , British Scientific Instrument Research Ass.,(SIRA), (1962), pp 9-42.

82. J.J. Bikerman, Adhesion and Cohesion,(Ed. P. Weiss), Elservier Pub. Co., New York, (1962), page 36.

83. L.H. Sharpe and H. Schonhorn, Contact Angle, Wettability and Adhesion, Adv. Chem. Ser. No.43,(Ed.R.F. Gould), (1964), page 189.

84. A. Duprè , Theorie Mechanique de la Chaleur, Gauthier - Villars, Paris , (1869), page 369.

85. D.H. Bangham and R.I. Razouk, Trans. Faraday Soc., 33, 1459 and 1463, (1937).

86. T. Young, Phil. Trans. Roy. Soc., 95, 65, (1805).

87. C.G. Sumner, Wetting and Detergency , (Ed. W. Clayton), A. Harvey Pub., London, (1937) , page 15.

88. J.J. Bikerman, J. of Appl. Chem., 11 , 81 , (1961).

89. H. Schonhorn , J. of Polym. Sci., B2 , 465, (1964).

90. V.K. Gromov, M.B. Neimann, V.L. Vakula, and S.S. Voyutski, Int. J. Appl. Radiation Isotopes, 14 , 351, (1963).

91. F.M. Fowkes, Industrial Engin. Chem., 56(12) , 40 , (1964).

92. J.J. Benbow, Proc. Phys. Soc. (London), 78 , 970, (1961).

93. D.R. Taylor and J.E. Rutzler, Indust. and Engng. Chem., 50(6), 928, (1958).

94. J.R. Huntsberger, J. Polym. Sci., 1 , 1339, (1963).

95. G.A. Ilkka and R.L. Scott, Adhesion and Cohesion,(Ed. P. Weiss) , Elsevier Publ. Co., New York, (1962), page 65.

96. E. Thelen, J. Appl. Polym. Sci., 6 , 150, (1962).

97. L.E. Raraty, Cited by D.D. Eley (Ed.) in Adhesion, Oxford Univ. Press, (1961) , page 273.

98. N.A. de Bruyne , Aero - Research Technical Notes, Bulletin No.168, (Dec. 1956).

99. M. Levine, G.A. Ilkka, and P. Weiss, Adhesive Age, 7(6) , 24, (1964).

100. W.A. Zisman, Contact angle, Wettability and Adhesion,(Ed.R.F. Gould), Advance Chem. Series No. 43, (1964), page 1.

101. M. Levine , G.A. Ilkka and P. Weiss, J. Polym. Sci., B2 , 915, (1964).

102. G. Kraus and J.E. Manson, J. Polym. Sci., 6(5) , 625, (1951).

103. S. Brunauer, The Adsorption of Gases and Vapours, Princeton Univ. Press, (1945), page 180.

104. B.V. Deryagin, Research, 8 , 70 , (1955).

105. J.M. Skinner, R.L. Savage, and J.E. Rutzler, J. Applied Physics, 24 , 438 , (1953).

106. V.J. Kabanov, Z.P. Grozinskaya, P.I. Zubov and V.I. Spitsyn, Doklady Akad. Nauk of SSSR, 165 (3), 626,(1965).

107. W.A. Zisman, Indust. Engng. Chem., 55 (10), 19, (1963).

108. J.R. Huntsberger, Contact angle, Wettability and Adhesion, Ed. R.F. Gould, Adv. Chem. Series No. 43, 180, (1964).

109. J.J. Bikerman, The Science of Adhesive Joints, Academic press, 2nd Edition, New York (1968), page 3.

110. J.J. Bikerman, J. Appl. Polym. Sci., 2, 216, (1959).

111. J.J. Bikerman and D.W. Marshall, J. Appl. Polym. Sci., 7, 1031, (1963).

112. J.J. Bikerman, Soc. of Plastic Eng. Trans., 2, 213, (1962).

113. J.P. Berry and A.M. Bueche in Adhesion and Cohesion, Ed. P. Weiss, Elsevier Pub. Co., New York,(1962)page 18.

114. H. Foulkes, J. Shields and W.C. Wake, J. Adhesion, 2, 254,(October 1970).

115. W.C. Wake, High temperature metal-to metal Adhesives, Report-2 to Directorate of Materials - Aviation Group, Ministry of Technology, (May 1970).

116. R.B. Krieger and R.E. Politi, Aspects of Adhesion,3,Ed. D.J. Alner, University of London Press,(1967) page 46.

117. G. Salomon in Adhesion and Adhesives,Ed. R. Houwink and G. Salomon, Elsevier, (1967), 2, page 68.

118. C.A.A. Rayner in Adhesion and Adhesives, Ed. R. Houwink and G. Salomon, Elsevier, (1967), 2, page 262.

119. G. Nomarski, A.R. Weill, Application à la metallographie, des méthodes interférentille à deux ondes polarisées, Revue de Métallurgie, L11, (1955) page 121. (Cited by Reichert ref. 120).

120. The interference contrast device and the microscope were made by: C.Reichert Optische Werke AG, Wein, Austria.

121. Cambridge Scientific Instruments Co.Ltd., Cambridge.

122. Associated Electrical Industries Limited, United Kingdom.

123. H. Ikawa, S. Shin and M. Morikawa, Technology reports by Osaka University, 19, 449, (1969).

124. H.R. Ogden and F.C. Holden, Metallography of Titanium Alloys, TML Report No.103, (May 29, 1958), Battle Memorial Institute, Columbus, Ohio.

125. P.J. Fopiano, M.B. Bever and B.L. Averbach, Trans. of ASM, 62 (2), 324, (1969).

126. D.F. Neal, IMI-Kynoch, Birmingham, Private communication.

127. F.A. Cotton and G. Wilkinson, Advanced Inorganic Chemistry, 2nd. Edition, Interscience Publishers, (1966), page 373.

128. A.I. Vogel, Quantitative Inorganic Analysis, 2nd Edition, Longmans, Green & Co., (1959), page 283.

129. F.A. Cotton and G. Wilkinson, Advanced Inorganic Chemistry , 2nd. Edition, Interscience Publishers, (1966), page 804.

130. E.R. Scheffer in Treatise on Analytical Chemistry, 5, Ed. I.M. Kolthoff and P.J. Elving, Interscience Publishers, (1961), page 52.

131. Araldite Adhesive - CIBA (A.R.L.) Ltd., Duxford.

132. De Solv-8090, obtained from Oxley Development Co. Ltd., Ulverston.

133. M. W. Holloway and Walker, J. of the oil and colour Chemists Assoc., 47 (10), 821. (October 1964).

134. Manufactured by MHH Engineering Company, Bramley, Guildford.

135. Torsional shear adhesive test apparatus - H.W. Wallace and Co.Ltd., Croydon (1969).

136. W.J. Roff and J.R. Scott, Fibres, films, plasics and rubbers, Butterworths, London (1972).

137. W.B. Pearson, Handbook of lattice spacings and structures of metals, Pergamon Press, London, (1958), page 872.

138. R.J. Good (a) Aspects of Adhesion, 7, Ed. D.J. Alner, University of London Press Limited, (to be published).
(b) American Chemical Society, Division of Organic Coatings and plastics chemistry, Washington meeting, 31 (2), 169, (1971).